Interreg France (Channel Manche) England
EuroSwac
European Regional Development Fund

EUROPEAN UNION
European Regional Development Fund

Highly efficient innovative shallow-water based Sea Water Air Conditioning solution for the Channel Area

EUROSWAC

WP T2.3 - Flexible Pipe Concept Model Calibration Report

Rev.	Status	Date	Author	Description	Checker	Approver
00	IFI	03/02/2023	Siane Lemoine	Issued for information	Benjamin Rousse	Claire Perez
01	IFI	31/03/2023	Siane Lemoine Alexandre Cinello	Issued for information	Benjamin Rousse	Claire Perez Alexandre Cinello

IFI = Issued for information

Table of contents

1. Introduction

1.1. Project Description

1.1.1. EuroSWAC Project

EUROSWAC is a highly efficient innovative shallow-water based Sea Water Air Conditioning solution for the Channel Area. It aims at designing and validating an innovative, cost-efficient, and environmentally friendly solution for cooling production, using English Channel's seawater (a renewable energy source) as a refrigerant, by exploiting temperature difference between the cold ocean water and the external air temperature.

While the need for cooling in large coastal cities is increasing at UK-FR levels (due to climate change), cooling is still mainly produced through chillers, a technology using large amounts of electricity generated partially by fossil fuels, slowing down the ability to meet Channel Area (CA) energy-climate objectives. EUROSWAC demonstrates the ability of using the Channel seawater for free cooling, adapting an existing technology used in tropical areas, to the low water depth and temperate of CA.

Building on the complementary expertise of 11 UK-FR partners from the academic and industrial fields and on the analysis of Channel's unique features, EUROSWAC aims to develop and test in real life conditions a SWAC prototype at the Brixham laboratory and National Lobster Hatchery in UK. This shallow-water based SWAC system will be the first to support an enhancing aquaculture food-stock, which will represent major benefits regarding CO2 emissions, lifespan, and costs compared to existing solutions.

The project will be complemented with R&D tasks focusing on:

- A self-burying system for the SWAC cold water pipes,
- A flexible pipe concept for the SWAC cold water pipes,
- Corrosion potential and temperature data logger.

These three R&D tasks will contribute to the reduction of the cost of the SWAC system by reducing the material cost and the installation cost. Validation of performance for the Brixham Laboratory and National Lobster Hatchery SWAC will pave the way for commercialization in CA and beyond. EUROSWAC will drive growth of SWAC solutions in FR-UK by de-risking the technology, and foster its deployment in CA, with positive environmental and economic benefits at local level. Solution's transferability is tremendous in coastal areas with high cooling needs and easy access to seawater, as up to 10% of cooling needs and 5% of heating needs of CA tertiary buildings could be met by shallow-water based SWAC by 2030.

The present document relates on the second R&D task, namely the use of a flexible pipe for the SWAC intake pipe.

1.1.2. Context of T2.3 – Flexible Pipe Concept

DORIS Engineering is using its experience to develop Sea Water Air Conditioning (SWAC) systems worldwide. Several studies have been performed previously highlighting the major importance of HDPE cost and marine operations in the Capital Expenditure (CAPEX) of the system. One promising solution to reduce SWAC CAPEX consists in using a flexible pipe instead of rigid pipe. First, the flexible pipe would be a low-cost alternative to HDPE pipe. Moreover, marine operations costs might be drastically reduced as flexible pipe can be stored on reels and installed by smaller and thus cheaper installation vessel.

The flexible pipe section is meant to transport sea water from the deep water (~1000m) up to the surface. The following sketch provides an overview of the desired system:

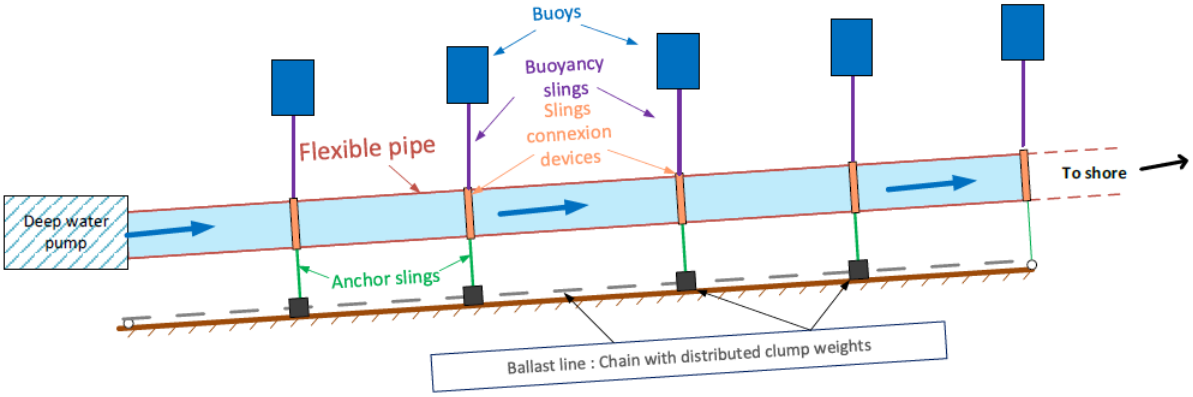

The hydrodynamic behavior of such a system is not known yet and previous numerical modelling of this flexible pipe under environmental loads has led to inconsistencies between two recognized software programs used by DORIS: Orcaflex (from Orcina) and Deeplines (from Principia).

As a result, DORIS and Océanide proposed to proceed with basin tests to validate the concept and provide experimental data for the calibration of the numerical model.

Three campaigns have been performed in April 2022 and in September 2022 using the same flexible pipe. The set-up, results, and main observations from these two campaigns are provided in Ref. 2 and Ref. 5. Additionally, a third campaign was conducted in January 2023, using both the initial flexible pipe, and a second one with a different mechanical behavior under pressure (Ref. 7).

1.2. Document Purpose

This document presents a study which aims at defining whether the OrcaFlex software is suitable for the numerical modelling of flexible pipes, and to identify potential program limitations.

The ultimate objective is to provide a step-by-step methodology to calibrate such numerical models reproducing a flexible pipe system designed for sections of SWAC intake/outtake pipes. The underlying goal is to bring to light the sensitive trends in such designs, in order to provide a basis for further SWAC/flexible pipe studies.

1.3. Executive Summary

1.3.1. 1st Campaign

For the first campaign, the set-up consists in a flexible pipe fixed at both ends, anchored to the basin floor through anchor slings, and supported by buoys through buoyancy slings. The main objectives of this first campaign were to first investigate the pipe hydrodynamic behavior using a 'simple' set-up under regular waves, with varying design criteria, and to assess the suitability of the Orcaflex software to reproduce the experimentally observed behaviors.

The principal studied design parameters of this first campaign were:

- the shape of the buoyancy modules and their distribution along the flexible pipe
- the flow pressure inside the flexible pipe
- the flow rate inside the flexible pipe
- the anchor slings' axial stiffness
- the pipe end fixation state (fixed/free)

It was observed during the experimental campaign that:

- the selected flexible pipe retracts when put under pressure, leading to a pressure specific definition of the axial, and bending stiffnesses of the flexible pipe.
- the designed flexible pipe system exhibits hyperstaticity, which is visible through the uneven and unpredictable repartition of the anchor sling tension in the basin.
- the flexible pipe axial end loads are very sensible to the distance between the two fixation points, when both ends of the flexible pipe are fixed (a few millimeters generate a difference of a dozen kN).

The numerical modelling calibration focused mainly on:

- the axial and bending stiffnesses in function of the internal pressure
- the axial end loads at both fixed pipe ends
- the tension signal of the anchor sling during slack events in function of the sling axial stiffness

It was found that the OrcaFlex numerical model of the flexible pipe system:

- predicts the general pattern and the amplitude of the motions time signals in both the x and z- directions
- identifies the anchor sling slack events occurring in the basin
- slightly overestimates the high-tension peaks of the tension time signals in the anchor slings, following slack events

Rather than software limitations, the calibration of the flexible pipe system numerical model was limited by the hyperstaticity of the designed flexible pipe system.

1.3.2. 2nd Campaign

Building on the 1st campaign observations and with the objective to test for a more realistic flexible pipe system, as part of a SWAC intake pipe, a new flexible pipe system is considered in this 2nd campaign.

The following design parameters were updated:

- addition of a strainer at one end of the flexible pipe,
- testing of 3 different anchoring systems (clump weights and/or chain),
- more realistic connecting devices between flexible pipe and anchors/buoyancy modules using soft collars.

By liberating one pipe end, and implementing anchoring components, the second campaign design allows to get rid of the limiting hyperstatism state observed during the first campaign.

The 2nd campaign test matrix included:

- underwater axial and bending stiffnesses characterization tests of the flexible pipe,
- seabed friction characterization of the anchoring components,
- irregular wave tests to investigate the anchor system dynamic behavior for each configuration,
- in-line regular wave tests to investigate potential "whiplash effect" at the pipe free end equipped with the strainer (amplification of the pipe end amplitude),
- both regular and irregular wave tests with an initial pipe buckling (i.e., local deformation) to assess the evolution of the buckling under given sea conditions.

During the second experimental campaign, it was observed that:

- During transverse irregular wave tests, the flexible pipe system oscillates around its initial position (i.e., rectilinear resting position).
- During transverse regular wave tests, the flexible pipe system adopts a circular arc shape and is then shifted in either transverse direction depending on the wave phase.
- During transverse current tests, the clump weights adopt a slanted position and are then shifted along.
- No resonance phenomena were observed at the pipe free end during in-line regular wave tests.
- It was not possible to obtain a none-collapsed buckling with the flexible pipe, due to its rigidity (i.e., retracting under pressure). As a results, these tests could not be reproduced on OrcaFlex, due to the deformation of a solid.

The calibration of the numerical models of the 2nd campaign, mainly focused on the axial and bending stiffnesses based on the updated underwater characterization tests, and the friction coefficients of the anchoring components. Overall, the numerical model yields similar flexible pipe system behaviors to the experimental recordings.

Now that the flexible pipe system is allowed to move laterally, a calibration of the hydrodynamic coefficients of the pipe for each sea condition is required to predict the true pipe transverse displacement.

1.3.3. 3rd Campaign

Finally, the objective of the third campaign is to complement the two previous ones by investigating:

- The use of a new flexible pipe featuring another mechanical response to the internal pressure variations. The pipe tested previously tends to shorten with the internal pressure increase while the new pipe elongates with the internal pressure increase, thus enabling buckling formation without collapse.
- Damage conditions considering one anchor sling, or one buoyancy sling lost at different locations along the flexible pipe.
- The potential seabed elevation variations by modelling a bump. Indeed, all tests of the first and second campaign are performed on a flat seabed.

The following remarks on the experimental campaign are summarized hereafter:

- A hysteresis behavior was characterized for pipe B during the preliminary in air axial stiffness check.
- The elongation under pressure feature of pipe B did indeed allow the formation of non-collapsed buckling.
- The end B buoy removal, for free end configurations (i.e., strainer presence), was unintentionally omitted during this third campaign.

For this third and last campaign, a calibration validation approach was adopted to validate the numerical model through a systematic and direct comparison of the results. This systematic comparison between the numerical model and physical model has shown that:

- The numerical model provides the same tendencies and the same orders of magnitude for most of the cases.
- The numerical model predicts the maximum tensions in the anchor slings for all cases.
- The numerical model exhibits more discrepancies regarding the flexible pipe motions. However, both numerical model and physical model show small motions of the pipe at the wave frequencies, demonstrating the consistent hydrodynamics behaviour of the modelled flexible pipe. In addition, it is highlighted here that the motions predicted for the anchoring configuration 1, with clump weights only, compare better to the numerical model than for the anchoring configuration 2, with chain only. It is reminded that the initial position of the chain is not similar between the numerical model and the physical model.

Finally, the calibration methodology developed using the results of the two first campaigns was applied to the cases investigated during the third campaign. The comparative analysis between the numerical model and physical model tends to demonstrate that OrcaFlex software can be used to investigate the hydrodynamic behavior of a flexible pipe system and to design the main elements of such a concept. In addition, the calibration methodology developed using results from tests with pipe A has been applied with success to another pipe material exhibiting a different response to internal pressure variation. As a conclusion, the developed numerical tool and associated calibration methodology can be used to design an actual flexible intake pipe for future SWAC systems.

1.4. References

N°	Name	Description
Ref. 1	216-T2.3-DEN-002 - SWAC-R&D - Basin Test specification rev00	First Basin Tests Campaign Specification
Ref. 2	21.2.024.R.004 1st basin tests campaign - Basin Tests Report	First Basin Tests Campaign – Basin Tests Report
Ref. 3	216-T2.3-DEN-007 Master Thesis HydroFlexible	Master Thesis Report acting as a detailed Calibration Report of the First Campaign
Ref. 4	216-T2.3-DEN-004 - Flexible Pipe Concept - Second Basin Model Tests - Campaign Specification rev. 01C	Second Basin Tests Campaign Specification
Ref. 5	216-T2.3-OCD-002 – 2nd basin tests campaign - Basin Tests Report rev. 00A	Second Basin Tests Campaign – Basin Tests Report
Ref. 6	216-DEN-006 - SWAC-RD - Basin Test specification 3 - Rev01	Third Basin Tests Campaign Specification
Ref. 7	216-T2.3-OCD-003 – 3rd basin tests campaign Basin Tests Report – Rev02	Third Basin Tests Campaign – Basin Tests Report
Ref. 8	C-DOC-VIA-1030_rev01 - Submaflex - Physical Model tests report	Developed by DORIS Engineering in previous projects
Ref. 9	C-DOC-VIA-1021_rev01 - SubmaFlex - Hydrodynamic Behaviour	Developed by DORIS Engineering in previous projects
Ref. 10	DNVGL-RP-C205 Environmental conditions and environmental loads	
Ref. 11	Offshore Structure Hydrodynamics by Bernard Molin	Hydrodynamics Handbook

1.5. Acronyms

AS: Anchor Sling
BS: Buoyancy Sling
C_A: Added mass coefficient
C_D: Drag coefficient
CW: Clump Weight
EA: Axial stiffness
EI: Bending Stiffness
H: Wave height
HDPE: High Density Polyethylene
ID: Internal Diameter
OD: Outer Diameter
Pi: Internal Pressure
SWAC: Sea Water Air Conditioning
T: Wave period
Tn: Natural wave period
QT: Qualysis Target
VIV: Vortex Induced Vibrations
WD: Water Depth

2. First Campaign

2.1. Model-Scale Experimental Campaign

2.1.1. Flexible Pipe System Design

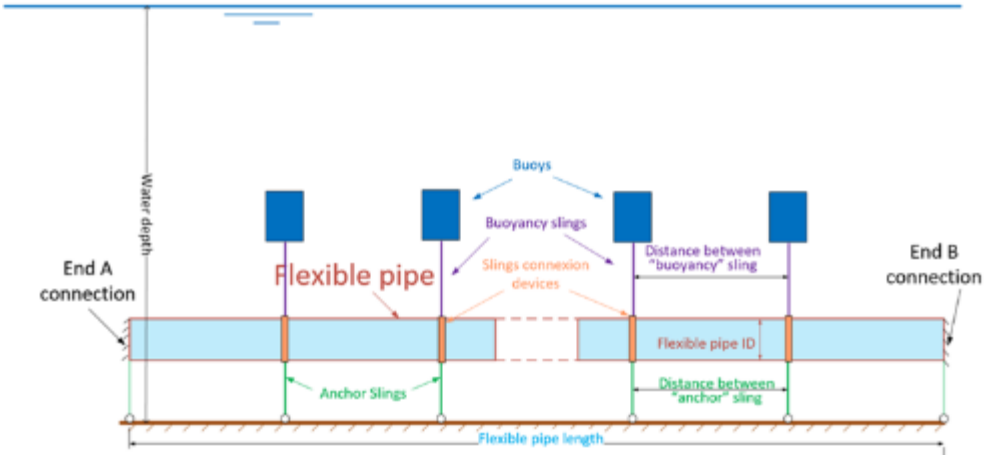

Figure 2-1: Longitudinal view of the 1st campaign flexible pipe system.

As detailed in Ref. 2 Section 5, the flexible pipe system design is composed of the following components:

- Flexible pipe in woven polyurethane (fixed at both end for this 1st campaign)
- Buoys : 3 different types (Picture 2-1)
  1. Cylinder; B = 37.08kN
  2. Cylinder; B = 74.14kN
  3. Ring; B = 49.00kN
- Buoyancy slings connecting the buoys to the flexible pipe
- Anchor slings connecting the flexible pipe to the seafloor (fixed connection at the seafloor for this 1st campaign)
- Clamping devices surrounding the flexible pipe and allowing the sling connection to the pipe (Picture 2-1)

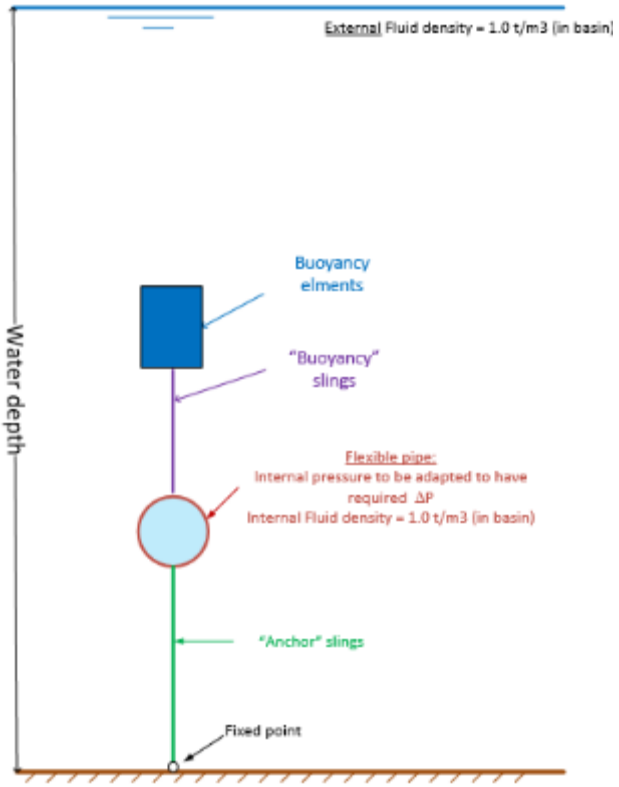

Figure 2-2: Transverse view of the 1st campaign flexible pipe system.

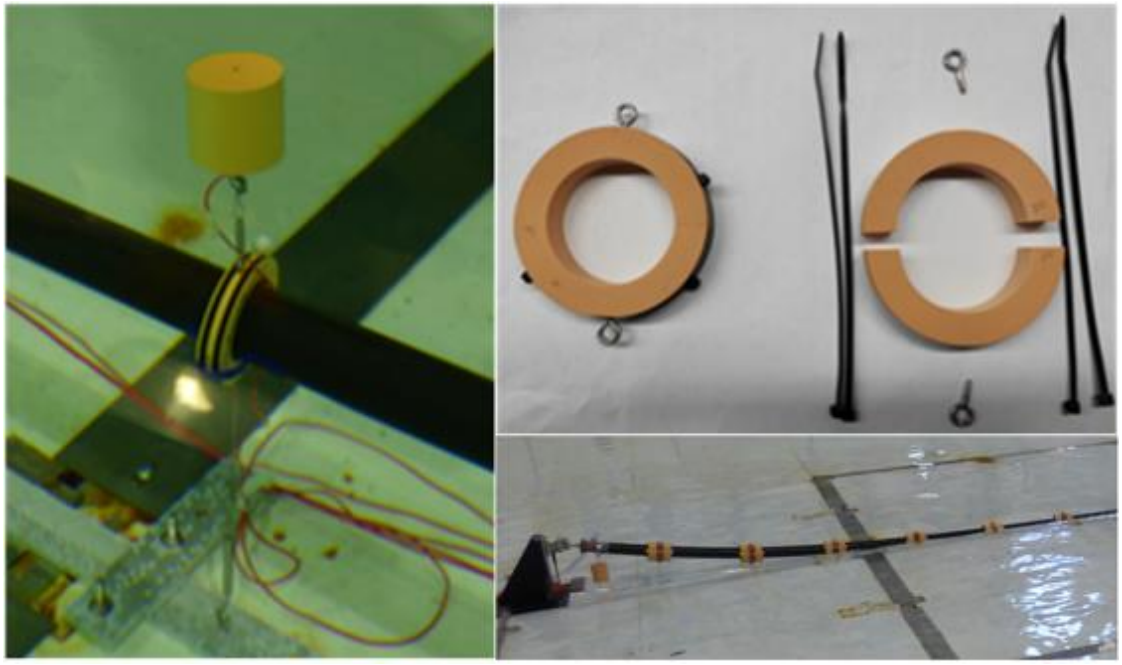

Picture 2-1: Left - Cylindrical buoy with rigid clamping device surrounding the flexible pipe, on which the slings are fixed. The clamping devices are maintained into position through the thermos-glued strap in the pipe axial direction. Right – Ring shape buoy before and after being assembled around the flexible pipe.

As explained in Ref. 3 Section 2.1.2. and 2.1.3., several scales are defined in this project (Figure 2-3):

- **Model-scale** of 1/20, used in the test basin during the experimental campaign (OD = 0.0702m). This model scale was dictated by both the available polyurethane commercialized flexible pipes and the extreme sea conditions limited by the experimental facility dimensions.
- **Full-scale** of 1 (i.e. OD = 1.404m), obtained with the Froude similitude (except for the hydrodynamic coefficients see Section 2.2.2 of this document for further details).
- **Real scale** referring to standard SWAC intake pipe dimensions (i.e. OD = 0.5m)

Thus the full and real scales are not identical due to the previously mentioned constraints. Note that all the numerical simulations were conducted at full scale.

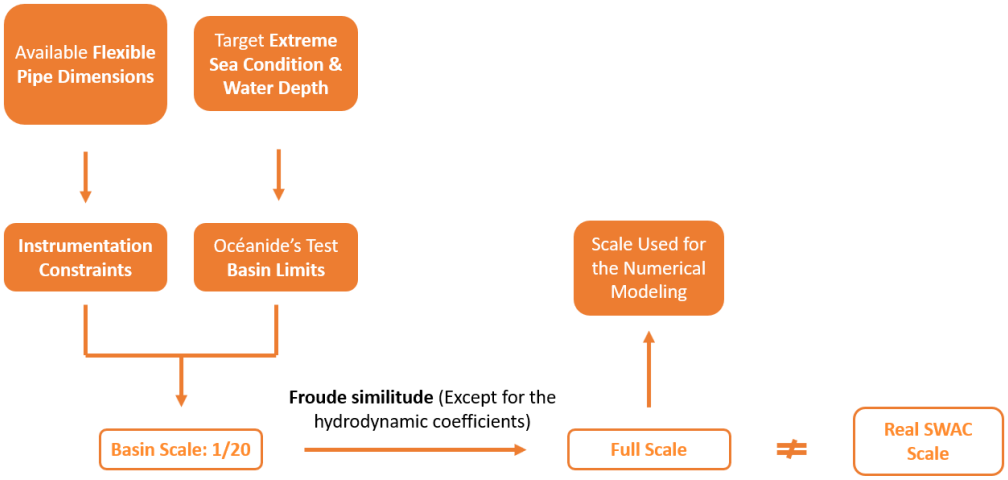

Figure 2-3: Schematic definition of the 3 different scales of flexible pipe systems.

The described flexible pipe system was defined through preliminary calculations with the Orcaflex software. A so-called base case was determined after having conducted several sensitivity studies on the design. Table 2-1 summarizes the selected parameters of interest. This preliminary study was carried out with a simplified Orcaflex model which did not consider the effect of the internal pressure on the flexible pipe EA and EI. Further details are provided in Ref. 3 Section 2.2.2.

Varying Parameter	Unit	Tested Value
Buoy type	-	1; 2; 3
Buoy spacing	m	10 ; 20
AS axial stiffness	kN	2000 ; 60000
Fixed/Free pipe end	-	Fixed-Fixed ; Fixed-Free
Pi	bar	0 ; 10 ; 40
Internal flow rate	t/s	0 ; 0.36 ; 0.5

Table 2-1: Selected parameters to be tested during the 1st experimental campaign (reported in full scale).

As a result, several flexible pipe configurations were tested. While the base case, previously presented is referred to as Configuration 1, the five additional configurations are listed in Table 2-2.

	Unit	Config. 1	Config. 2	Config. 3	Config. 4	Config. 5	Config. 6
Buoy distribution	m	10	10	**20**	**20**	10	10
Buoy shape	-	Cylinder	Cylinder	Cylinder	Cylinder	**Ring**	Cylinder
Buoy volume	m3	3.78	3.78	3.78	**7.56**	3.78	3.78
AS EA	kN	2000	**60000**	2000	2000	2000	2000
End B state	-	fixed	fixed	fixed	fixed	fixed	**free**

Table 2-2: Main features of the six flexible pipe system configurations tested during the 1st experimental campaign.

2.1.2. Experimental Procedures & Observations

2.1.2.1. Preliminary Flexible Pipe Characterization Tests

The flexible pipe selected for this 1st campaign is the "Techflex PU Extra DN65" made in woven polyurethane and produced by the French company Delannoy Frères. The main pipe dimensions are provided in detail in Ref. 3 Section 2.1.3., for the 3 scales. Note that this flexible pipe is flat when empty, and when filled with air or water, it gains its cylindrical shape and becomes more rigid, as can be seen in Picture 2-2.

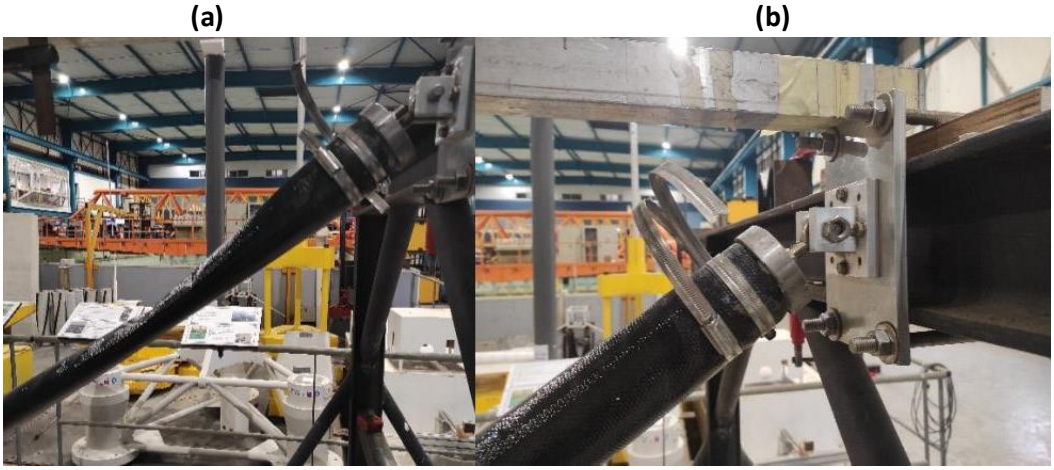

Picture 2-2: Flexible pipe without (a) and with (b) air-induced internal pressure.

As a result, the pipe was thus experimentally characterized, prior to the experimental campaign, both for the axial stiffness and the bending stiffness, with a model-scale 6 meter-long protype.

The axial flexible pipe EA was characterized by testing for the elongation of the flexible pipe under air-induced pressure. The flexible pipe was hung from the ceiling and the internal pressure, and the axial tension applied axially on the pipe bottom end were gradually increased, by respectively adding more air inside the pipe and increasing the attached weight mass (Figure 2-4a). The results are reported at full scale in Figure 2-4b.

(a) *(b)*

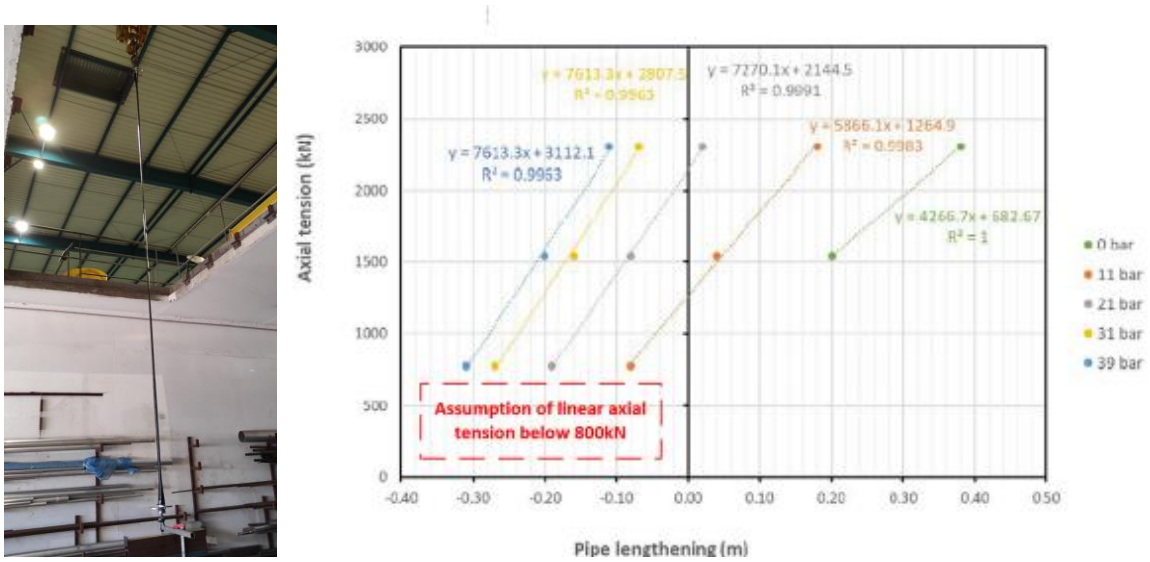

Figure 2-4: Experimental of the elongation under pressure of the flexible pipe, and (b) flexible pipe lengthening in function of the internal pressure and the applied axial tension.

Several observations can be made about Figure 2-4:

- the higher the internal pressure, the higher the pipe stiffness
- starting a Pi of approximatively 30bar, the stiffness seems to have reach its peak and stagnates
- the studied flexible pipe shortens under pressure (unexpected behavior based on the previous flexible pipe behaviors reported on the past DORIS SWAC reports & ViaMarina reports → depending on the constituting fiber arrangement angle of incidence)

Note that 800kN was the minimum axial tension tested for. It was thus hypothesized in the further sections, that the flexible pipe EA also evolves linearly below 800kN of applied tension.

The flexible pipe EI was also tested for. This was done by fixing the flexible pipe ends in a horizontal position above the ground and hanging a weight of increasing mass. The flexible pipe distance to the horizontal line joining both pipe ends was then recorded at several fixed sections.

(a)

(b)

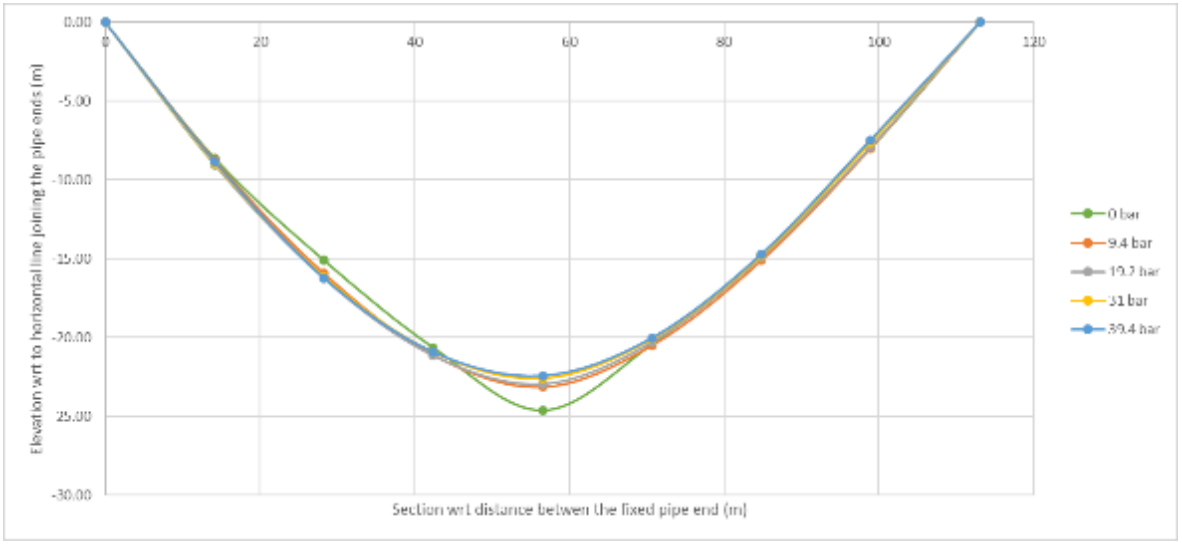

Figure 2-5: (a) Experimental setup to measure the vertical profile of the flexible pipe in function of the internal pressure and the applied tension at the pipe mid-length and (b) flexible pipe elevation profile for a weight of 34.6 tons attached at the pipe mid-length and increasing internal pressures.

From Figure 2-5b, one can deduct that the higher the internal pressure, the higher the flexible pipe EI.

Further details about the flexible pipe EA and EI characterization are provided in Ref. 3 Section 2.1.3. and in Ref. 2 Sections 5.1.1 - 5.1.3.

2.1.2.2. *Experimental Campaign Main Features*

This section is meant to briefly introduce the experimental setup and the selected sea conditions tested in the BGO First at Océanide in La Seyne-sur-Mer, and to report some unexpected behaviors of the scale prototype during the experimental campaign. A more thorough description is provided in Ref. 2 Sections 2.2. for the referential conventions, 5. for the setup description, and 10.3. for the main observations noted during this experimental campaign.

2.1.2.2.1. Model scale Experimental Setup

The tested experimental setup slightly differed from the simplified numerical model built for the sensitivity studies carried out previously. The following divergences are listed as follows:

- Weighting pipe end connections allowing a closed-loop water circuit and a connection of the setup to the weighting scales; made neutrally buoyant with dedicated buoys (Picture 2-3)
- Clamping devices with a larger internal diameter as the flexible pipe outer diameter and with a fixing strap with a loose fit (Picture 2-4)
- Tensiometers were added to some slings changing the overall mass and diameter (Picture 2-4)
- Small buckles and eyebolts enabling the assembly of the setup (Picture 2-4)

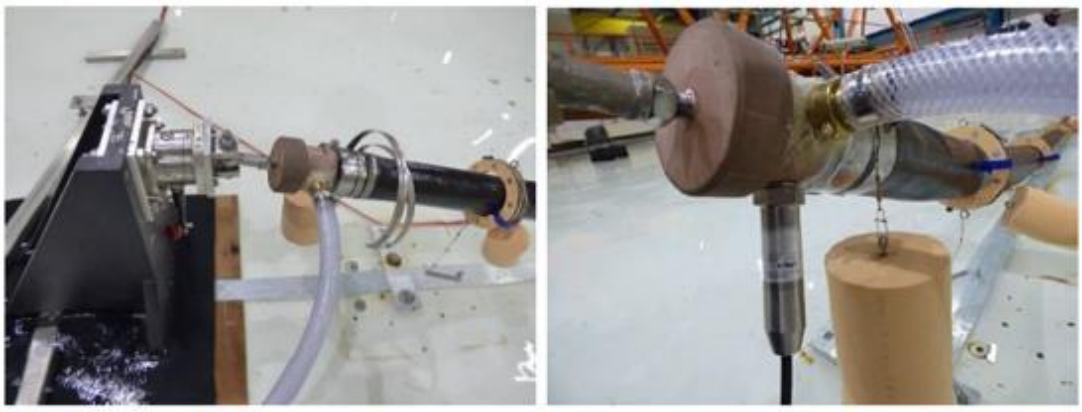

Picture 2-3: Flexible pipe end connections and their associated end connection buoys.

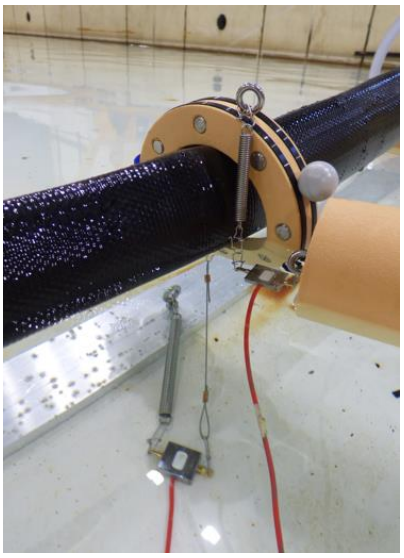

Picture 2-4: Collar-shaped clamping device allowing the connection of the slings to the flexible pipe, with a tensiometers and visible assembly pieces.

2.1.2.2.2. Selected Sea Conditions

Environmental conditions include regular wave alone tests, current alone tests, and regular and current tests.

The current was set to 0.8 m/s. Three regular waves are modelled, based on the wave height (double amplitude) H; and the wave period T:

- REG1: H = 4 m; T = 8.5 s
- REG2: H = 8 m; T = 11.0 s
- REG3: H = 10 m; T = 12.0 s

Three incidences were considered: 0°, 45°, and 90°. When combined, current and wave shared the same incidence.

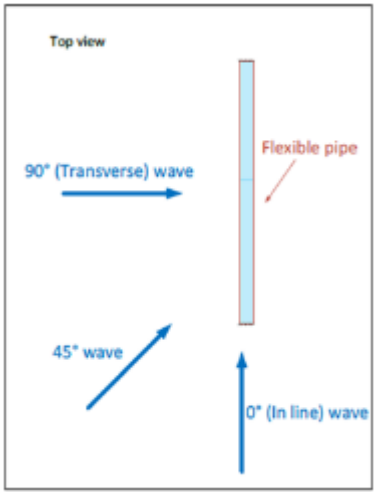

Figure 2-6: Schematic representation of the sea conditions incidence.

2.1.2.2.3. Experimental Unexpected Observations

The main unexpected features observed during the experimental campaign are reported hereafter to taken into consideration during the calibration process described in Section 2.2.

- The designed flexible pipe system was found to be hyperstatic. In fact, given that the flexible pipe is fixed to the seabed at each anchor sling end, and that the flexible pipe ends are constrained in all directions, the pipe being flexible, compensate for any king of irregularity in the experimental setup (i.e., seabed imperfection, small variation of anchor slings length, initial deformation of the pipe, …). Consequently, due to this unpredictable compensation, the load is not evenly spread between the anchor slings as observed in a 'perfect' numerical model.

- During the tests, an initial deformation of the flexible pipe was observed, namely at the pipe end, as illustrated in Picture 2-5. This initial deformation led to initial constraints measured at the end connections.

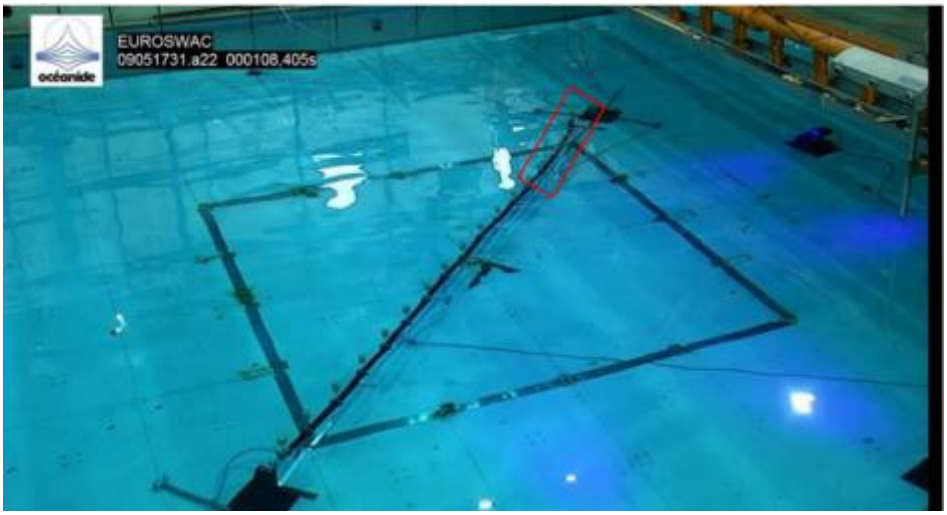

Picture 2-5: Experimental setup of the flexible pipe system of Configuration 6 (fixed-free pipe end connection) with a visible pipe initial deformation at the free end.

2.2. Numerical Model Implementation

2.2.1. Numerical Model Description

2.2.1.1. Orcaflex Numerical Model

The numerical model was built on the Orcaflex software. The flexible pipe system was decomposed into the following constituents:

- Flexible pipe & Pipe ends connections ➔ 1 Orcaflex Line (divided into 3 sections)
- Anchor slings ➔ Orcaflex Lines
- Buoyancy slings ➔ Orcaflex Lines
- Buoys ➔ Orcaflex 3D Buoys
- Clamping devices ➔ not included as an Orcaflex object (since it is neutrally buoyant) but taken into account as connection offsets

For further details, refer to Ref. 3. Sections 2.2.2. for the basic introduction of the numerical model and 2.3.1. for the precise dimensions of each component.

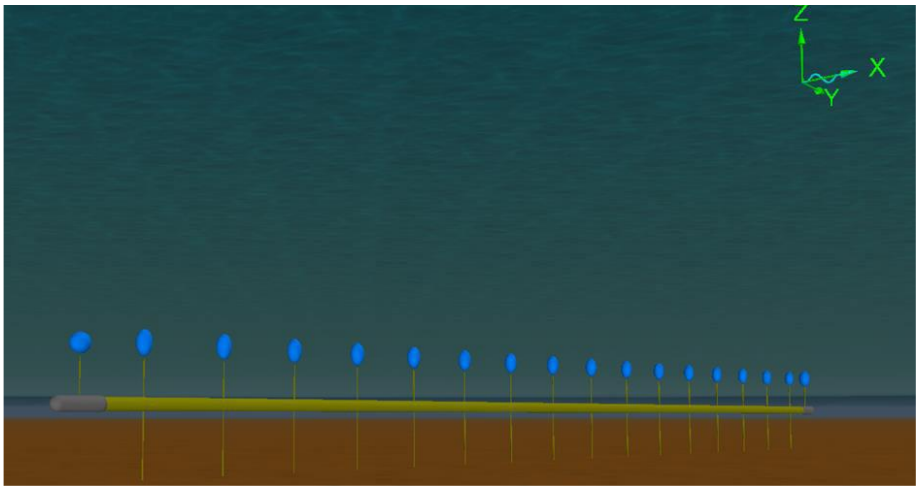

Figure 2-7: Shaded longitudinal view of the flexible pipe system numerical model (Configuration 1).

2.2.1.2. Adjustments to Fit the Experimental Setup

As introduced in Section 2.1.2.2, a few additional features which were not taken into account in the preliminary numerical Orcaflex model were noted. This section provides a succinct explanation as to how they were included in the numerical model. In Ref. 3. Section 2.4.2., an extensive description for the inclusion of the pipe end connection and the sling modeling is given.

- **Pipe end connections:** These complex shapes were simplified to two hollow cylinder of same ID as flexible pipe ID and OD calculated so to obtain the same experimental masses in the water.

- **Slings:** Given that torsion was not included in the model, the connection between the Orcaflex Lines modelling the flexible pipe and those accounting for the slings could only be done at the pipe longitudinal center axis. It was chosen to add an additional sling length including the pipe thickness, and the extra elevations added by the clamping device and by the eyebolt. The sling EA was modified accordingly.

- **Spring/Sting & Tensiometers:** To achieve the desired sling EA, specific springs were added to the string acting as slings. Additionally, tensiometers were placed in the axis of some of the slings. To account for these elements, both the masses and the diameters were calculated by averaging the values of each component.

2.2.2. Hydrodynamic Coefficients

This section explains how the hydrodynamic coefficients of the flexible pipe, as well as those of the slings and buoys were estimated for the numerical model. Rather than a precise study, the goal was to get an order of magnitude of those values.

The viscous forces at the model scale characterized by the Reynolds number allowed the approximate estimation of the C_D for the flexible pipe. Given that the Froude similitude was used for the scale transition, it was chosen to retain the C_D range obtained for the model scale for the full scale, in order to conserve the same viscous regime observed in the basin at model scale.

The flexible pipe C_A was set to 1 following the Sarpkaya referential graphs reported in Ref. 3.

Note the that the same C_D defined for the flexible pipe was used for the slings and for the buoys. The added mass coefficient was however set to 1 for the slings and 0.62 for the buoys, according to the recommended practice of DNVGL-RP-C205 Ref. 10. in Appendix D.

The values for the C_D and the C_A of the flexible pipe system main components are reported in the following Table, and the complete definition procedure of the hydrodynamic coefficients are provided in Ref. 3. Section 2.1.2.2.

	Flexible Pipe	Slings	Buoys
C_D	1.2	1.2	1.2
C_A	1	1	0.62

Table 2-3: Hydrodynamic coefficients estimated for the flexible pipe, slings, and buoys for the numerical model of the 1st campaign.

2.3. Numerical Model Calibration Axes

This section presents the main topics that were treated in an effort to obtain a more realistic numerical model. These so-called calibration axes refer to either the integration of the experiment tests to characterize both the axial stiffness and the bending stiffness in function of the internal pressure; or to account for non-anticipated phenomena that were witnessed during the test campaign: axial end loads and anchor sling behavior with a high EA.

2.3.1. Axial Stiffness

The calibration methodology of the axial stiffness of the flexible pipe is described in detail in Ref. 3. Sections 2.4.1.1. and 3.1.1. A succinct step-by-step summary is provided in this Section.

- The axial stiffness behavior can be specifically defined through a strain/wall tension function in Orcaflex. It was chosen to define the pressure-specific axial stiffness for a strain associated to an externally applied tension of 0N (excluding the strain due to the internal pressure), and for a strain of 100%. Since the experimental tests characterized linear trends, two points were hypothesized to be sufficient.

- Next, the effective tension Te was calculated from which the wall tension Tw could be derived. The EA was derived from the slope of the tension/pipe lengthening characteristic curves multiplied by the pipe initial length.

$$T_e = EA \cdot \frac{\Delta l}{l_0}$$
$$T_w = T_e + (p_i a_i - p_o a_o)$$

- The second axial stiffness characterization point was calculated for a strain of 100%.

$$T_{w_{\varepsilon=100\%}} = EA \cdot \frac{\Delta l}{l_{0_{\varepsilon=100\%}}} + T_{w_{T_e=0}} \text{ where } \frac{\Delta l}{l_{0_{\varepsilon=100\%}}} = 1 - \frac{\Delta l}{l_{0_{T_e=0}}}$$

- The obtained axial stiffness was then tested for each internal pressure. The pipe length evolution was checked to be equal to 10% of the initial length with an EA of 10%.

- The internal pressures that were not directly characterized during the axial stiffness test were linearly interpolated from the available data.

- However, given that the characterization tests were done in the air and that the experimental campaign of the flexible pipe system was conducted in the basin, the effect of the hydrostatic pressure had to be accounted for. This was achieved by considering the pressure differential ΔP, instead of the internal pressure.

Table 2-4 provides the obtained strain/wall tension curves for three recorded experimental Pi.

Pi	Pe	ΔP	$\varepsilon_{Te=0}$	T_w for $\varepsilon_{Te=0}$	$\varepsilon_{100\%}$	T_w for $\varepsilon_{100\%}$
[bar]	[bar]	[bar]	[%]	[kN]	[%]	[kN]
13.2	4.19	9.01	-0.019	1089	100	675220
25.4	4.19	21.2	-0.092	2708	100	878672
39.6	4.19	35.4	-0.167	4593	100	919810

Table 2-4: Interpolated axial strain/wall tension curves used as axial stiffness customized Orcaflex input data based on experimental pressures.

2.3.2. Bending Stiffness

Further details about the bending stiffness calibration are given in Ref. 3. Sections 2.4.1.2. and 3.1.2.

- The calibration of the EI was more straightforward, as the EI was kept as a constant input data in the Orcaflex model, for a specified Pi.
- For a given Pi, the EI was defined by iteratively verifying if the obtained vertical offsets to the imaginary horizontal line joining the 2 fixed ends were identical to those recorded during the experimental characterization test (Figure 2-5b).
- Similarly, the EI for the Pi not experimentally characterized were derived through linear interpolation.

Table 2-5Table 2-4 provides the obtained EI values for three recorded experimental Pi.

Pi	Pe	ΔP	EI
[bar]	[bar]	[bar]	[kN.m^2]
13.2	4.19	9.01	95115
25.4	4.19	21.2	203697
39.6	*4.19*	*35.4*	*340668*

Table 2-5: Interpolated EI values used Orcaflex input data based on experimental pressures.

2.3.3. Axial End Forces

The recorded axial end loads measured with the 3D load transducers at the pipe end connections, showed some unexpected trends, when looking at the Configuration 1 test batch for 90° incident sea conditions:

- asymmetric axial tension results at the pipe ends, despite the symmetry of the experimental setup
- significant variability for a same Pi (end A: -360kN to -510kN, end B: -540kN to -650kN)
- the end loads recorded negative values → compression at the 3D load cell → pipe is extending (which is the contrary of what was characterized)

The validity of these axial pipe end loads was thus questioned. To investigate the reliability of the experimental end loads, a calibration test recording the axial end loads at the balances while being immerged, for an internal pressure of 1000kPa, was used (Figure 2-8).

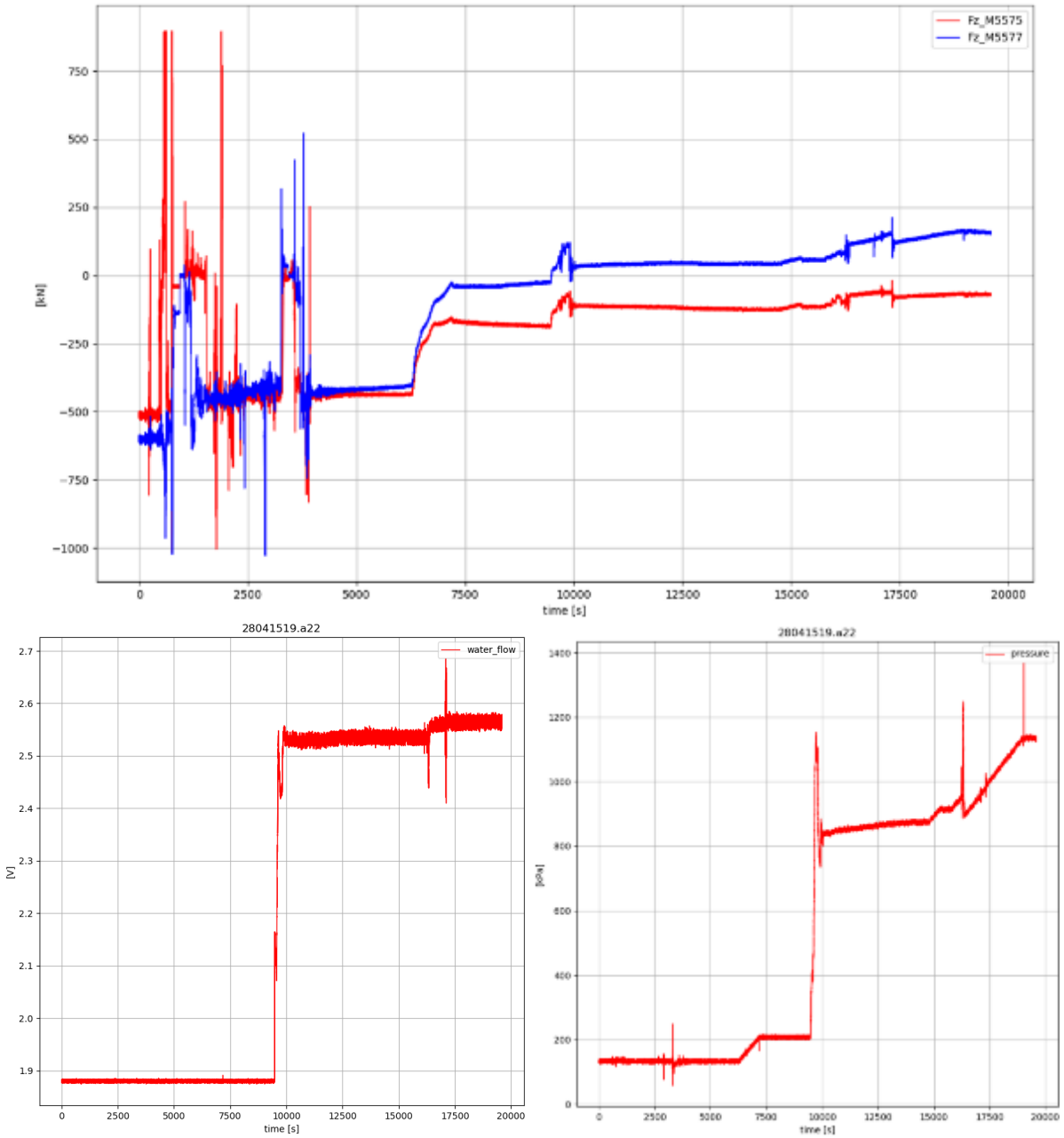

Figure 2-8: Axial end load at the pipe extremities, water flow and internal pressure time signals during the end scale calibration test. Note that the basin referential frame of the basin differed from the one used throughout this study and that as a result, the plotted Fz are indeed the axial forces and that Fz_5575 has to be corrected with a factor of -1.

This exercise revealed that in Figure 2-8:

- seafloor descent starts at 6500s (gradual increase of the hydrostatic pressure)
- just before 10000s, the water flow is increased, and in turn the pressure, and the axial loads
- at 16500s, the collars were re-adjusted to ensure a non-slanted position (explain the peaks)
- it is visible that the Fz_M5577 downstream axial end load tends to drift away during the axial end loads stabilized time intervals (unlike the Fz-M5575 upstream axial end load which remained constant)
- the final upstream axial end load (+70kN) was thus considered as the reference value to obtain the distance between the pipe fixation points for the numerical model
- this distance between the pipe fixation points was maintained for the tests with different Pi

With this calibration process, the pipe is now retracting as characterized during the axial tension tests. It should however be mentioned that :

- the flexible pipe system axial loads are hypersensitive to the inter distance between the 2 pipe end fixation points (i.e. at full scale a reduction of a few mm between the fixation points yields a gain of a few dozen of kN in terms of axial end loads)
- the axial end loads during the tests mostly fall within the linear interpolation assumption of the EA Orcaflex input curves range (below the first tension measurement), refer to Figure 2-4.

In Ref. 3. Sections 2.4.3. and 3.1.4., additional information can be found to complete the given correction procedure applied on the numerical model.

2.3.4. High Anchor Sling Stiffness

A summary of Ref. 3. Sections 2.4.3.2. and 3.1.3. is provided hereafter.

As the AS with a high EA (60000kN) were anticipated to cause slack events, and that one of the objectives of this study was to determine the capacity of the Orcaflex software to identify and accurately handle them, specific care was put into the calibration of Configuration 2, featuring this increased AS EA, especially when subjected to the highest regular wave REG3 (**test 21**). A first comparison between the experimental data and the results obtained with refined numerical model, showed that:

- slack events are identified by the numerical model and main tension signal pattern is well predicted
- but during slack events, high tension peaks are overestimated by the model

After investigation, it was found that the specified AS EA of 60000kN was most likely not correctly implanted in the basin. Figure 2-9 shows a visual explanation of the above comments. By gradually decreasing the AS EA from 60000kN to 12000kN, the tension peaks are getting closer to the experimental signal.

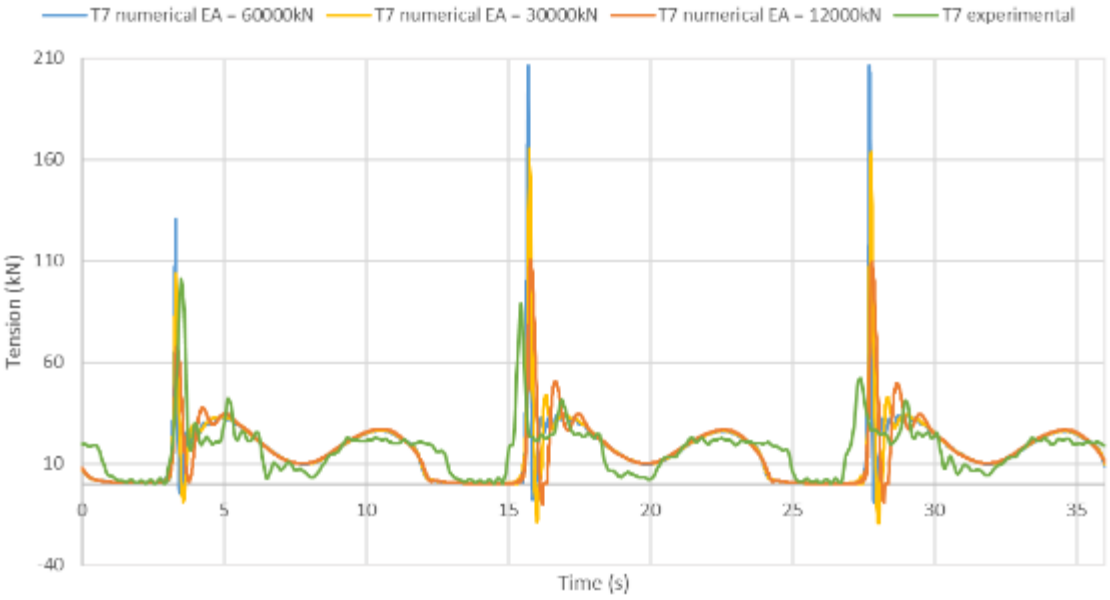

Figure 2-9: Comparison of the tension time signal of the AS15 for Configuration 2 under a 90° incident REG3, between the experimental signal and different numerical model using decreasing AS EA.

It was conjectured the buckles and fasteners included in the experimental setup to connect the different sling components made the experimental sling more flexible than desired. Additionally, when considering the technical sheet of the spring used during the experimental campaign (Ref. 3. Appendix 6), the stiffness behavior for a load inferior to 72kN is nonlinear. As this condition is met during slack events, this could also be responsible for the divergence in the peak tensions for this test.

2.4. Comparative Study between the Experimental and Numerical Data

The comparison between the recorded experimental data and the calibrated numerical model of this first campaign is provided in this section. To complete this comparative study some additional information are available in Ref. 3 Section 3.2 for the pipe motions, and Section 3.3 for the sling tensions.

Note that this comparative study is restricted to the nominal configuration (i.e., Configuration 1) for 90° incident sea conditions due to time restraints. Some general remarks of the experimental behavior of the remaining configurations are however drawn in Section 0.

In the basin, the flexible pipe was placed along the y-axis of the reference frame. The x-axis is defined as positive towards the wave absorber, and the z-axis is vertical and pointing upwards (Sketch 2-1). The flexible pipe motions of interest are thus in the x- and the z-direction.

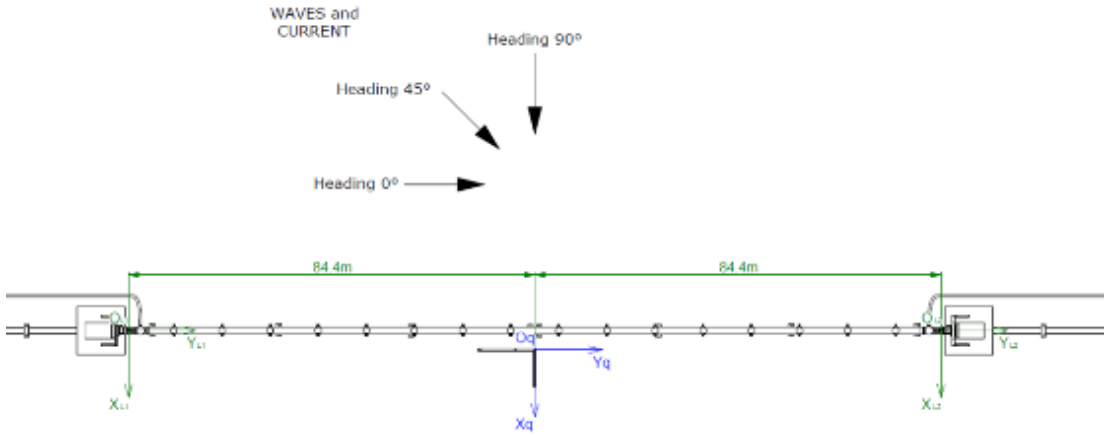

Sketch 2-1: Reference frame used in the experimental campaign and in Orcaflex.

2.4.1. General Motion Behavior of the Flexible Pipe

To assess the predictive ability of the numerical model to reproduce the general motion behavior of the flexible pipe system in Configuration 1, the maximum displacements of the flexible pipe with respect to its resting position are investigated. By plotting these maximum displacements, in both the x- and z-directions, at different pipe arc lengths, the position of the flexible pipe under the 3 regular waves is visible. Figure 2-10 and Figure 2-11 respectively depicts the extremum pipe transverse and vertical offsets for the nominal Pi of 10 bar, subjected successively to REG1, REG2, and REG3, with a 90° incidence (**tests 8, 9, 10**).

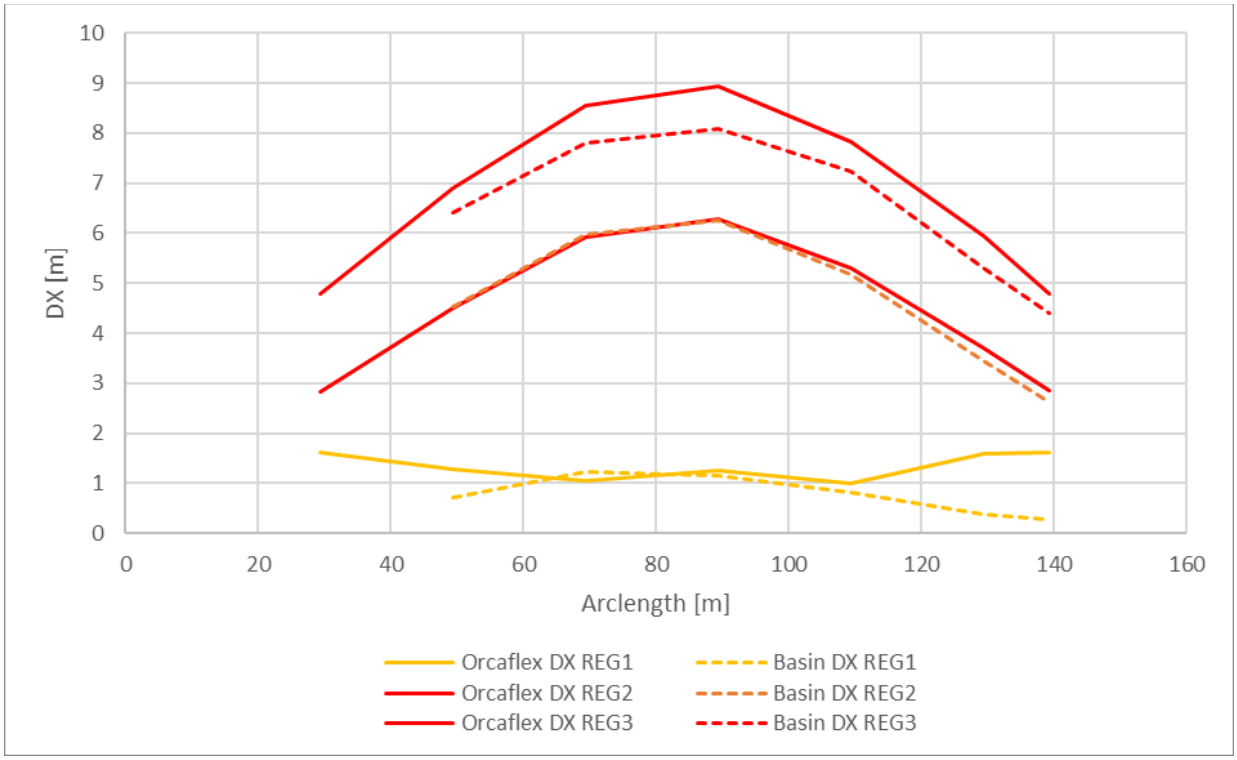

Figure 2-10: Extremum flexible pipe X-position (Configuration 1) for Pi = 10 bar, under 90° incident RE1, REG2, and REG3.

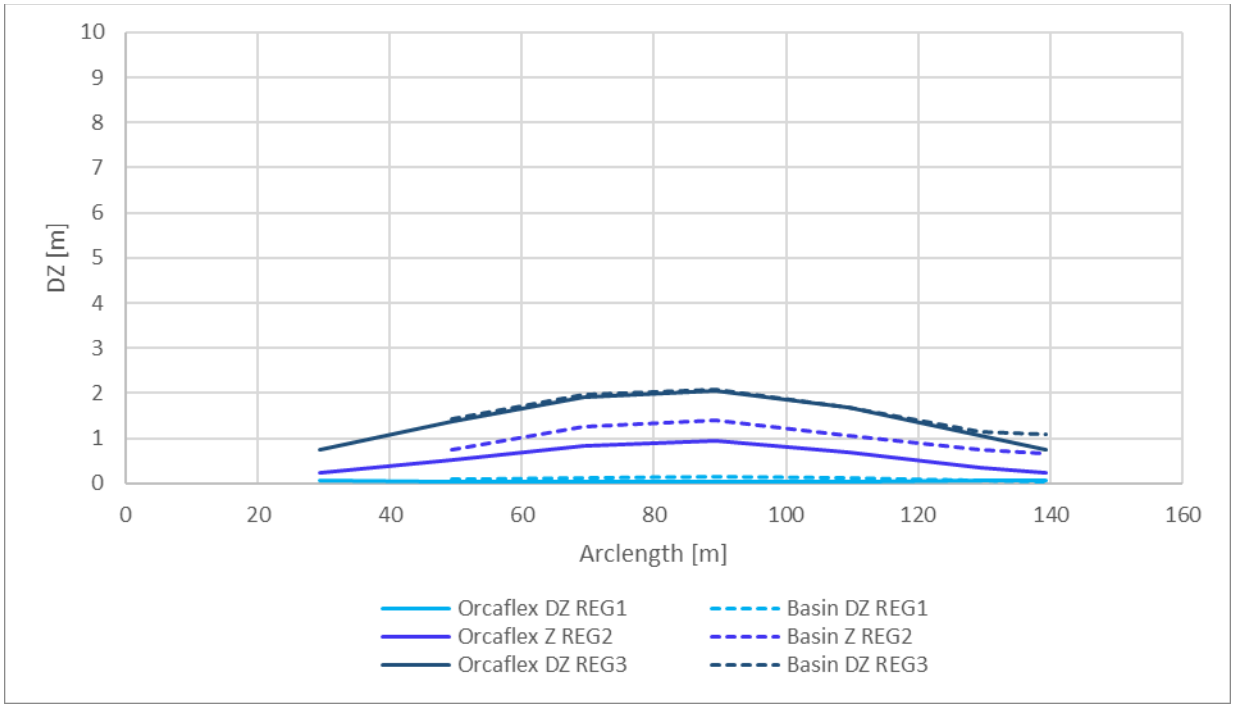

Figure 2-11: Extremum flexible pipe Z-position (Configuration 1) for Pi = 10 bar, under 90° incident RE1, REG2, and REG3.

- Being fixed at both ends, the flexible pipe adopts a circular arc shape in both the x- and the z-directions.
- The higher the regular wave height, the larger the offsets with respect to the initial position.

- The offsets in the x-direction are larger than in the z-direction, given that the flexible pipe system is constrained by anchor sling fixation points in the z-direction. For example, at REG3, the maximum x-offset reaches 9m at the pipe mid length, for only 2m in the z-direction.
- Globally, the numerical model offsets, depicted with a solid line, are well predicted with respect to the experimental data represented with a dashed line.
- The x-offsets under REG3 are however slightly overestimated by the numerical model.

To further test the predictability of the numerical model, a similar comparison between the experimental and numerical pipe maximum offsets is made in Figure 2-12 (x-direction) and Figure 2-13 (z-direction), taking the internal pressure as a variable. The flexible pipe offsets are plotted for a 90° incident REG2 for a Pi of 10bar, 25bar, and 40bar (**tests 9, 15, 16**). Additionally, the 1st mode in the x-direction for both the experimental setup (**test 75 and 77**) and the numerical reproduction are provided in Table 2-6, as the internal pressure has a direct impact on the flexible pipe bending stiffness and thus the natural mode. Table 2-6 also contains the axial end loads measured experimentally at the upstream balance and its numerical analog.

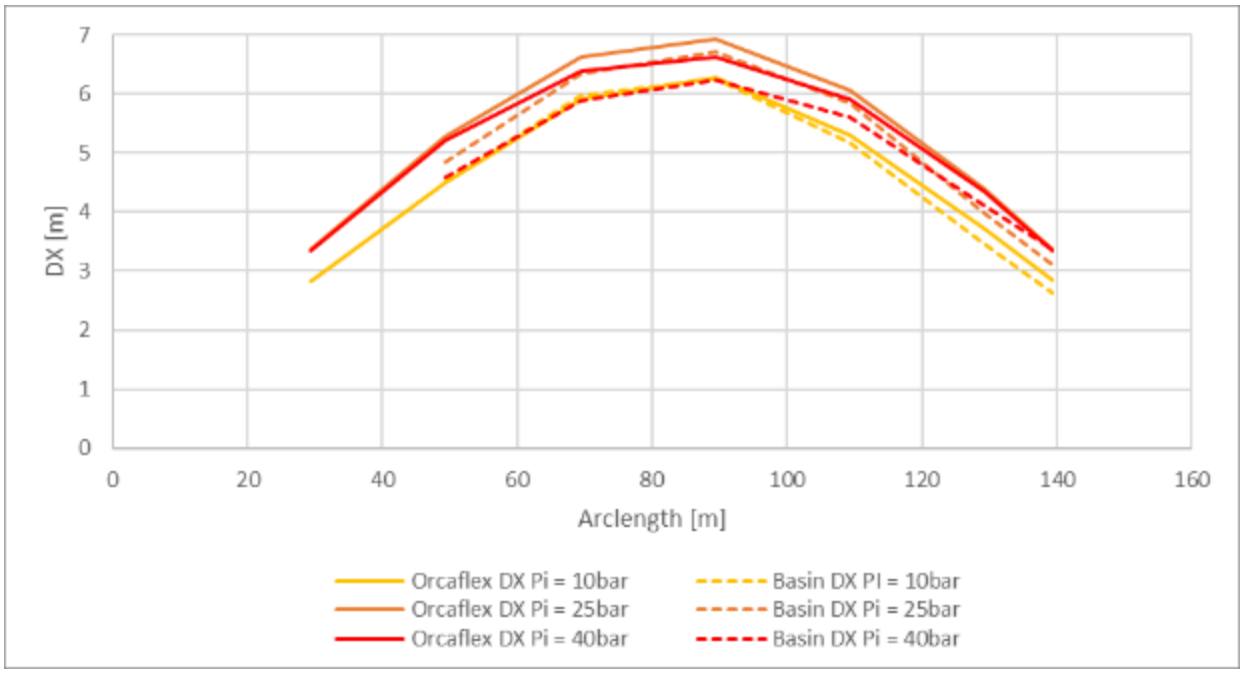

Figure 2-12: Extremum flexible pipe X-position (Configuration 1) under a 90° incident REG2, for Pi = 10bar, Pi = 25 bar, and Pi = 40bar.

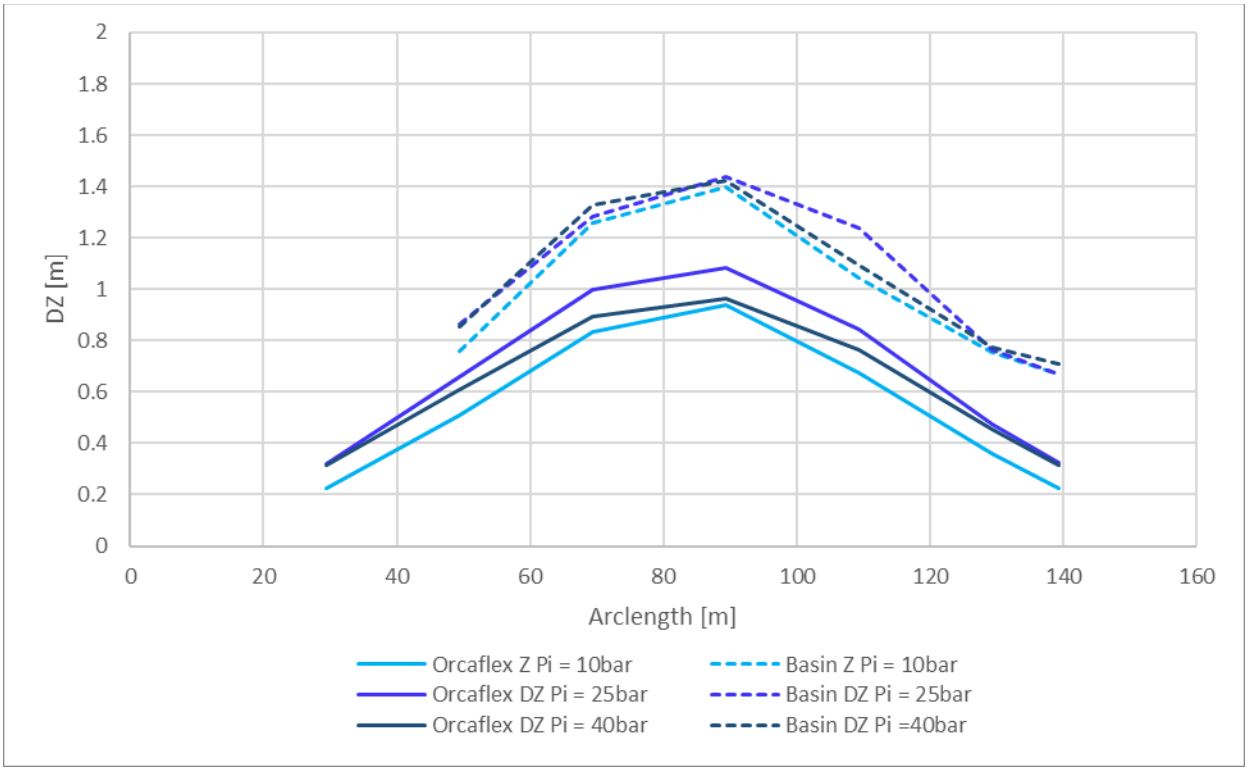

Figure 2-13: Extremum flexible pipe Z-position (Configuration 1) under a 90° incident REG2, for Pi = 10bar, Pi = 25 bar, and Pi = 40bar.

- Counter-intuitively, both the offsets in the x- and z-directions are larger for Pi = 25bar, rather than Pi = 10bar which is theoretically supposed to yield the larger offsets, given that the higher the Pi, the higher the bending stiffness; and that the flexible pipe retracts under pressure.
- However, the numerical model predicts the same tendency as the one observed in the basin: the x- and z-offsets are the largest for Pi = 25bar, then for Pi=40bar, and finally Pi=10bar has the lowest offsets for the same sea condition.
- While the x-offsets are slightly overestimated by the numerical model, the inverse is visible for the z-offsets.

	Basin Tn X	Orcaflex Tn X	Basin Fy_M5575	Orcaflex Fy_M5575 (end A)
	[s]	[s]	[kN]	[kN]
Pi = 10 bar	20	21	+79(2)	+79(1)
Pi = 25 bar	- *	16	+400(2)	+747(1)
Pi = 40 bar	15	13	+1300(2)	+1469(1)

Table 2-6: Flexible pipe natural modes in the x-direction according to both the basin tests and the Orcaflex numerical model.

Note *: No decay test was conducted at Pi = 25bar.

Note 1: The Orcaflex axial end loads are those obtained once the initial distance between the two pipe fixation points has been adjusted to obtain the reference value of +79kN (Figure 2-8). Given that for Pi = 10 bar, the static axial end load was measured to be -420kN, a correction factor of 500kN was defined to reach the +80kN reference value, for the higher Pi tests.

Note 2: The reported static experimental axial end loads are not the one which can be found in the provided Océanide data. The correction factor of 500kN has been added to the raw static end loads (Pi = 25bar → Fy_5575 = -100kN; and Pi = 40 bar → Fy_5575 = 800kN).

From Table 2-6, the following remarks can be made:

- The higher the internal pressure, the lower the natural period of the flexible pipe, which was to be expected given that the higher the Pi, the stiffer the flexible pipe.
- The numerical natural 1st modes in the x-direction, are slightly different from the experimental ones (2s difference at most).
- Despite the calibration step of the axial end loads, the numerical values still present an offset with the experimental values (maximum of 347kN for Pi = 25bar).
- The divergences between the experimental and numerical natural modes and axial end loads are most likely due to:
    - The approximative accuracy of the correction factor applied on the axial end loads data due to a lack of experimental checking on the end scales measuring drift, and its evolution in function of the internal pressure
    - A decreasing mean internal pressure, especially for Pi = 40 bar (Figure 2-14)

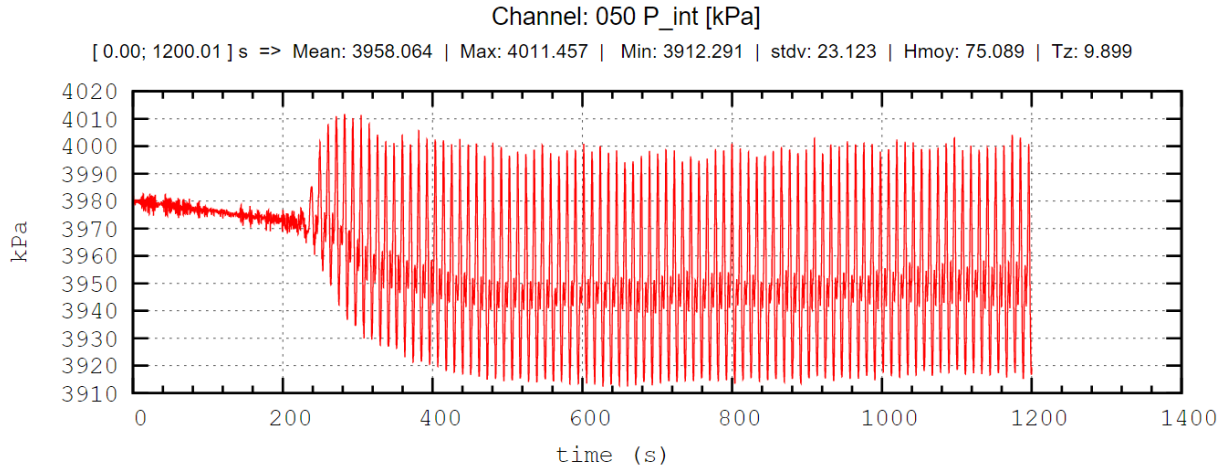

Figure 2-14: Time evolution of the internal pressure for test 16 specified at Pi = 40 bar.

2.4.2. Pipe Motions

A more detailed study of the pipe motion is provided in this section. The time evolution of the flexible pipe motions in both the x- and z-directions, are presented hereafter at two different locations along the pipe length:

- At Q3 which is located approximatively at the pipe mid length
- At Q7 which is located at the right pipe extremity

Sketch 2-2 locates each measuring devices used during this first campaign for the Configuration 1 of the flexible pipe system under 90° sea conditions. Both the qualysis targets (Q#) for the motion targets, and the tensiometers are reported (T#). A close-up sketch is additionally provided in Sketch 2-3.

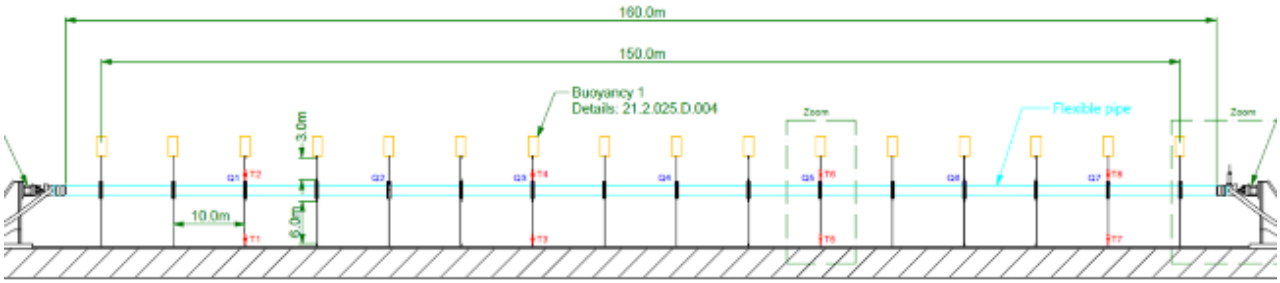

Sketch 2-2: Measuring device locations on the flexible pipe system: Q – Qualysis target for pipe motion, and T – Tensiometers for sling tension.

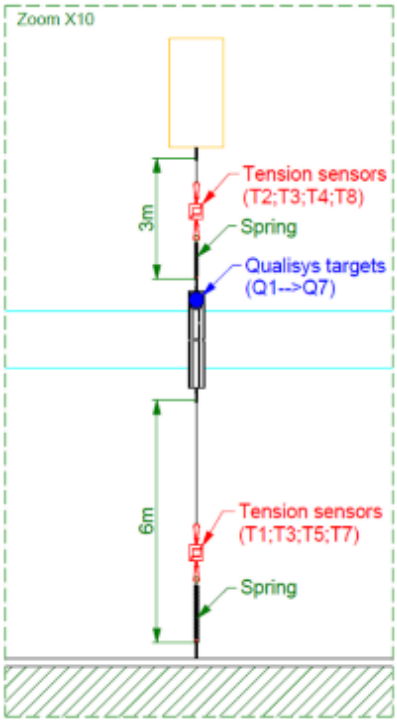

Sketch 2-3: Detailed measuring device locations.

- Motion time signal under different regular waves
  - X: REG1, REG2, REG3 for Q3 & Q7
  - Z: REG1, REG2, REG3 for Q3 & Q7

Figure 2-15 depicts the time evolution of the pipe motions in the x-direction at Q3 (pipe mid length) and Figure 2-16 at Q7 (close to the right/downstream pipe extremity).

Figure 2-17 depicts the time evolution of the pipe motions in the z-direction at Q3 (pipe mid length) and Figure 2-18 at Q7 (close to the right/downstream pipe extremity).

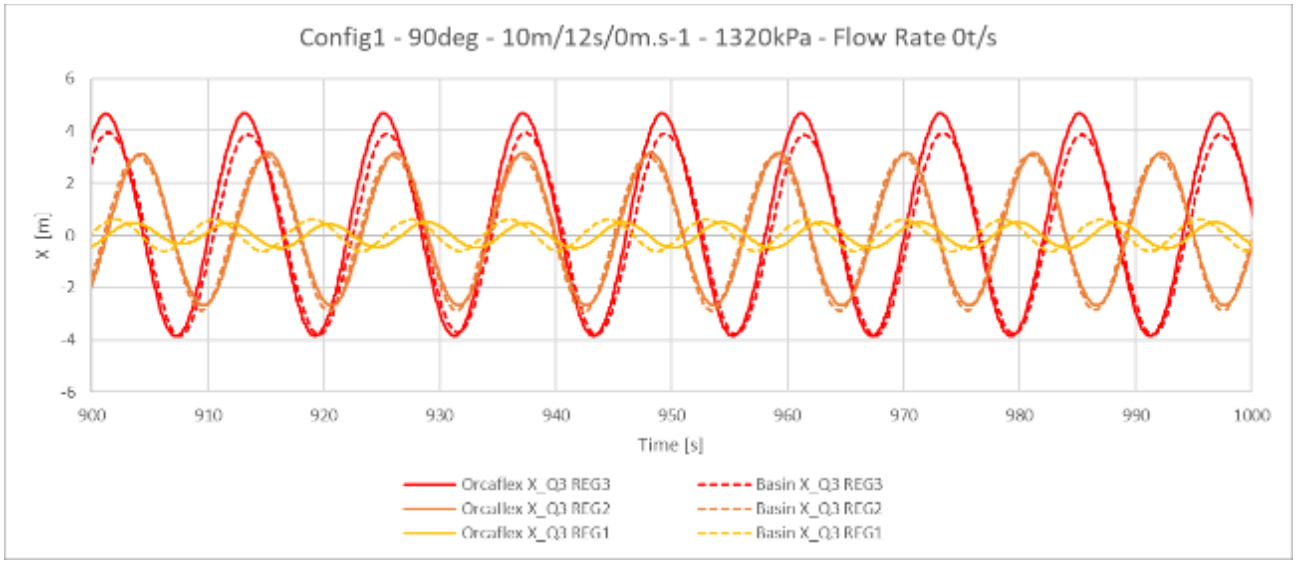

Figure 2-15: Time evolution of the flexible pipe motion in the x-direction at Q3 (approximatively at pipe mid length) for Pi = 10bar, under REG1, REG2, and REG3.

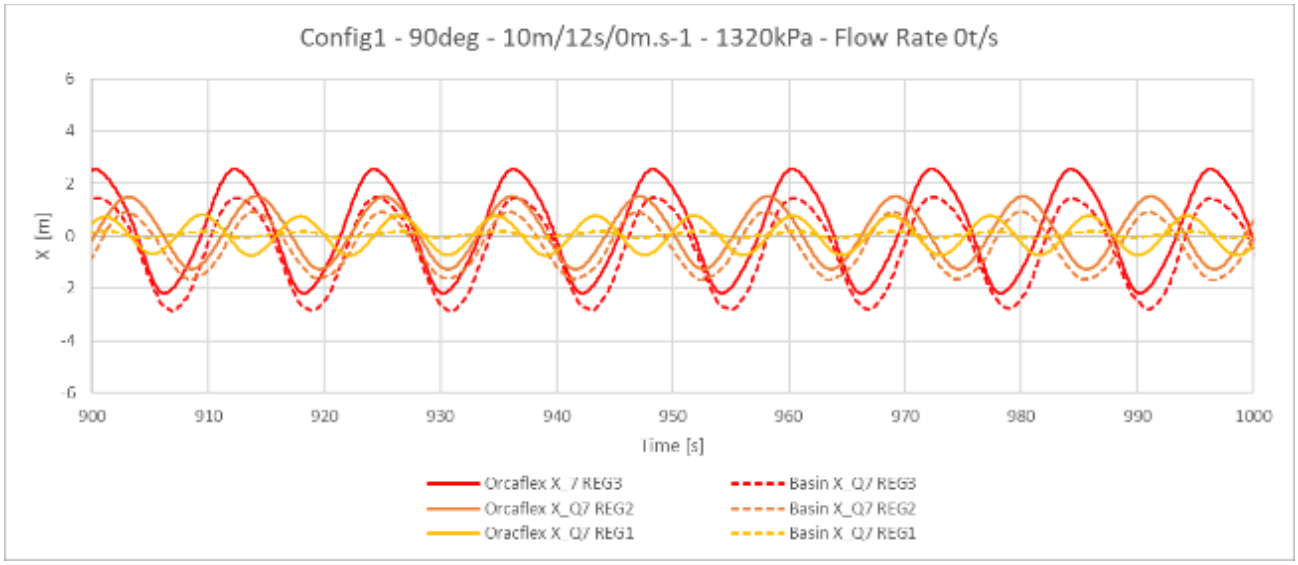

Figure 2-16: Time evolution of the flexible pipe motion in the x-direction at Q7 (approximatively at pipe right extremity) for Pi = 10bar, under REG1, REG2, and REG3.

- The flexible pipe x-motion time signals follow the sinusoidal shape of the sea water elevation induced by the regular waves.
- Again, the higher the regular wave height, the larger the motion amplitude.
- Being closer to the pipe end fixation point, Q7 registered lower x-motion amplitudes than Q3.
- The numerical model yields very similar pipe motions in the x-direction, to the experimental results. A slight overestimation is however visible, especially at the pipe extremity (Q7).

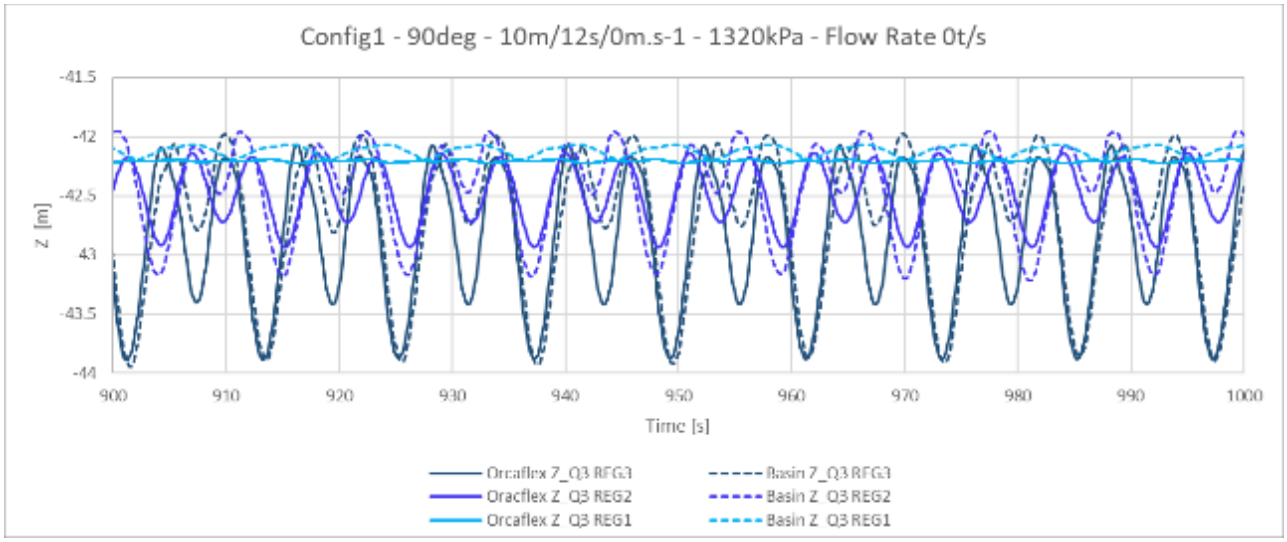

Figure 2-17: Time evolution of the flexible pipe motion in the z-direction at Q3 (approximatively at pipe mid length) for Pi = 10bar, under REG1, REG2, and REG3.

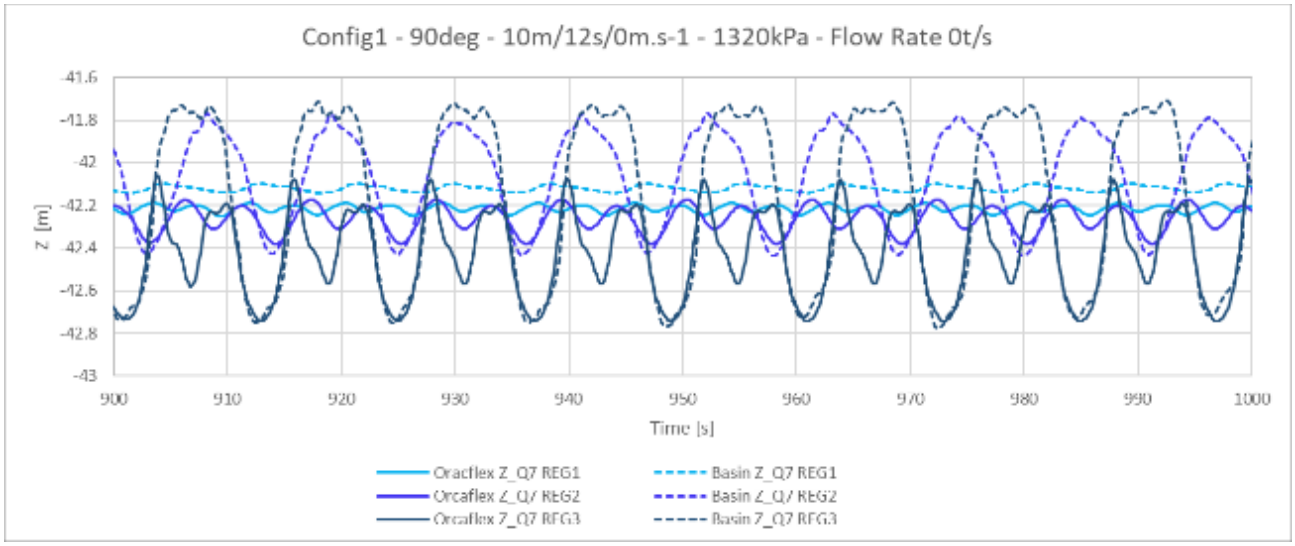

Figure 2-18: Time evolution of the flexible pipe motion in the z-direction at Q7 (approximatively at pipe right extremity) for Pi = 10bar, under REG1, REG2, and REG3.

- Again, the motion amplitudes recorded at Q7 are smaller than at Q3.
- At Q3, starting REG2, the z-motion time signals are double-peaked and not sinusoidal anymore.
- At Q7, however this double-peak pattern is only visible at REG3, and it less pronounced.
- The numerical model pipe z-motions tend to display a more pronounced double-peaked pattern than the experimental signals.

2.4.3. Sling Tension

The sling tensions are assessed in this section. The experimental tension signals are compared to their numerical analog, namely in terms of static values, amplitude, and signal pattern. First the anchor sling tensions are studied in Section 2.4.3.1 (with T1, T3, T5, and T7), and then the buoyancy sling tensions in Section 0 (with T2, T4, T6, and T8). As a reminder, Sketch 2-2 and Sketch 2-3 locates the measuring devices on the flexible pipe system.

2.4.3.1. Anchor Sling

Figure 2-19 illustrates the time evolution of the anchor sling tensions measured at the four tensiometers locations, approximately evenly spread along the flexible pipe system length; subjected to a 90° incident current of 0.8m/s.

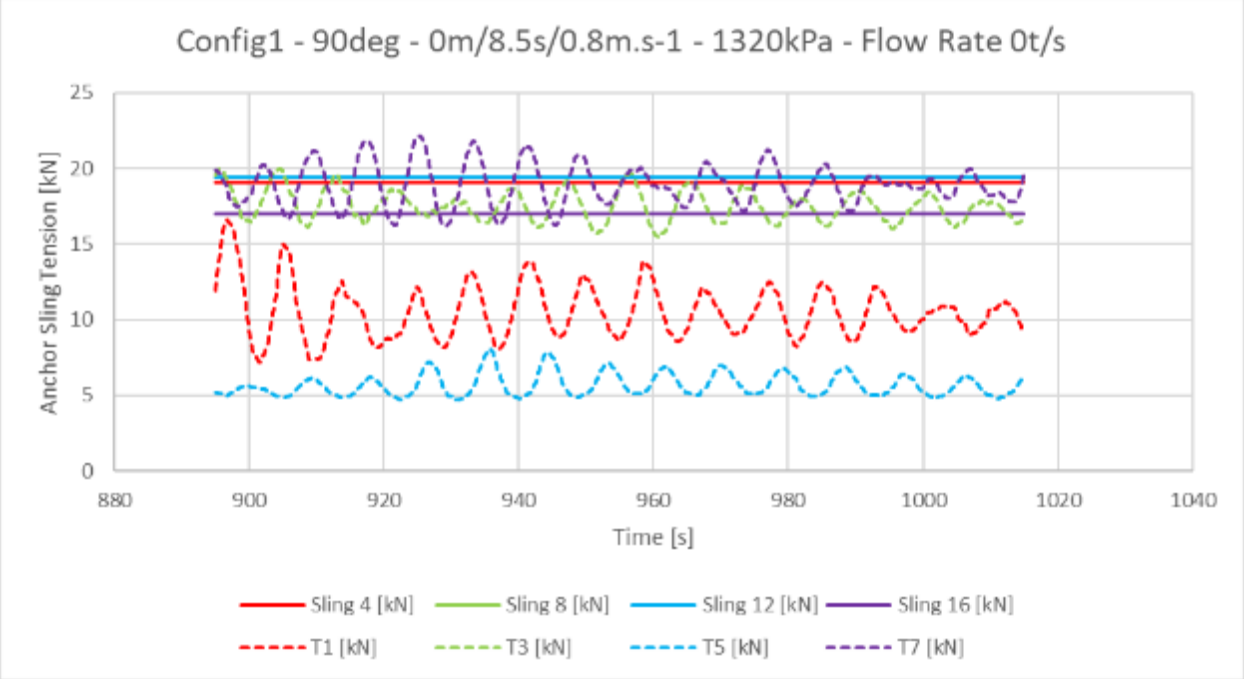

Figure 2-19: Time evolution of the anchor sling tensions along the flexible pipe system, under a 90° incident current of 0.8 m/s.

- The experimental tension signals are oscillating due to the VIV, while the numerical tensions signals are completely constant, given that the VIV were not implemented in the numerical model.
- The experimental AS tensions do not share the same static value:
  - T1 → 10kN, T3 → 17kN, T5 → 6kN and T7 → 19kN.
  - This is a visual proof of the hyperstatic sate of the flexible pipe system (introduced in Section 2.1.2.2.3).
  - Note that during the experimental campaign, some AS were adjusted in length to attempt to compensate the uneven AS tension repartition.
- The numerical AS tensions are all equal to the theoretical design tension of approximately 19kN, to the exception of T7 which recorded a slightly lower tension (17kN) which is most probably due to the implementation of the weighting pipe ends in the numerical model.

To assess the predictive ability of the numerical model to identify and reproduce slack events in the AS, a specific study on T3 (defined as the most prone location to slack events) is conducted by comparing the AS tension signals for the three 90° incident regular waves (Figure 2-20).

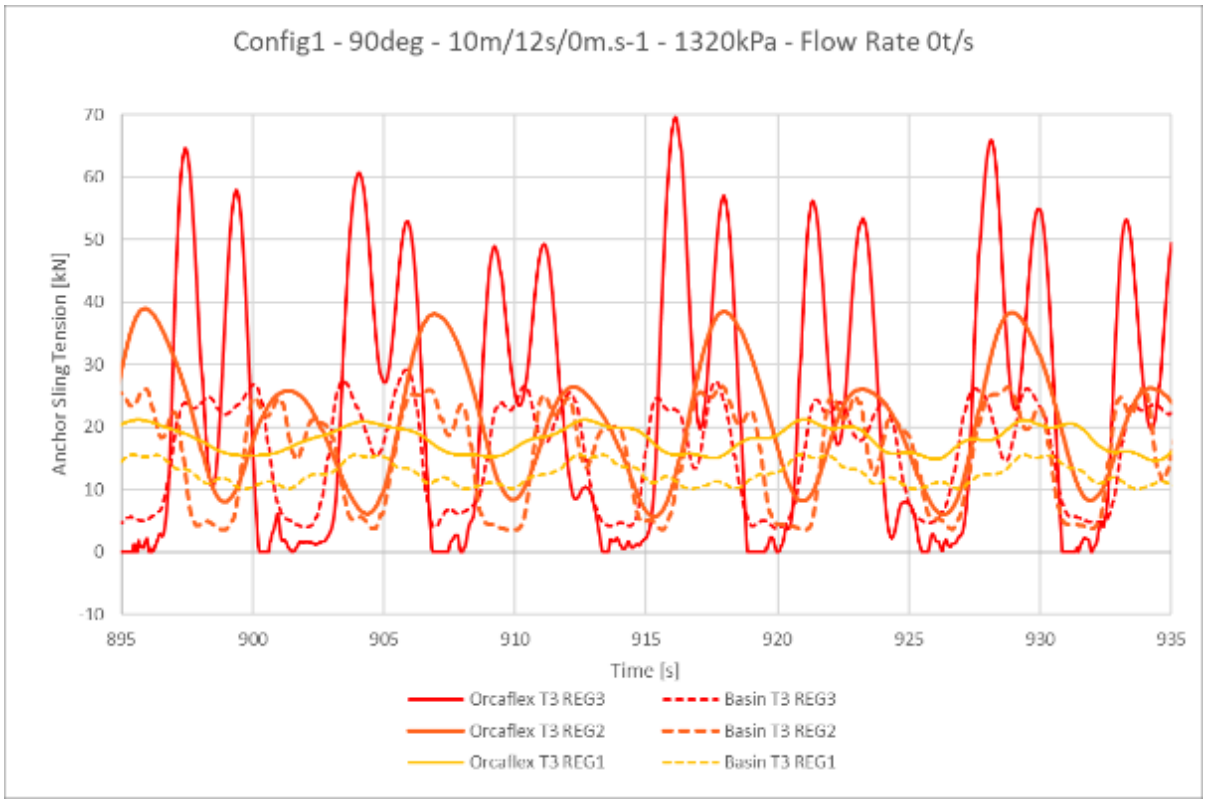

Figure 2-20: Time evolution of the anchor sling tension T3 (approximately at pipe mid length), under 90° incident REG1, REG2, and REG3.

- Slack events occur at REG2 and REG3 and are identified by the numerical model, which is visible through the very low tension intervals immediately followed by a high tension peak.
- The amplitudes of the experimental AS tension signals are estimated as follows:
  - REG1: 2.5kN
  - REG2: 10kN
  - REG3: 12.5kN
- Globally, the experimental signal patterns are well reproduced by the numerical model. However, the following remarks are made:
  - The experimental signals contain additional high frequency components which are not visible and the smooth numerical AS tension signals.
  - For REG2 and REG3, the AS tensions are overestimated by the numerical model. This trend is especially observed for REG3, during the high tension peak phase of the slack events. As an example, the maximum recorded AS experimental tension during this plotted time interval almost reaches 30kN, while its numerical analog goes as high as 70kN.

2.4.3.2. *Buoyancy Sling*

The BS tension time signals are compared at T4 which is approximately at the flexible pipe mid length, for the three 90° incident regular waves in Figure 2-21.

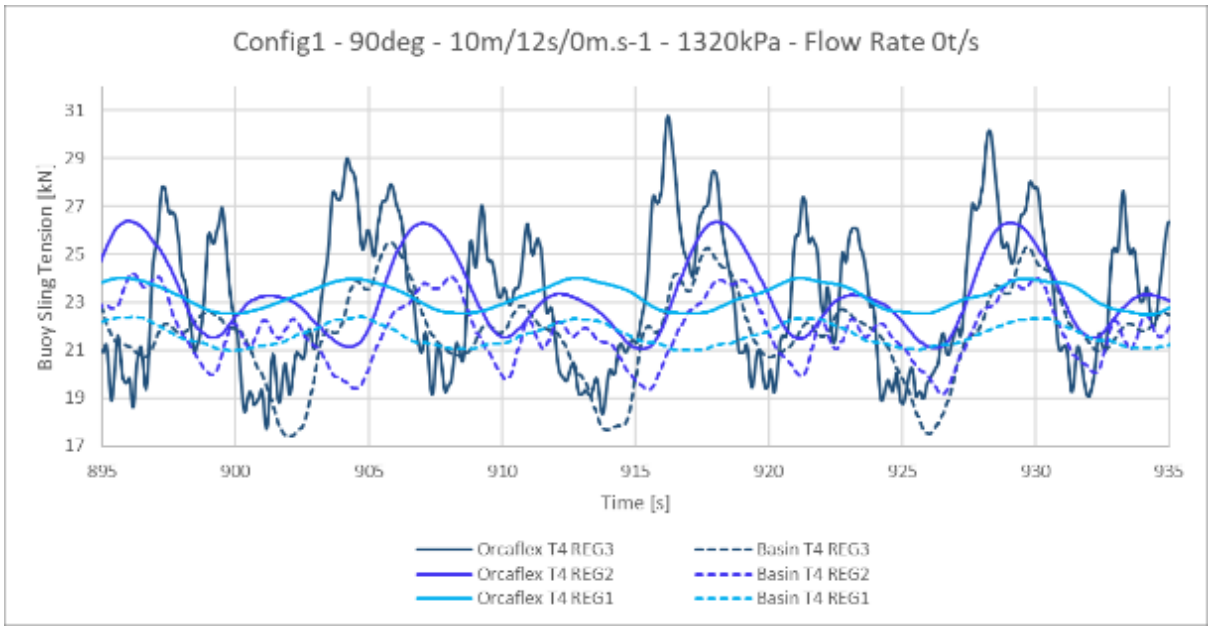

Figure 2-21: Time evolution of the buoyancy sling tension T4 (approximately at pipe mid length), under 90° incident REG1, REG2, and REG3.

- Globally the BS tension signal pattern is well reproduced by the numerical model. Additionally, both in terms in amplitude and static value.
- The amplitude of the BS tension signals (4kN for REG3) are smaller than the AS tension amplitudes.
- Regarding the specific signal shape of the BS tension signals, it can be said that:
  - At REG1, both the experimental and numerical BS tension signal are sinusoidal.
  - At REG2, the signal is double-peaked over one period, but the experimental signal contains some faint additional high frequency components, which are not visible on the numerical BS tension signal.
  - At REG3, the signal is also double-peaked. The numerical signal now also contains additional high components. The signal tension maxima are however slightly overestimated.

2.4.4. Experimental Observations of the Remaining Configurations

The purpose of this last section is to provide a succinct summary of the global behavior of the remaining flexible pipe system configurations. Ref. 3. Section 3.4. provides an extensive description while this document briefly lists the main difference noted to the nominal configuration.

Thus, the configurations which were not addressed in the previous comparative studies to the numerical model results, are introduced in this section, but solely based on the experimental data, given that the calibration of the numerical models for these configurations could not be done due to time restraints. These experimental observations could be used as calibration checking points, should the numerical model be further developed.

The varying parameters of the different flexible pipe configurations are presented in Table 2-2, and recalled hereafter:

- Configuration 3 - 20m spacing with cylindrical buoys of nominal volume
- Configuration 4 - 20m spacing with cylindrical buoys of doubled volume
- Configuration 5 – ring shaped buoys of nominal volume
- Configuration 6 - one pipe end let free

2.4.4.1. Configuration 3

Configuration 3 has two times less buoys than Configuration 1. The flexible pipe system should consequently be less stable when excited since less buoys are supporting it. Additionally, the tension in the system has thus less distribution options, given that the fixation points are also divided by two.

When considering Configuration 3 subjected to REG3 (**test 23**), it is readily observable that the anchor sling tensions are more than twice as high, than those registered for Configuration 1 (Figure 2-22). The tension peaks can reach up to 250kN. The general loss in buoyancy of Configuration 3 seems to make it more vulnerable to slack events.

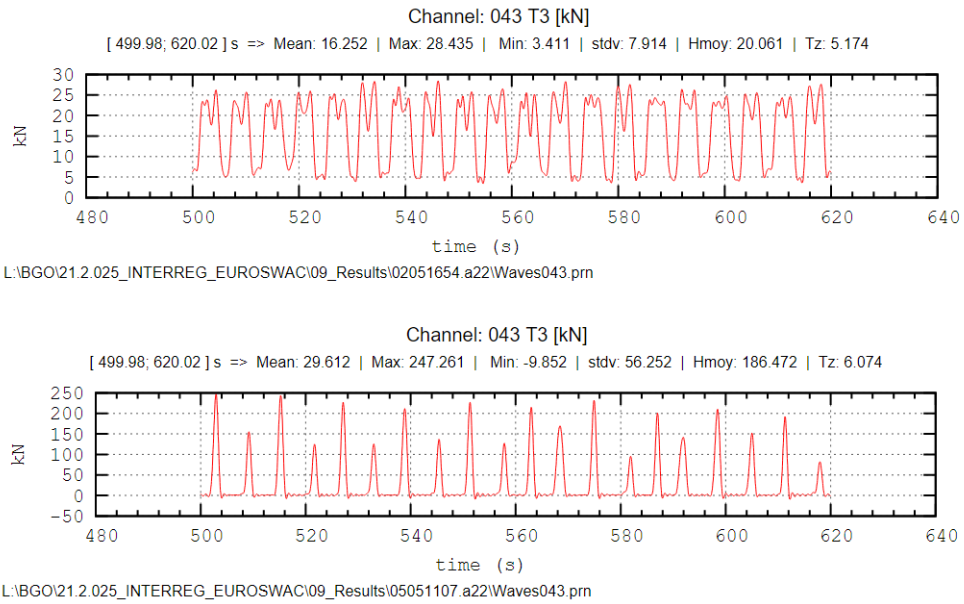

Figure 2-22: Time evolution of the anchor sling tension at T3 under a 90° incident REG3 for (top) Configuration 1 and (bottom) Configuration 3.

2.4.4.2. Configuration 4

Configuration 4 was also designed with a 20m spacing between each buoy, but with two time more buoyant floaters. As a result, the tensions measured at the tensiometers are supposed to be multiplied by two.

REG1 was considered to ensure slack free recording. The comparison between Configuration 1 and Configuration 4, respectively **tests 8 and 25**, reveals indeed an overall tension which is approximatively two times greater for Configuration 4. This observation holds for both the buoyancy and anchor sling tensions (Figure 2-23). Consequently, the impact on the flexible pipe motions is such that the x-displacements have lower amplitudes.

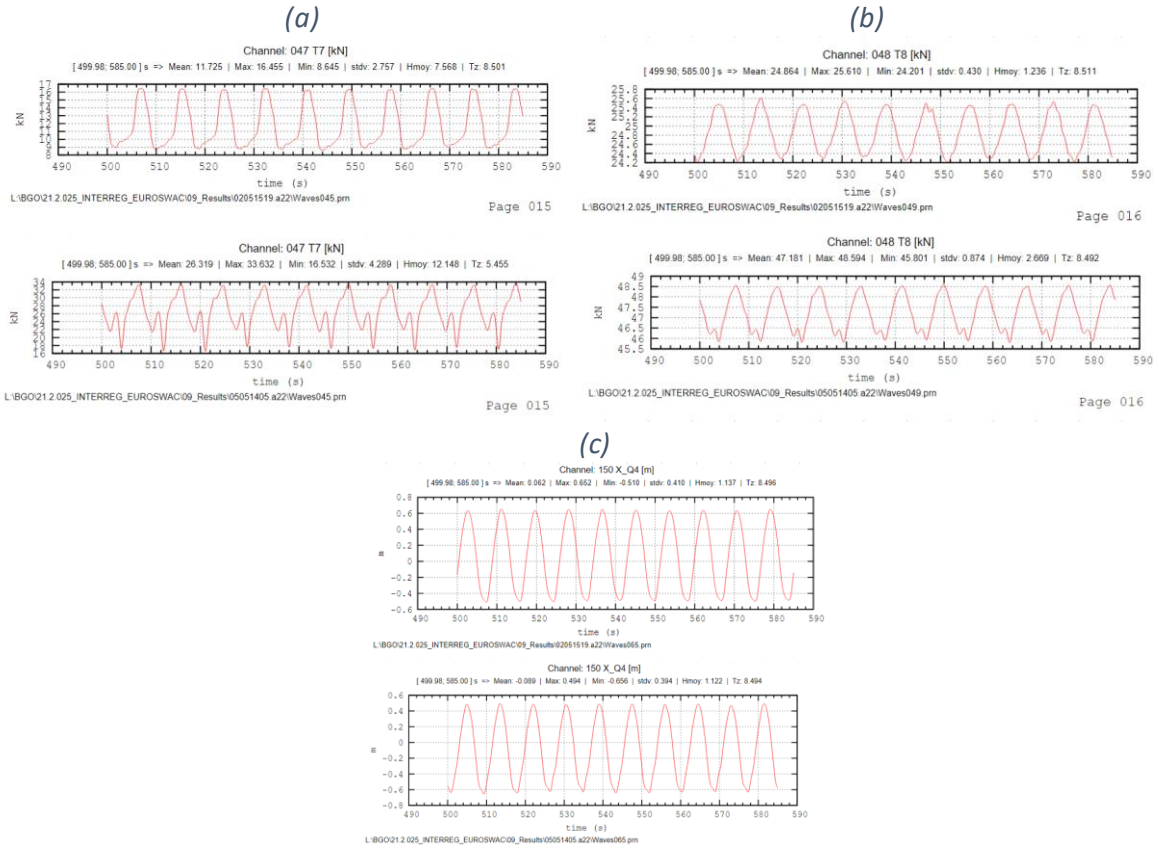

Figure 2-23: Time signal of (a) the anchor sling tension at T7, (b) the buoyancy sling tension at T8, and (c) the flexible pipe motion at Q4, under a 90° incident REG1.

2.4.4.3. Configuration 5

The experimental data of Configuration 5 comprised of the ring-shaped buoys demonstrated an even more hyperstatic state of the flexible pipe system. The anchor sling signals at REG1 showed a more pronounced uneven repartition of the tension. The comparison of REG3 demonstrated that Configuration 5 is more prone to slack events, and to high tension peaks.

2.4.4.4. Configuration 6

Finally, the comparison of Configuration 6 with the nominal configuration confirmed the anticipated results: the motion at the freed pipe end was greater since it was free to move. Additionally, the pipe end load at the pipe end still fixed, is subjected to a lesser axial end load. It was also noted that when exposed to high waves like REG3, the system is generating higher anchor sling tension peaks.

2.5. 1st Campaign Conclusions

The first campaign main objectives were to provide data to both conduct a hydrodynamic study of the flexible pipe system and to enable the calibration of the associated Orcaflex numerical model within its limitations. The project research statement status will first be addressed in Section 2.5.1, and an opening towards the 2nd experimental campaign of the EUROSWAC project is made in Section 2.5.2.

2.5.1. 1st Campaign Key Points

- A nominal flexible pipe system configuration with both its extremities fixed and supported by floating modules distributed with a 10m spacing was defined. In this designed system, the buoys are linked to the flexible pipe with buoyancy slings, themselves mounted on a collar-shaped connecting device arranged around the pipe. The flexible pipe is then fixed to the ground through anchor slings, also connected to the collar.
- Five other configurations of this nominal flexible pipe system were also defined by varying some design parameters, such as the buoys volume, shape, or spacing, or the anchor sling axial stiffness.

- During the experimental campaign, conducted at Océanide in the BGO FIRST, the following observations were made:

    - The selected flexible pipe made of woven polyurethane, was characterized to retract under pressure.
    - The flexible pipe system exhibits hyperstaticity, which is visible through the uneven and unpredictable repartition of the AS tension in the basin.
    - The flexible pipe axial end loads are very sensible to the distance between the fixation points of the pipe ends.
    - At configuration 6 (one free pipe end), the initial deformation at the pipe end is clearly visible.
    - the free space between the internal clamping device cross sectional area and the pipe, created sling inclinations, and in turn pipe misalignment and thus additional constraints which were not accounted for in the numerical model

- The experimental setup was then reproduced numerically on the Orcaflex software, the closest possible to the reality and calibrated according to 4 specific topics:
    - Flexible pipe axial stiffness varying in function of the internal pressure
    - Flexible pipe bending stiffness varying in function of the internal pressure
    - Flexible pipe axial end forces obtained through a calibrated pipe fixation points distance
    - Anchor sling tension at Configuration 2 (high AS EA)

- The nominal Configuration for the 90° incident regular waves and current tests, were then reproduced with the calibrated numerical model, to conduct a comparative study between the experimental data recorded by Océanide and the numerical results obtained with the Orcaflex model.

- Overall, the general pattern of x- and z-motion time signals of the flexible pipe were well predicted by the numerical model. Under the action of the regular waves, the x-motions were sinusoidal and the z-motion double-peaked. The x-motions amplitudes were larger than the z-motion amplitudes.
- The tension signals were also well captured by the numerical model. The model was even able to identify the slack events, when occurring in the basin. The high tension peaks of slack events were however slightly overestimated by the numerical model. The buoyancy sling tension were lower than the anchor sling tension, as expected, given that less buoyant elements are placed above the buoyancy sling than the anchor slings.

- Rather than software limitations, the calibration of the flexible pipe system numerical model was mainly limited by the hyperstaticity of the system.

- A general conclusion about the capacity of the Orcaflex software to model a flexible pipe system such the one for the EuroSWAC project would be that the higher the effort of precision in the input data, the closer the numerical results will be to the experimental ones. The reported divergencies between the numerical results and the experimental data are mainly due to the level of preciseness of the input data in the numerical software.

2.5.2. Towards the 2nd campaign

- The 2nd campaign will be introducing 3 different anchoring systems consisting of clump weights and/or a chain which serves the double objectives of getting closer to a more realistic anchoring system and of absorbing the flexible pipe irregularities due to the fixed anchoring points (hyperstaticity)

- With the same double objective as cited previously, the new flexible pipe system will be designed with a free end equipped with a strainer (to get rid of tension related uncertainties and get closer to the real design)

- The new flexible pipe design will also include a new sling-to-pipe connection mechanism to avoid the free space between the pipe and the clamping device and the slanting position of the clamping devices impacting on the slings' inclination.

- Improve flexible pipe characterization methodology: test for the axial stiffness underwater with the pipe filled with water AND for smaller tensions (under 800kN, where the linear evolution was hypothesized during the 1st campaign) for the same internal pressures.

3.Second Campaign

3.1. Flexible Pipe System Design

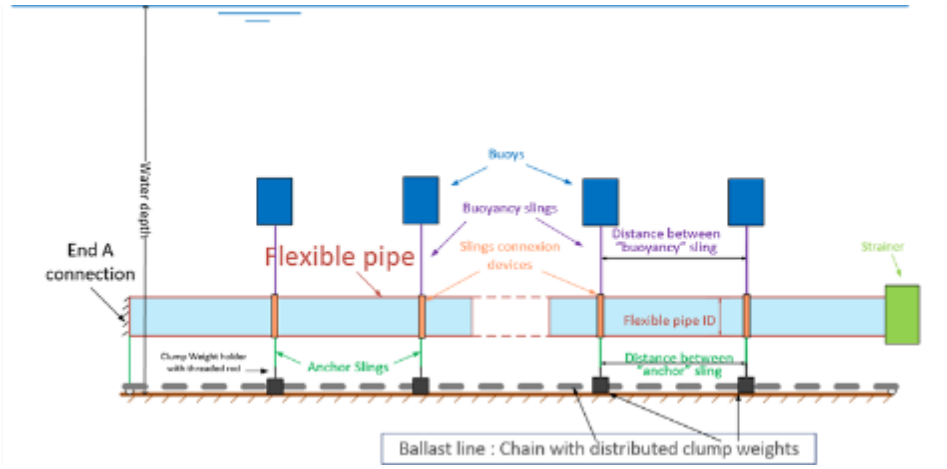

Figure 3-1: Side view of the flexible pipe concept tested during the 2nd experimental campaign.

As detailed in Ref. 6, the 2nd campaign aims for a more realistic flexible pipe system design. The main changes, when compared to the 1st campaign prototype, are reminded as follows:

- One of the pipe extremities is let free and a strainer is mounted on this same pipe end (filtering needed at the entrance of the admission pipe)
- Three different anchoring systems of the same linear wet mass are considered :
  - Clump Weights at each anchor sling end (*Configuration 1*)
  - A chain (*Configuration 2*)
  - A combination of both (*Configuration 3*)
- Addition of rigid CW holders, designed as a circular flat base on which a threaded rod is fixed to allow a modular stacking of weights (Picture 3-1).
- New clamping device in soft webbing to suppress the free space between the pipe and the interior wall of the clamping device (which allowed a slanting position of the previous clamping devices, and in turn, slanting sling) (Picture 3-2).

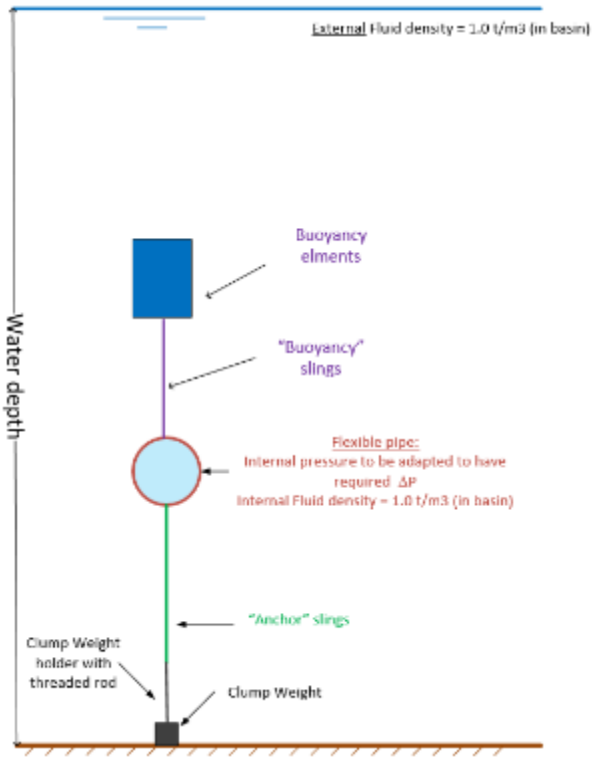

Figure 3-2: Transversal view of flexible pipe system.

Picture 3-1: Rigid clump weight holders.

(a)

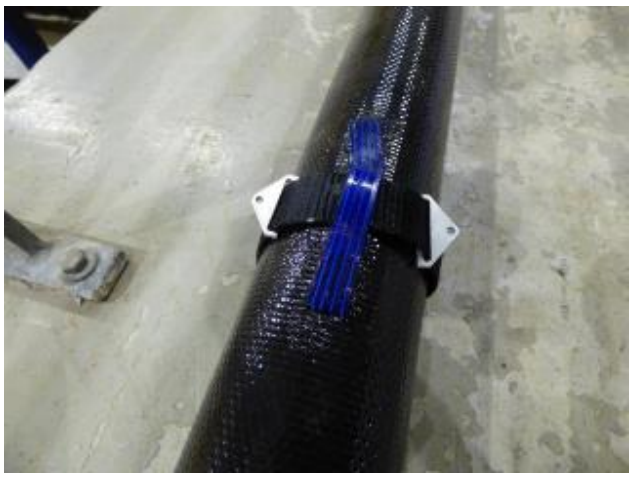

(b)

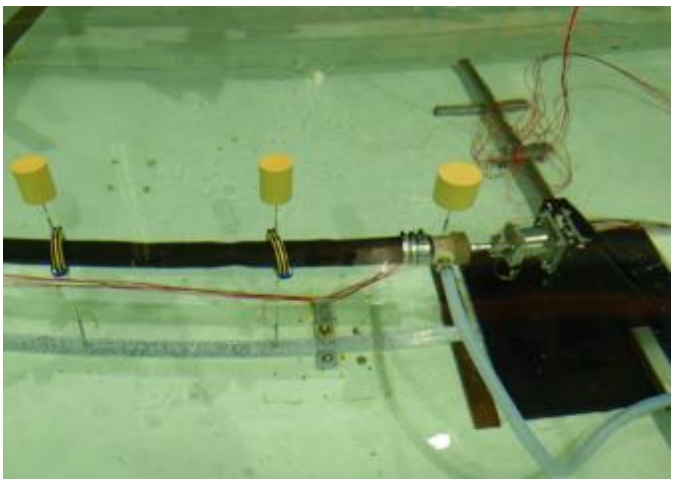

Picture 3-2: (a) Second campaign soft webbing clamping device preventing slanting position and (b) previous solid clamping device used during the 1st campaign with visible oblique position of the clamping device on the second sling axis from the left.

Note that this new design also permits to get rid of the issues associated to the hyperstatism of the flexible pipe system of the 1st campaign. In fact, during the first campaign, the following issues were noted:

1- The two pipe extremities were rigidly fixed, leading to uncontrolled pipe axial tension variation with internal pressure. Besides, the axial load measurement has not worked properly, leading to pipe axial tension uncertainties.

2- The anchor slings were fixed on the basin floor, leading to uncontrolled vertical load repartition, mainly due to pipe permanent deformation (shape memory).

3.2. Numerical Model Implementation

This section contains all the input data and information needed to reproduce the Orcaflex numerical model established for this second campaign. Most results will be further detailed in the Section 3.3, dedicated to the calibration of the associated numerical model.

3.2.1. Flexible Pipe, End Connections & Strainer

	Length	OD	ID	Mass per unit (air)	Mass (water)	EI	EA
-	[m]	[m]	[m]	[t/m]	[kg]	[kN.m2]	[KN]
TechFlex PU Extra 1404mm	160	1.404	1.3	0.257	7862.8	Note 1	Note 1
End A	4.392	1.037	0	1.837	4363	8.58E+07	9.07E07
End B	2.4	1.199	0	1.861	-3041(3)	8.58E+07	9.07E07
Strainer	5.008	2.9	0	5.2		8.58E+07	9.07E07

Table 3-1: Orcaflex input data concerning the flexible pipe "TechFlex PU extra", both end connections, and the strainer.

Note 1: This result depends on the internal pressure specified. Section 3.3.1 & 3.3.2 respectively describe the evolution of the axial and bending stiffnesses as function of the internal pressure.

Note 2: For the sake of simplicity, it was chosen to only implement the correct masses (in air and water) in the numerical model, when the object to model had a complex shape.

Note 3: Since End B and the strainer were embedded together, and that the experimental mass in water was verified by combining both elements by Océanide, the mass in water is provided for both elements combined.

The normal drag and added mass coefficients were derived from both the detailed study conducted during the 1st campaign and reported in Section 2.2.2; and detailed in Ref. 3. Section 2.1.2.2. Given that the numerical model outer diameters of the strainer and of both pipe ends were revised in accordance with the wet mass and not the actual outer diameters, the following coefficients were adjusted accordingly.

	Normal Drag Coefficients	Normal Added Mass Coefficients
-	[-]	[-]
TechFlex PU Extra 1404mm	1.2	1
Strainer	1.2	0.645
End A	1.6	1.83
End B	1.4	1.37

Table 3-2: Hydrodynamic coefficients used in the numerical model of the 2nd campaign flexible pipe system.

3.2.2. Buoyancy Modules

The 1st campaign flexible pipe design recycled the buoyancy modules of "Buoyancy type 2" of the 1st campaign (Section 2.1.1). Similarly, the buoy used to cancel out the wet mass of the end connection remained unchanged. Note that the end connections were interchanged due to the pressure sensor location perturbating the mounting of the strainer at the free end. Thus, the end buoys were interchanged as well: in the 2nd campaign, the previously end A was used as end B, and inversely.

3.2.3. Slings

In the same way of the 1st campaign, an additional length covering the pipe radius and the height of the connection device between the soft webbing and the sling (0.707+0.3); was added to the numerical sling experimental length (Figure 3-3). This is done to avoid the inclusion of torsion to the model but still respect the height of each component in the flexible pipe system. Again, the OD were calculated to respect the provided wet masses. No differentiations were made for the slings which included a tensiometer during the 2nd campaign.

Note that for this campaign CW holder of a height of 3.6m were used to facilitate the CW change between each Configuration and to allow the CW displacement measurement with the Qualisys tracking system. This object is included as a connection offset between the slings and the CW. This explains the shorter AS length, when compared to the first campaign (Figure 3-3).

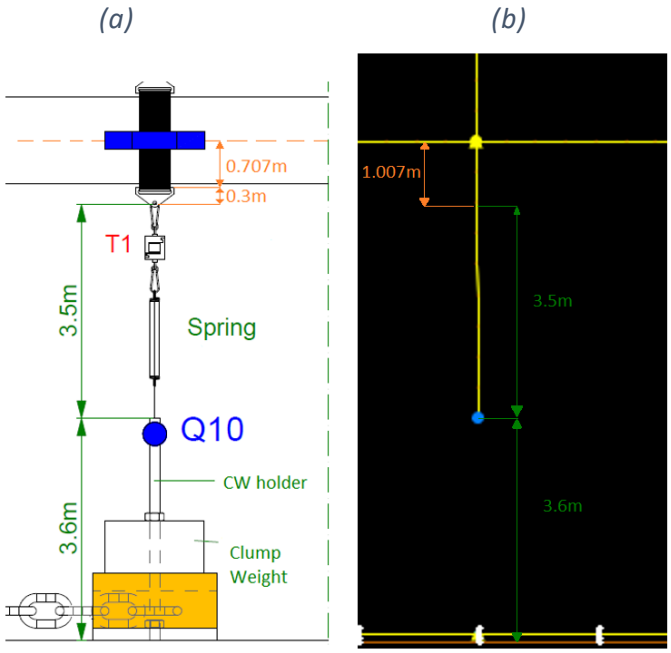

Figure 3-3: (a) Sling experimental setup (with Tensiometer T1 and Qualysis target Q10) and (b) Sling numerical modeling of the experimental setup.

	Length	OD	Mass	Wet mass	Mass per unit	EA	EI
-	[m]	[m]	[kg]	[kg]	[t/m]	[kN.m2]	[KN]
Real AS	3.5	0.123	93.3	81.4	0.0267	1148	0
Numerical AS	4.5	0.123	93.3	81.4	0.0207	1478	0
Real BS	3	0.0896	49.3	43	0.0164	2040	0
Numerical BS	4	0.0896	49.3	43	0.0123	2725	0

Table 3-3: Orcaflex sling input data.

	Normal Drag Coefficients	Normal Added Mass Coefficients
-	[-]	[-]
Real AS	1.2	1
Numerical AS	1.2	1
Real BS	1.2	1
Numerical BS	1.2	1

Table 3-4: Orcaflex hydrodynamic coefficients for the slings.

3.2.4. Anchoring Configurations

The CWs were modelled as 3D Buoys Orcaflex objects. The objective is to model only the CW translations since the CW rotations are not measured in the basin (only one motion target is put on the CW).

Similarly to the previous components, the volume of the CWs and the diameters of the chains were adjusted to fit the provided mass in water.

		Mass	Mass per unit	Volume	OD	Seabed Friction (1)	
		[t]	[t/m]	[m3]	[m]	Axial [-]	Lateral [-]
Config. 1	CW 1-7	10.828	-	1.388	-	0.57	0.57
	CW 8	18.353	-	2.353	-	0.44	0.44
Config. 2	Chain		0.542	-	0.306	0.48	0.38
	CW 8	12.939	-	1.659	-	0.44	0.44
Config. 3	Chain	-	0.3126	-	0.2274	0.49	0.44
	CW 1-7	4.588	-	0.588	-	0.57	0.57
	CW 8	15.233	-	1.953	-	0.44	0.44

Table 3-5: Orcaflex main input data for the components of the three different anchoring configurations.

Note 1: The friction coefficients values are detailed in Section 3.3.3, dedicated to their calibration.

The drag coefficients for the chain were obtained from the Orcaflex line wizard. The added mass and drag coefficients for the CWs were roughly estimated from Ref.10. No further calibration was conducted on these values because it is not of interest in this study.

3.3. Numerical Model Calibration Axes

This section provides a description of the identified topics to be refined in the numerical model. This refining process is mainly divided in 3 calibration axes for this 2nd campaign:

- Axial stiffness calibration with a new experimental characterization procedure (immerged)
- Bending stiffness calibration with a new experimental characterization procedure (immerged)
- Friction coefficients of the different anchoring components

3.3.1. Axial Stiffness

The axial stiffness of the selected flexible pipe is pressure dependent. Orcaflex allows to model a non-linear axial stiffness with a strain/Wall tension curve only. For each internal pipe pressure, a strain/wall tension curve (Figure 3-4) is thus defined in the calibrated model.

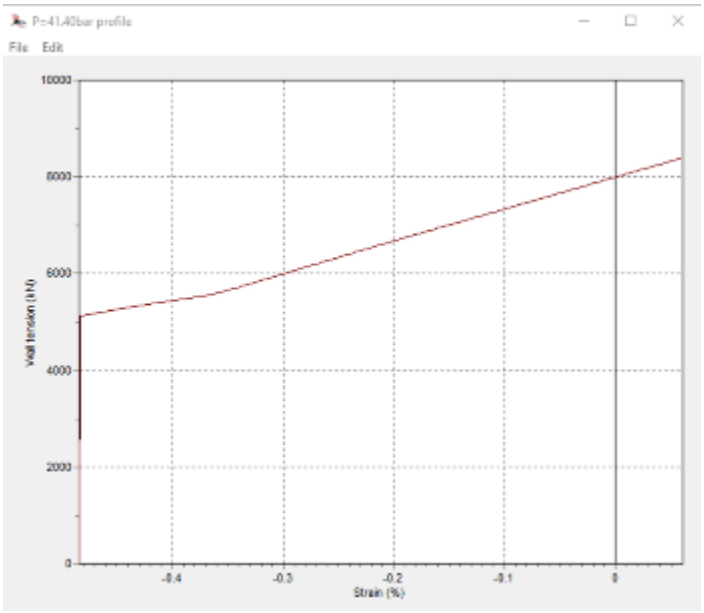

Figure 3-4: Strain/wall tension customized characterization curve used as an input Orcaflex data for the specification of the axial stiffness of test 72 with Pi= 41.40bar.

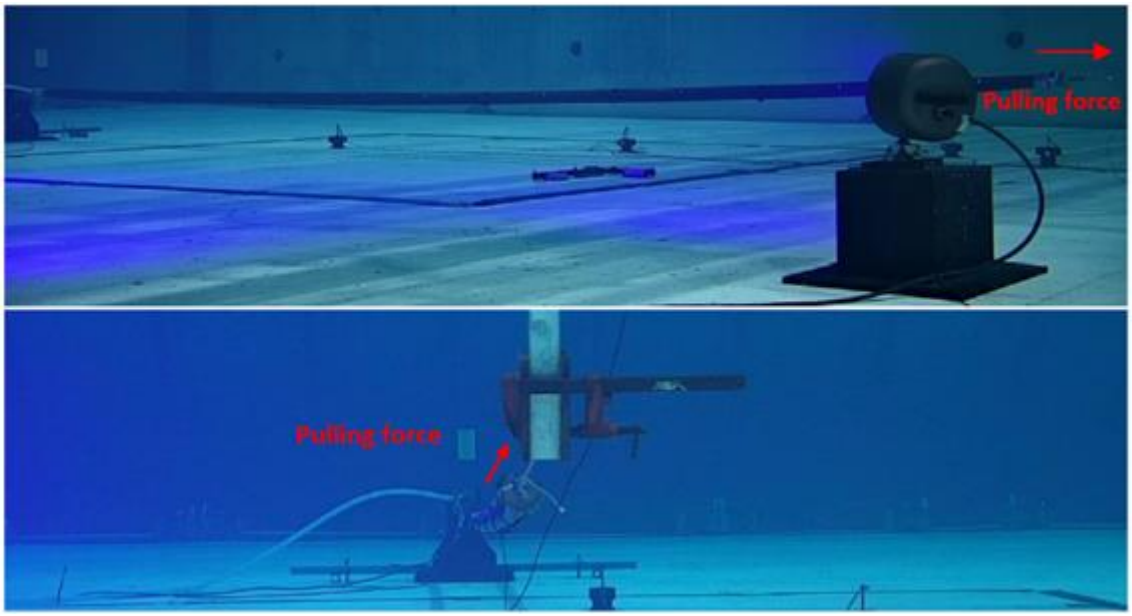

Picture 3-3: Experimental setup of test 116 (Pi = 4.2 bar and pulling force = 110kN) with the pulley traction system (a) transversal view, and (b) longitudinal view.

The tests 116-119 investigate the flexible pipe axial stiffness under the effect of internal pressure. To do so, the flexible pipe was placed underwater and fixed at one end and was then horizontally connected to a winch through an additional sling and subjected to an increasing tension and internal pressure (Picture 3-3). Note that the tension range that was assumed to be associated with a linear EA behavior during the first campaign (axial tension under 800kN were not tested for in Figure 2-4), is covered during these immerged tests (approx. 200kN -1200kN: Figure 3-5).

To assess whether the preliminary EA calibration conducted in the air medium during the first campaign is valid, a comparison of the elevation profiles obtained during these tests and a numerical reproduction was made. However, the elevation profiles did not overlap, especially for pulling forces below 800kN. The tendency is showing that the flexible pipe in the model is too stiff, especially for low tensions (higher Z values obtained from the model).

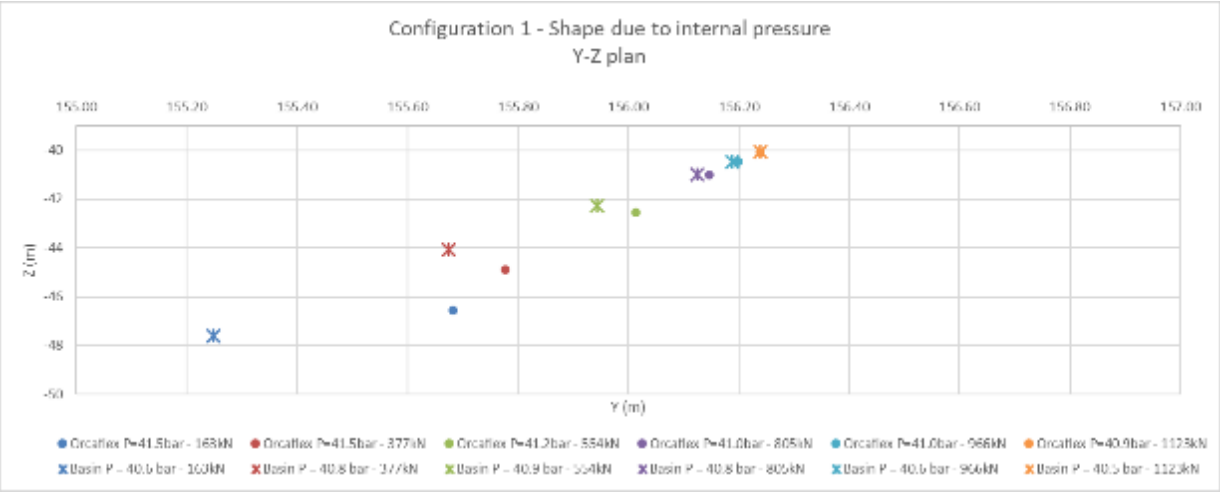

Figure 3-5: Flexible pipe elevation measured with Q3 obtained with the pipe EA calibration of the 1st campaign. Q3 is the Qualysis target located the closest to end B (at pipe arc length = 159.392m). Note that the flexible pipe is positioned along the y-axis, and that the Z-direction refers to the vertical axis.

It was hypothesized that this divergence was not only due to the EA linear hypothesis for pulling forces below 800kN, but also linked to the fact that the catenary shape dictated by gravity was also at play in the elevation profile, especially for the low traction forces, and low Pi (Picture 3-3). For each internal pressure, the low nonlinear axial tension curve is thus adjusted iteratively, to fit with the elevation profiles obtained in the basin. This calibration provides the nonlinear axial stiffness curve for each pressure (Figure 3-8) where initial pipe length L0(Pi) is obtained from **test 1** (Picture 3-4). Test 1 recorded the evolution of the axial tension at the fixed pipe ends with a discontinuously increasing Pi.

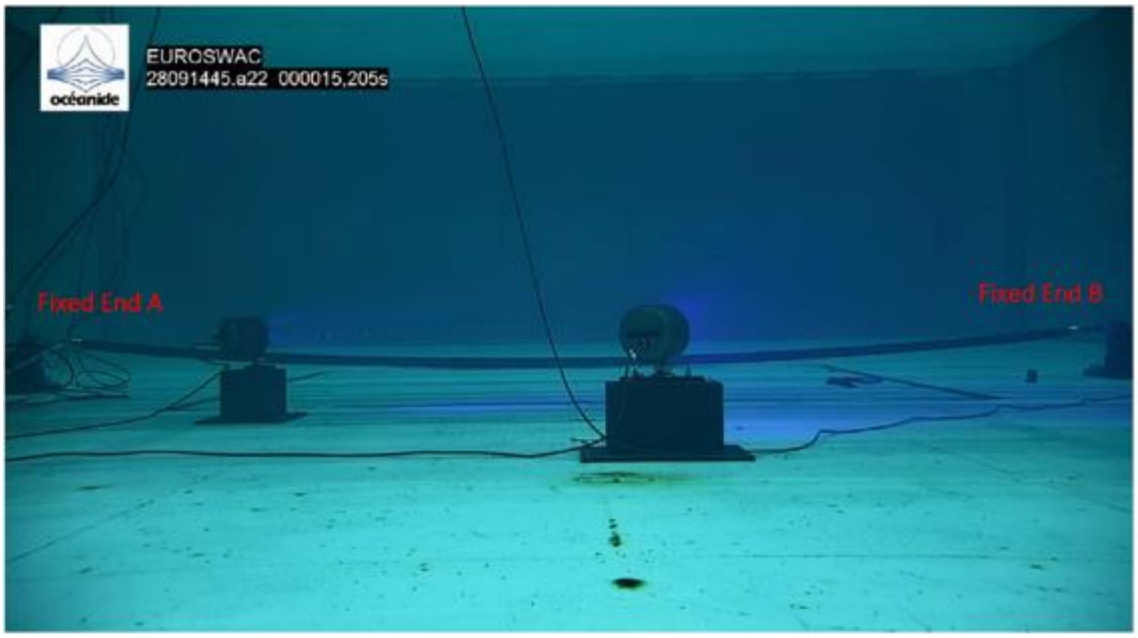

Picture 3-4: Test 1 – Axial tension characterization for Pi = 4.24bar and tension = 310.7kN.

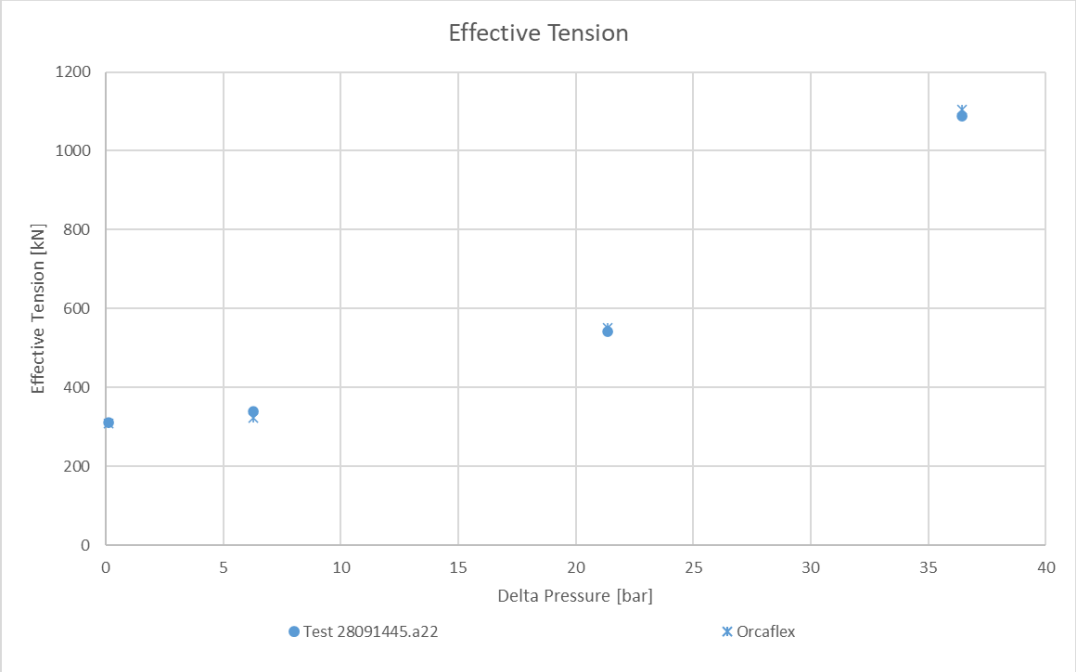

Figure 3-6: Calibrated evolution of the flexible pipe effective tension for the axial tension characterization (test 1), in function of the internal pressure.

The final calibrated results showing overlapping elevation profiles for **test 1** are presented in Figure 3-7.

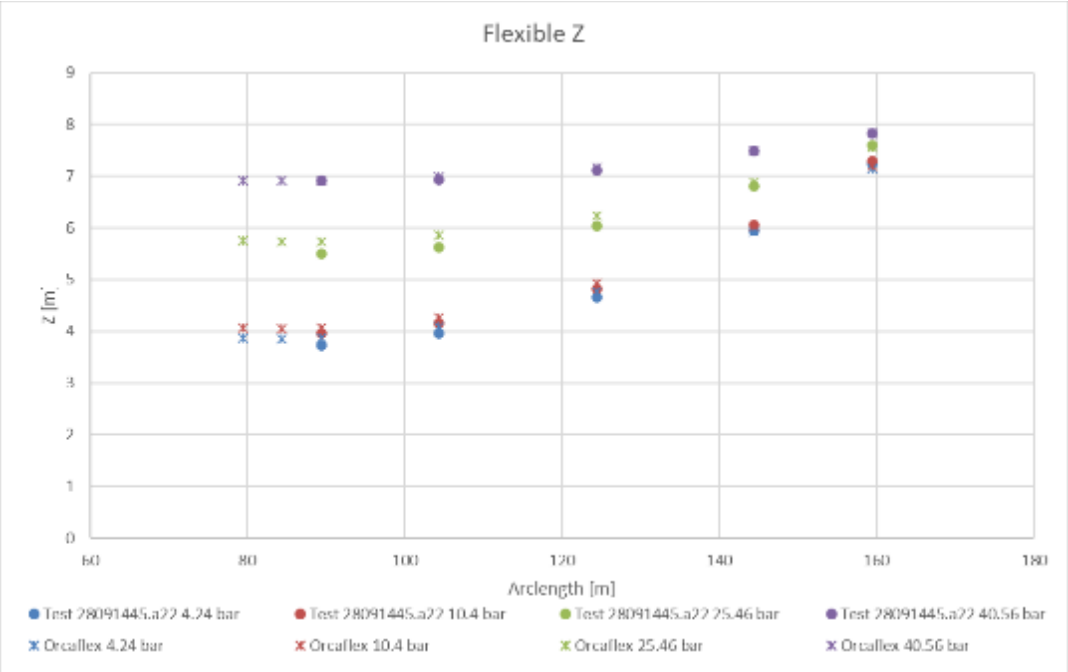

Figure 3-7: Calibrated evolution of the flexible pipe elevation profile for the axial tension characterization test (test 1), in function of the internal pressure.

The mass per unit length of the flexible pipe was modified to get the Z elevation profile for the two lower Pi (4bar and 10bar) on point with the experimental data. In fact, when using the provided pipe mass per unit length, only the elevation profiles for the 25bar and 40bar were superimposed with the experimental data. Given that the tests the lower Pi are more sensitive to the inertia forces, than the high Pi that rigidify the flexible pipe, the mass per unit length was changed from 0.270 t/m to 0.257 t/m (reduction of 4.81%). This assumption was considered given the fact that the flexible pipe mass in the air is well defined, but it is not precisely the case of the mass in the water, taking into account that the pipe thickness is measured to be equal to 2.6mm at basin scale, the tolerance of this measured value makes this 4.81% mass change acceptable.

The following EA curves are the final curves obtained after the calibration axes mentionned above. They were used to build a MathCad sheet enabling an estimation of the EA curve in function of the Pi, through linear interpolation. The first Tw was specified to 0kN, to avoid excessive retraction because Orcaflex interpolates linearly outside the specified range.

(a)

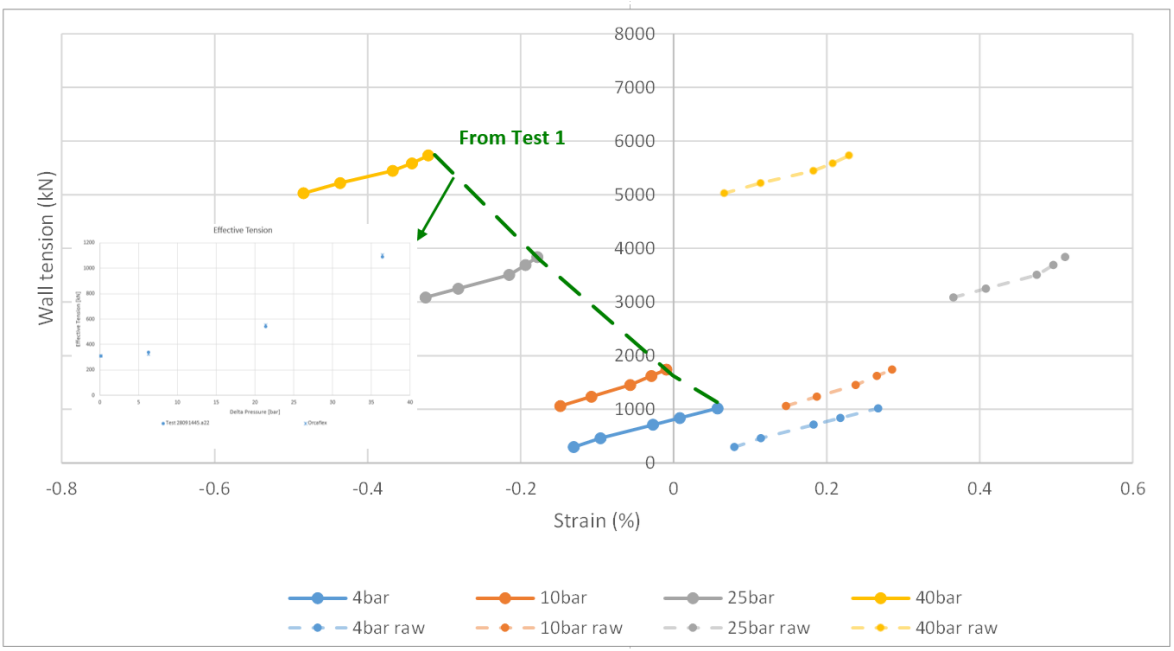

(b)

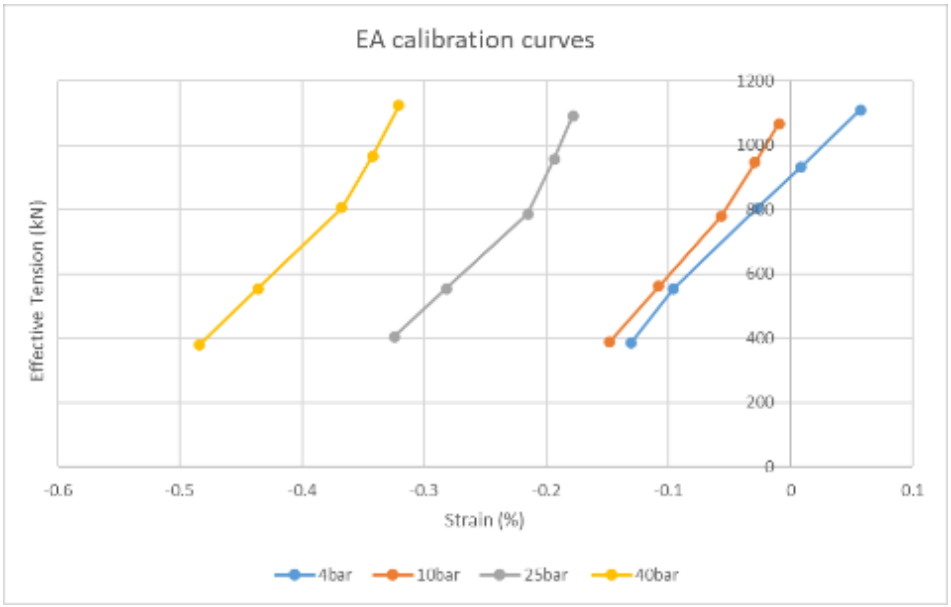

Figure 3-8: *Calibrated EA curves obtained from the 2nd campaign calibration* expressed through (a) wall tension in function of the strain (%) *, and (b)* effective tension in function of the strain (%) .

To further investigate the validity of the obtained EA curves, **test 1B** was reproduced numerically and the elevation profiles of the flexible pipe were compared. Test 1B is the same as test 1, to the exception that a buoy was added at the flexible pipe mid length, to test for lower axial tensions (Picture 3-5).

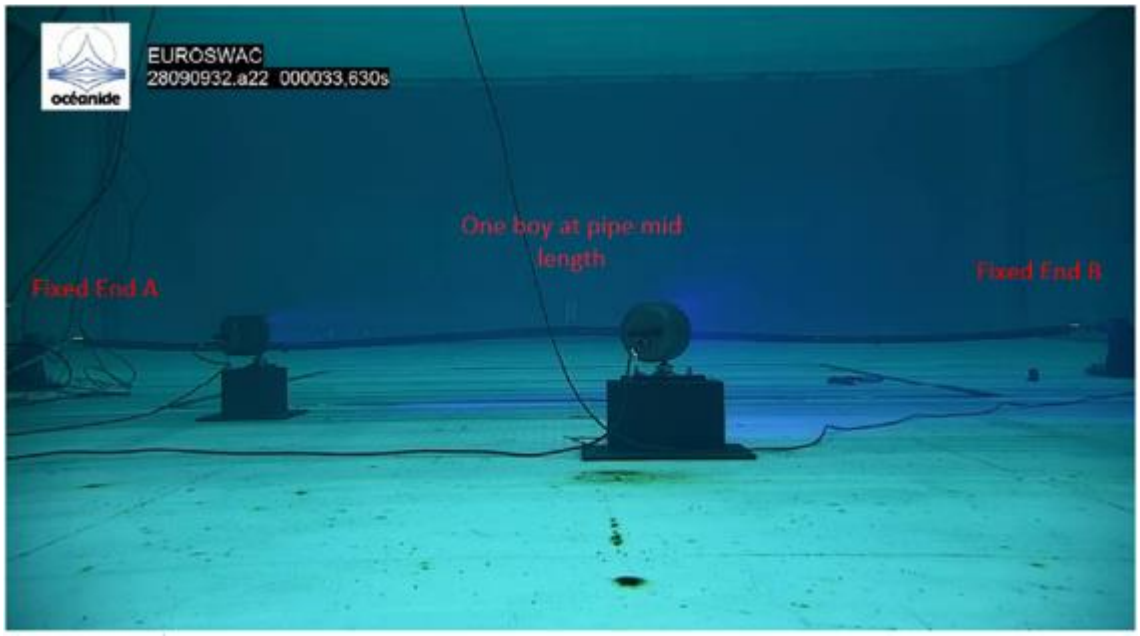

Picture 3-5: Test 1B – Axial tension characterization for Pi = 4.23bar and tension = 103.2kN.

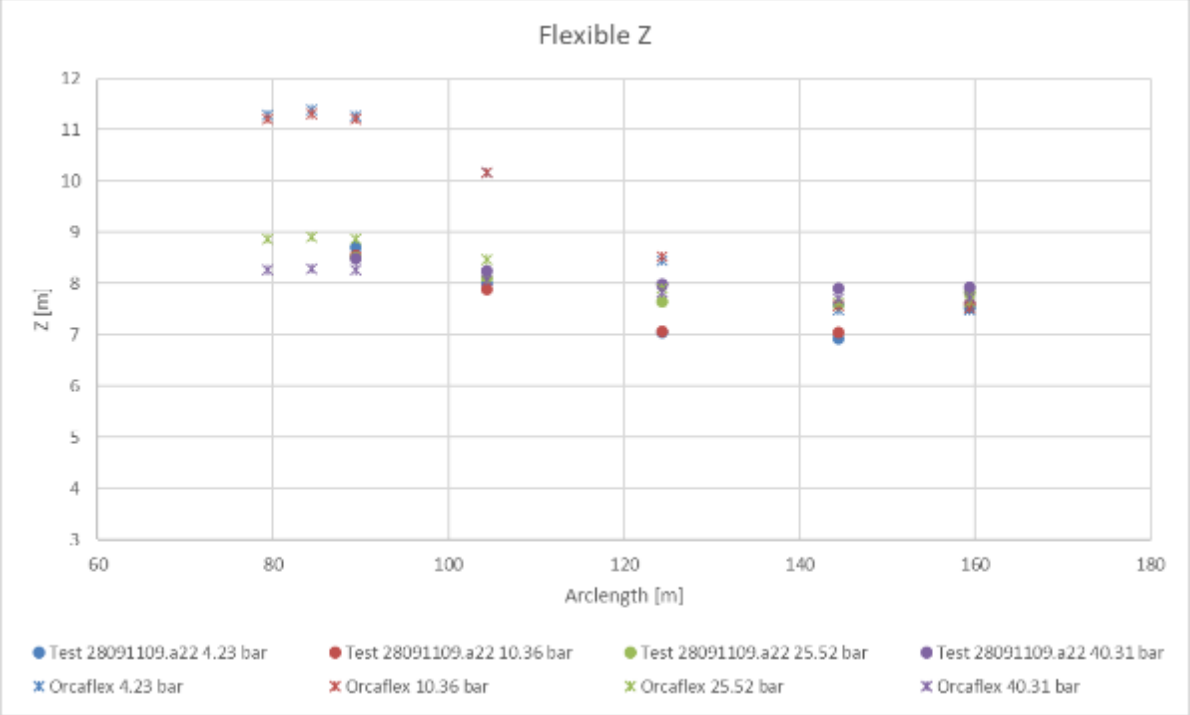

Figure 3-9: Numerical model with a flexible pipe mass per unit length of 0.257t/m.

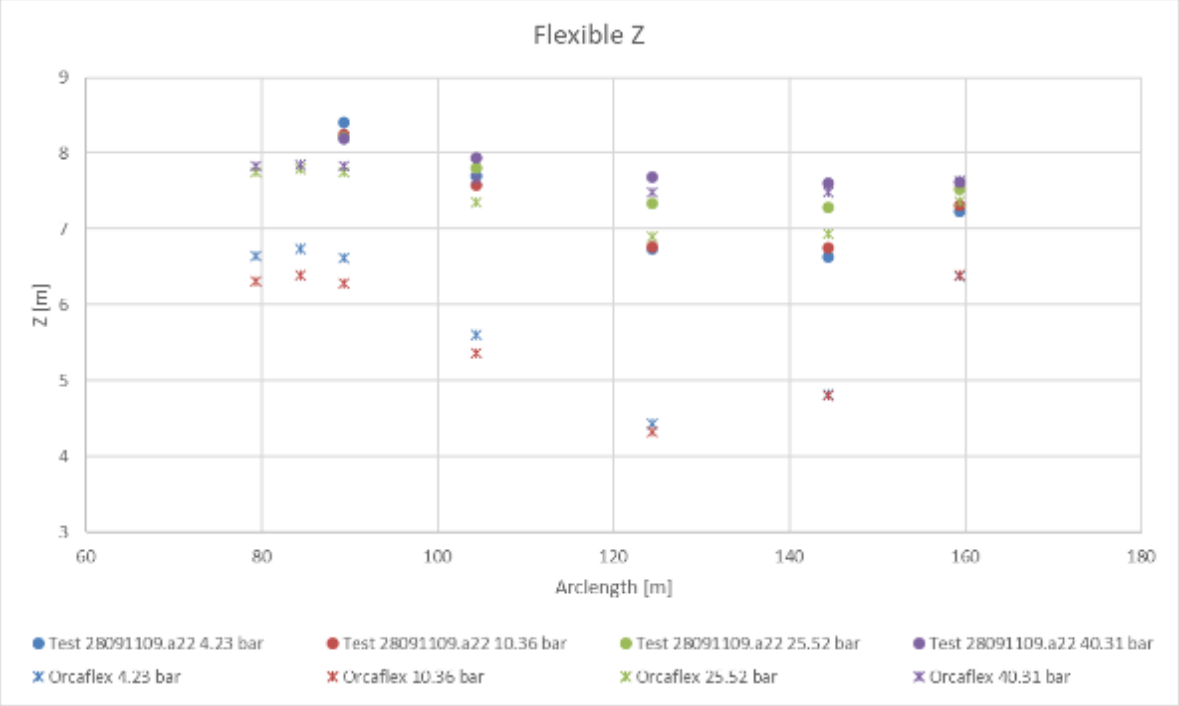

Figure 3-10: Numerical model with a flexible pipe mass per unit length of 0.270 t/m.

When looking at the elevation profiles of the numerical model with a lighter mass per unit for the two lowest Pi (Figure 3-9), the Z elevation points of the numerical model are overestimated, while they were underestimated by the numerical model with the initial mass per unit length of 0.270 t/m (Figure 3-10).

This leads to think that the iterative process of the EA calibration should also include the EI and not solely the mass of the flexible pipe. This hypothesis was not verified due to time restraints.

Note that the EI values used for the EA calibration are those presented in Section 3.3.2, as derived from the elevation profiles of tests 14-16 (first option).

3.3.2. Bending Stiffness

In order to calibrate the EI behavior of the flexible pipe in function of the Pi, two calibration methods were tested.

Option 1: Iterative calibration of the EI based on the profile elevation of **tests 14, 15, and 16**.

The first method relied on tests 14, 15, and 16 which recorded the static equilibrium of the three flexible pipe configurations tested during the 2nd campaign. Given that the pipe end to which the strainer is connected is not fixed, the flexible pipe is free to bend under the action of the Pi, according to the associated EI (Figure 3-11).

Figure 3-11: Experimental setup of test 14 – Bending stiffness test on Configuration 1 at Pi = 4bar and Pi = 40bar.

The experimental elevation profiles of test 14 (Configuration 1) were used as a reference to calibrate the EI in function of the Pi.

Pi	EI
[kPa]	[kN.m2]
447	31000
1030	36000
2454	52000
4081	85000

Table 3-6: EI values obtained from the elevation profile method, as a function of the internal pressure.

The following elevation profiles were obtained for Configuration 2 (test 15), and Configuration 3 (test 16) using the calibrated EI reported in Table 3-6.

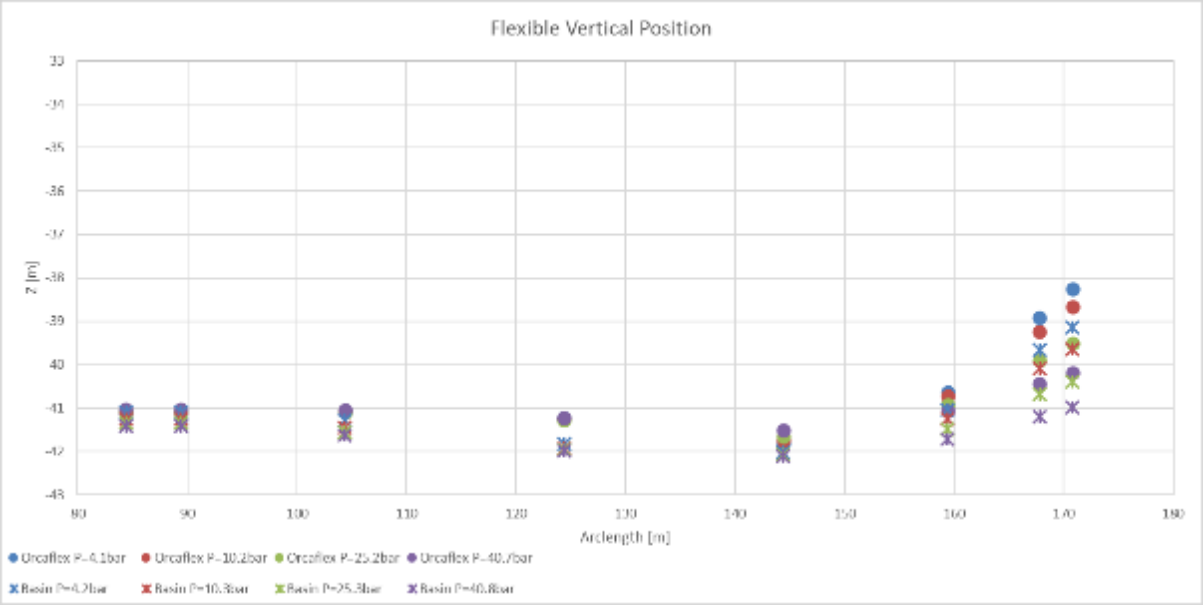

Figure 3-12: Elevation profile of test 15 (Configuration 2).

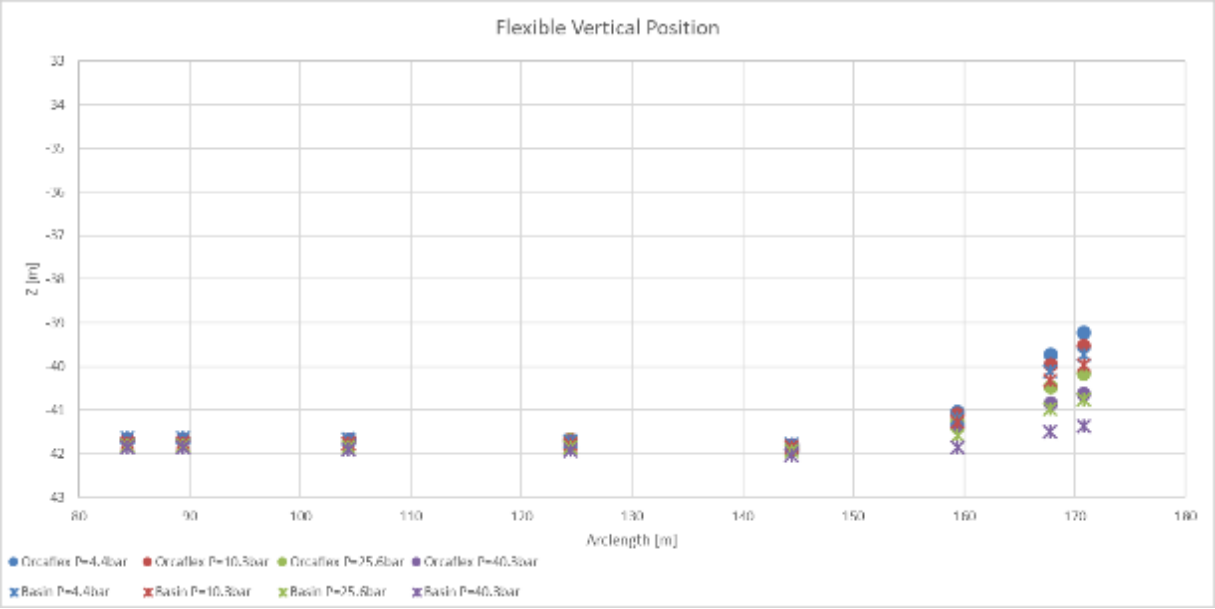

Figure 3-13: Elevation profile of test 16 (Configuration 3).

The elevation profiles of Configuration 2 and 3, depicted in Figure 3-12 and Figure 3-13 are not completely overlapping, especially at the free end part which is sensitive to the EI value. After investigation, it was observed that the free end pipe extremity of test 14 (Configuration 1), on which the calibration was made, was particularly bend transversally (Picture 3-6). It was hypothesized that the offsets in the Configurations 2 and 3 were due to this transverse offset of Configuration 1 in test 14.

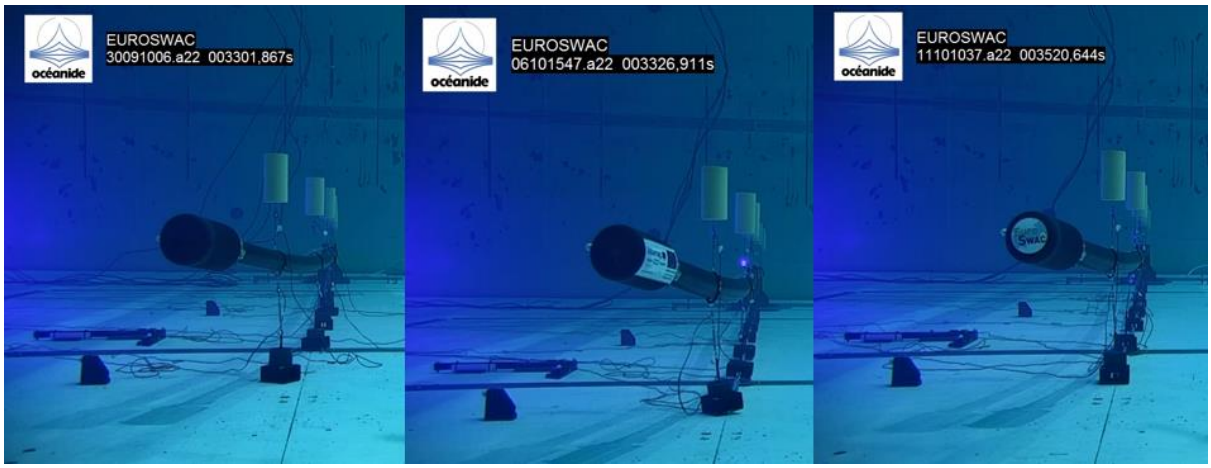

Configuration 1 *Configuration 2* *Configuration 3*

Picture 3-6: Initial transverse offset at the pipe free end, during the bending stiffness tests (14-16).

Looking at the profile view of each anchoring configuration during the EI tests, the third configuration has the most rectilinear position. However, the EI were not calibrated on the Configuration 3 EI elevation profile test because configurations with chain as anchoring components were anticipated to be problematic in the sense that the Orcaflex does not have the 'history' of the chain motions due to the seabed immersion (axial friction unknown).

Additionally, it was noted that the elevation profile of Configuration 2 obtained from the numerical model presents an offset ranging from 0.37m to 0.61m along the flexible pipe between the arclengths 80m to 150m (Figure 3-12). The video records show indeed a lifting of the CWs in the basin test, as well as a slight inclination which lead to slightly slanted slings. Similarly, the numerical model reproduced the lifting and the slanted position but overestimates the lifting. It was double checked that the numerical model with the initial mass per unit length of 0.270t/m did not yield the same elevation profile as the test 15. However, the change in value was not found sensitive enough to cover the elevation profile divergence. The most plausible hypothesis would be linked to the previous comment. Given the unknown exact chain starting position during this specific test by the Orcaflex software; the value of the lifting and inclination of the CW, and in turn those of the slings, might differ mainly due to the axial friction estimation, and thus, cause this divergence.

- Option 2: Iterative calibration of the EI based on the decay **tests 6, 7, 8, and 9**.

The tests 6, 7, 8, and 9 are the decay tests performed on Configuration 1 at the respective following pressures: 5, 10, 25, and 40bar. Despite the supposedly vertical excitation of the flexible pipe system during the decay tests, it was found that the small amplitude excitations were generated in the x-direction as well (Figure 3-14). Furthermore, when looking at the frequency response of these decay tests, a double-peaked signal is visible. The oscillations in the x-direction are responsible for this second frequency peak. Additionally, it is straightforward that the energetic contribution of the frequency response is significantly larger in the x-direction.

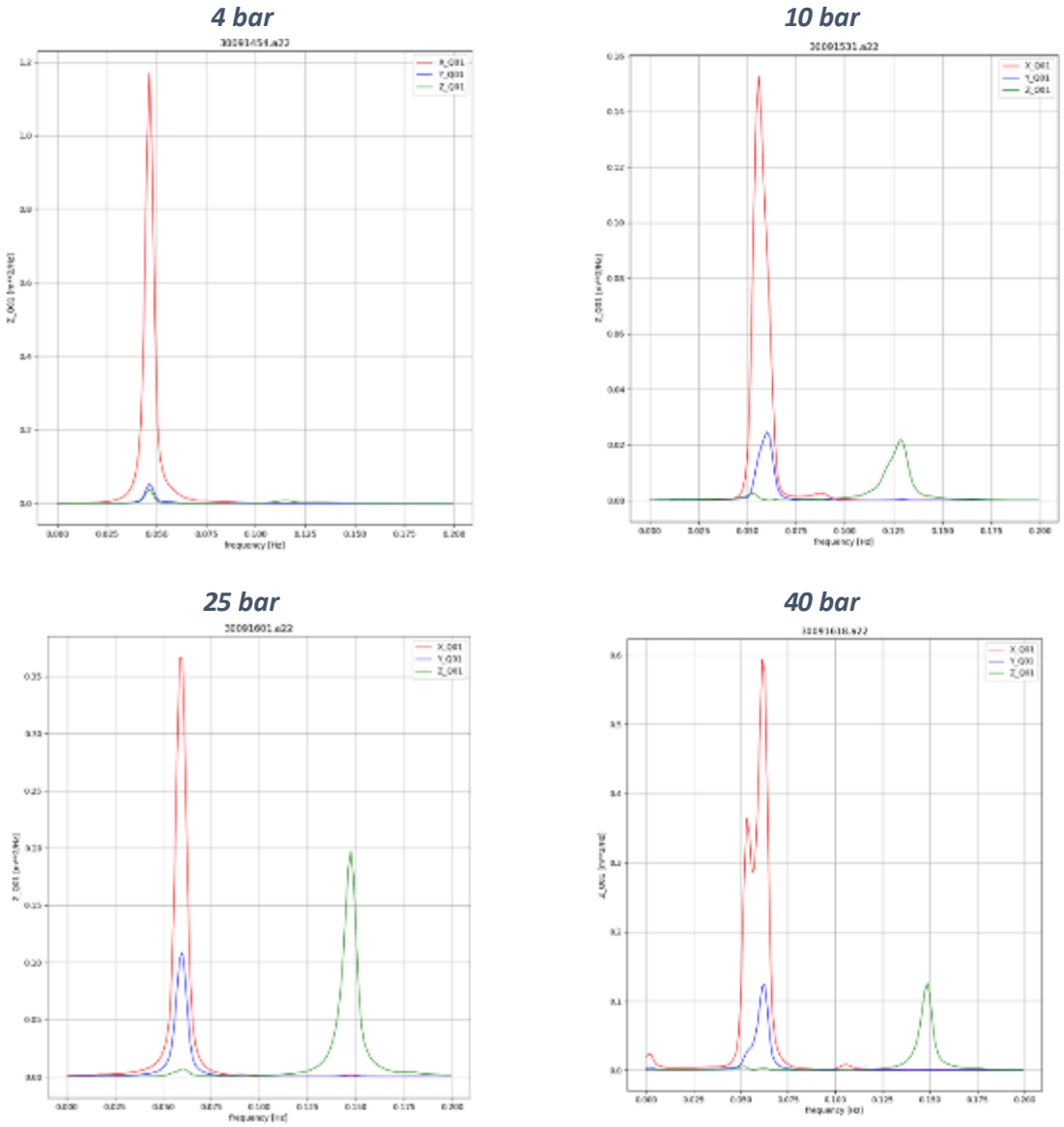

Figure 3-14: Frequency responses in the x, y, and z-directions of the flexible pipe system decay test, for the four considered Pi.

It was conjectured that the decay test in the z direction could not be conducted properly given the presence of the slings preventing a free return to equilibrium position.

The second EI calibration method was thus based on the natural modes in the x-direction. The idea is that the natural period Tn is directly dictated by the flexible pipe EI in the x-direction. This second EI calibration method was also tested to validate the previously calibrated EI. Table 3-7 reports the Tn X that were reported in the basin during the decay test of Configuration 1, and the EI obtained while calibrating the numerical model to obtain the same Tn X for the four different tested Pi.

Basin Decay Test		Numerical Decay Tests (6-9)		Numerical EI Test (14)	
Pi	Tn X exp	Tn X num	EI (Tn X)	Pi	EI (Z)
[kPa]	[s]	[s]	[kN.m2]	[kPa]	[kN.m2]
422	21.73	21.728	31100	447	31000
960	17.88	17.88	47060	1030	36000
2443	17.06	17.06	51900	2454	52000
3921	16.27	16.27	57380	4080	87000

Table 3-7: Comparison of the EI calibrated from the elevation profile method to the EI obtained from the X- natural modes.

When comparing the EI values obtained from the two calibration methods for approximatively the same Pi, it is visible that while the EI for the Pi of 4 and 25 bar are almost identical, it is not the case for the test conducted for the two other Pi. This could be explained by the double peaked response in the x-direction for the two problematic tests (Pi of 10 and 40 bar). In fact, despite the very low magnitude, it can be seen in Figure 3-14 that a second mode in the x-direction is present around respectively 0.085Hz (10 bar) and 0.11Hz (40 bar).

3.3.3. Seabed Friction Coefficients of the Anchoring Components

Seabed friction characterization tests were conducted to determine the friction coefficients between the seabed and the different anchoring components.

Tests 17 and 17b consisted in pulling a CW1-7 of Configuration 1 with a pulley system, horizontally with respect to the seabed (Picture 3-7a). The pulling tension was recorded which allowed to determine the friction coefficient of a CW 1-7 by considering the peak tension for each stop-and-go traction event.

(a) *(b)*

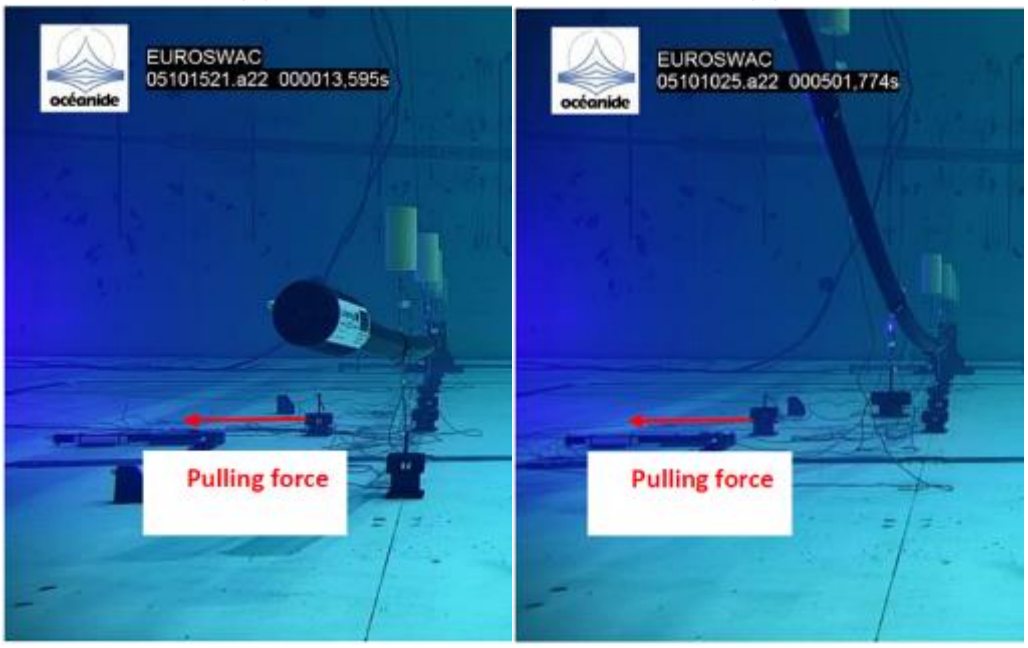

Picture 3-7: Test 17 and 17c – Seabed friction characterization of (a) CW1-7 (left) and (b) CW8. Note that the CW are completely detached from the flexible pipe system visible in the right hand side of both pictures.

Given that Orcaflex does not differentiate between the static and the dynamic friction coefficient, it was chosen to use the static friction coefficient to get a good estimation of the force needed to put the object into motion, even if it means that the motions will be underestimated in the simulations, given that the dynamic friction coefficient is lower than the static one.

The static friction coefficient was estimated with the following formula, considering the mass in water, and the static force F_s required to put the object into motion:

$$\mu_s = \frac{F_s}{m_{water} * g}$$

The static friction coefficient was calculated for each tension peak, and the averaged value was considered in the numerical model. **Test 17c** allowed to calucluate the static friction coefficient for CW8 of Configuration 1 (Picture 3-7b). Note that the friction coefficients obtained for the CW of Configuration 1, were also used for the numerical CW of the two other Configurations, given that same CW holder is used for all the CW, and that in turn, the contact area and material are the same.

	Test 17		Test 17b		Test 17c	
	Fstat [kN]	μ_s [-]	Fstat [kN]	μ_s [-]	Fstat [kN]	μ_s [-]
Peak 1	58.56	0.63	61.83	0.67	63.12	0.40
Peak 2	50.96	0.55	51.22	0.55	62.54	0.40
Peak 3	46.78	0.51	49.23	0.53	72.52	0.46
Peak 4	-	-	-	-	71.36	0.45
Peak 5	-	-	-	-	79.47	0.51

Table 3-8: Reporting of the static forces and the derived static friction coefficents from the experimental CW seabed friction tests.

Theoretically, the static friction coefficients were expected to be identical given the common CW holder object for eah CW. The order of magnitude of the friction coefficient for the CW was found to be of 0.50, by averaging all the estimates. From the Table 3-8, the CW are put into motion for a pulling tension ranging from 47 to 79kN .

Tests 18 and 20 respectively recorded the pulling tension and the transverse displacement of CW4 until the two neighboring CW were displaced; and the pulling tension and the axial displacement of CW8 connected to the entire chain (Picture 3-8). These two tests were designed to derive the lateral and axial seabed coefficients of the chain of Configuration 2.

Tests 19 and 21 lead to the same derivations for the chain of Configuration 3.

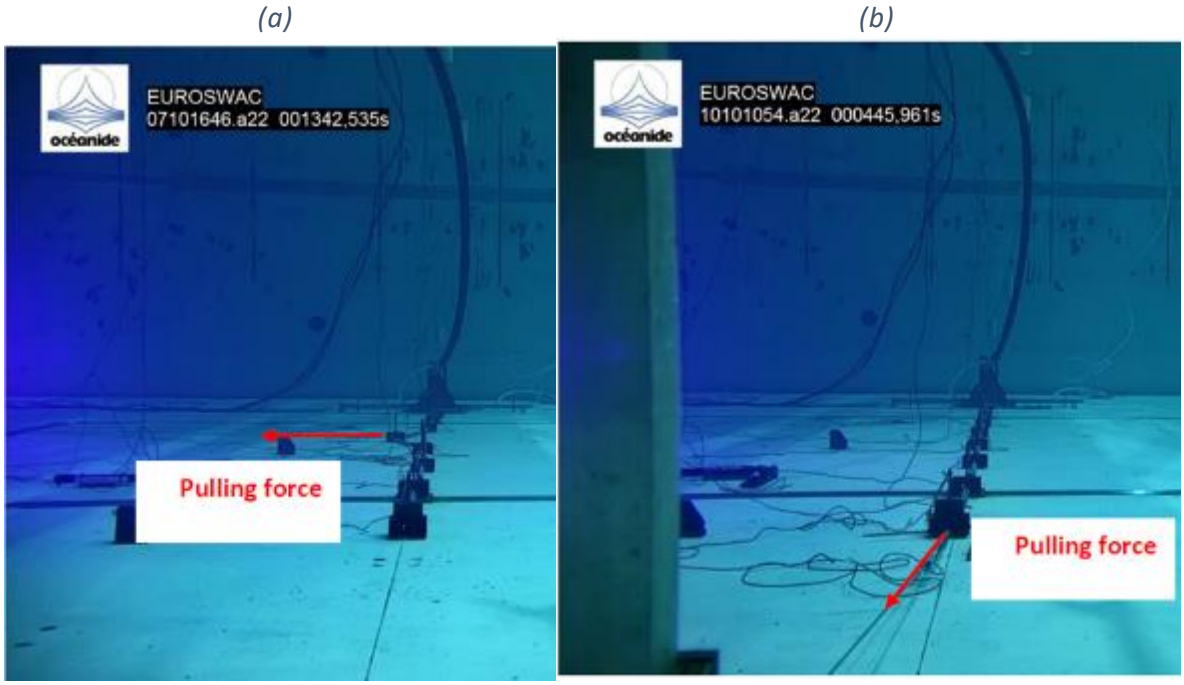

Picture 3-8: (a) Test 18 – Transverse seabed friction characterization of Configuration 2 chain, and (b) lateral seabed friction of Configuration 2 characterization.

The following Orcaflex methodology was used to calibrate the axial (i.e., "in-line") and lateral (i.e. "transverse") seabed friction coefficients of the chains:

- The pulley system was reproduced with a winch Orcaflex object with a "Specific payout rate" of -0.1 m/s. The payout rate is negative, given that the length of the winch wire is to be hauled in.
- The winch wire axial stiffness and pulley location were respected for each friction test (specified in Ref. 5).

- In-line tests: The axial friction coefficient was iteratively calibrated to get the desired tension peak, once stabilized in order to get rid of the dynamical effects of the winch wire payout rate (Figure 3-15). Note that the calibration is performed on the pulling tension rather than the y-displacement, given that in the experimental tests, the winch wire payout was conducted discontinuously, while the winch wire was constantly hauled in, in the simulation (no punctual displacements to calibrate on). Additionally, the peak tension considered was estimated based on the averaged value of all the experimental tension peaks. The two axial friction coefficients are reported in Section 3.2.4, in Table 3-5.

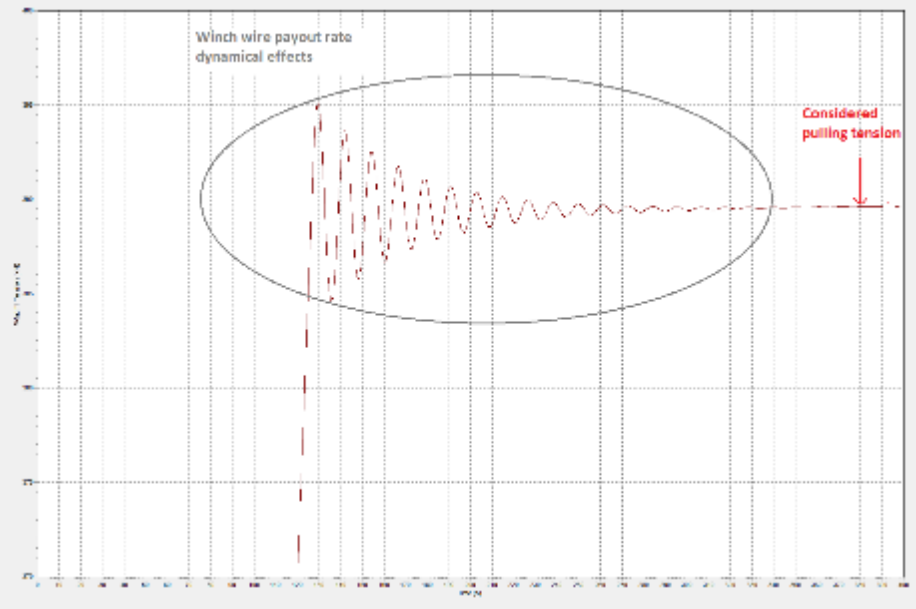

Figure 3-15: Stabilized Orcaflex winch wire tension of 389.50kN for an axial seabed friction coefficient of 0.48 (Configuration 2 chain).

- Transverse tests: In the second phase, the calibration of the lateral friction coefficient was conducted such as to get the desired x-displacement/tension couple, according to the pulling tension recorded in the basin. The lateral friction coefficient calibration was less straightforward, given that the transverse friction coefficient is dependent on the portion of chain involved . In fact, the greater the transverse offset, the greater the length of chain is being pulled, and thus the greater the contact area at play as well (Figure 3-16). As a result this calibration also takes into account the x-displacement associated with the target pulling tension. Note that the y-displacement was also cross-checked to validate the order of magnitude obtained in the numerical model. For the transverse friction coefficient, the calibration was not done of the averaged value of the 5 recorded peaks, but on the first one only. The obtained results are listed in Table 3-9.

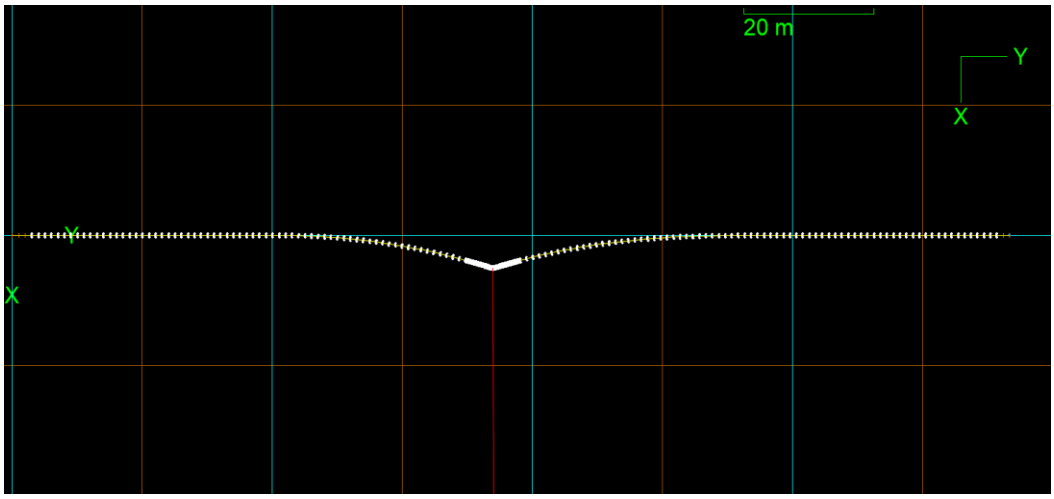

Figure 3-16: Numerical reproduction of the transverse friction coefficient caracterization test (Configuration 2 chain).

		Tension	X_Q12	Y_Q12
		[kN]	[m]	[m]
Test 20 - Peak 1	*Experimental*	**67.5**	**1.67**	**-0.018**
	Numerical (Cf =0.38)	**67.5**	**1.67**	**-0.093**
Test 20 - Peak 2	*Experimental*	98.8	2.91	-0.026
	Numerical (Cf =0.38)	98.8	3.14	-0.3
Test 21 - Peak 1	*Experimental*	**37.8**	**0.250**	**-0.003**
	Numerical (Cf =0.44)	**37.9**	**0.252**	**-0.010**
Test 21 - Peak 3	*Experimental*	69.8	1.33	-0.010
	Numerical (Cf =0.44)	69.9	1.42	-0.07

Table 3-9: Comparison of the x and y displacements obtained for the selected lateral friction coefficients in the numerical model with the experimental associated data (Configuration 2: Test 20 and Configuration 3: Test 21).

As stated, the lateral friction coefficients were calibrated on the x-displacements of the first peak. When focusing on the x-displacement of a subsequent peak (peak 2 or peak 3), it is visible that the x-displacements do not match. This is most likely due to the unknown alignment of the chain links which was most probably not rectilinear during the first pulling event. The evolution tendency with respect to the pulling tension is however respected. Additionally, when considering the y-displacements, the same remarks can be made.

3.4. Comparative Study between the Experimental and Numerical Data

3.4.1. Preliminary Study

The following tests are conducted with regular waves to mainly assess the order of magnitude of the measured outputs. For a 0° wave heading, specific care about potential amplification phenomena of the pipe motion at the free end, possibly resulting in a so-called "whiplash effect", was taken.

Additionally, the tests were repeated with a Pi of 40bar approximately, to validate the calibration of the EA and EI. This batch of tests is solely conducted on the Configuration 3, for wave headings of 90° and 0°.

- Whiplash 90° (REG1 RE1+current REG2 REG3)
  - Config 3 at Pi=10bar: **tests 75-78**
  - Config 3 at Pi=40bar: **tests 79-82**

- Whiplash 0° (REG1 REG2 REG3 RE3+current)
  - Config 3 at Pi=10bar: **tests 67-70**
  - Config 3 at Pi=40bar: **tests 71-74**

During the experimental campaign some unexpected and unaccounted event/phenomena occurred which are not reported in the numerical model but exposed and discussed in Section 3.4.1.1 to understand the reason of some misalignment between the numerical results and the experimental data.

The general behavior of the flexible pipe system in the basin is then briefly described in Section 3.4.1.2 and compared with the numerical results, for each sea conditions. Some specific comparisons are also provided about CW displacement, pipe displacement and the sling tension (static values and temporal evolution). These comparisons are either provided for illustrative purposes or to investigate a potential divergence between the experimental data and the numerical results obtained with the Orcaflex model.

3.4.1.1. Experimental hindrances

3.4.1.1.1. Transverse offset of the flexible pipe system toward the free end

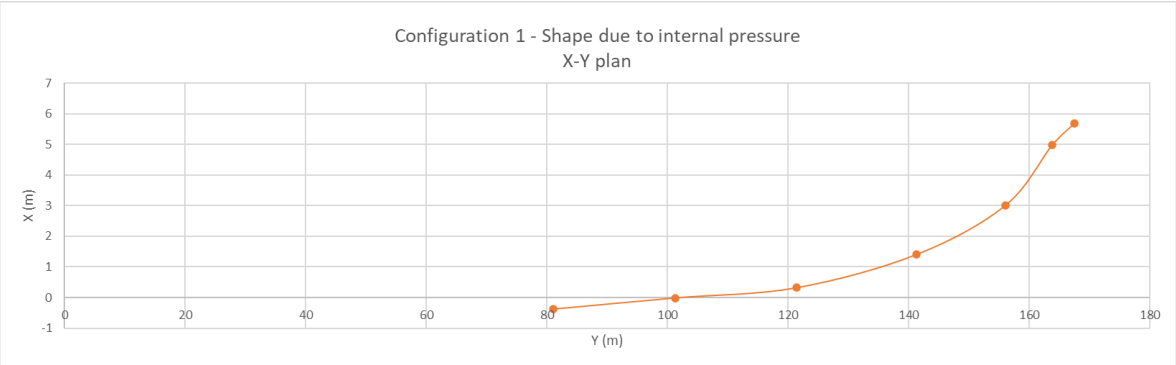

Figure 3-17: Plan view of the *flexible pipe initial transverse offset for test 3 (Decay test on Configuration 1).*

Firstly, as mentioned previously, the flexible pipe system presented a transverse offset (x-direction) at the free extremity (Figure 3-17). Given that the flexible pipe system was arbitrary repositioned in a rectilinear position during the experimental campaign, this offset was never exactly the same. In fact, this initial deformation was present in the first campaign, and was accentuated due to the pipe free end state.

The flexible pipe position being conditioned by the CW position, the latter also presented some unaccounted differences, since the initial flexible pipe system was not modified in the numerical model and kept rectilinear. This x-offset measured during the basin tests results in a different starting position with the numerical model where the pipe and the anchoring components were always rectilinearly placed at each test start. This led to some minor flexible pipe system different responses which are detailed further.

3.4.1.1.2. Basin floor irregularity under CW8

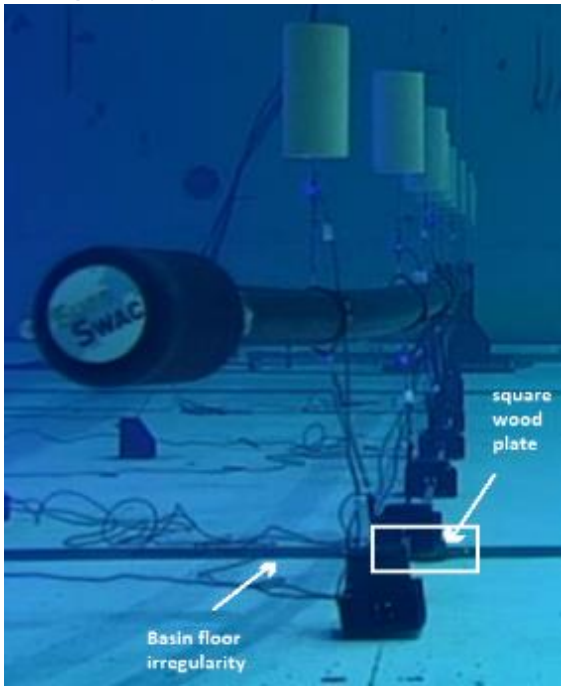

Picture 3-9: Addition of a square wood plate to avoid difference in seabed friction coefficient for the fore last CW.

Furthermore, the CW7 which displacement was measured by Q11 happened to be placed on a basin floor irregularity. To remedy this issue, a small square plate of wood was added underneath the CW7 to prevent a difference in seabed friction coefficient (Picture 3-9). However, as presented in Section 3.4.1.2, this wood plate was of a certain thickness which led to a modified CW transverse motion response, depending on the sent wave height.

3.4.1.1.3. Slanted Clump Weights

It was also observed that the CW adopted an inclined position towards the x-direction (Picture 3-10) or the y-direction which is respectively due to respectively the moment induced by the current on the CW holders, and the axial friction of the chain. However, the CW were modelled with 3D buoys. The slanted position of the CW can thus not be reproduced with the current numerical model.

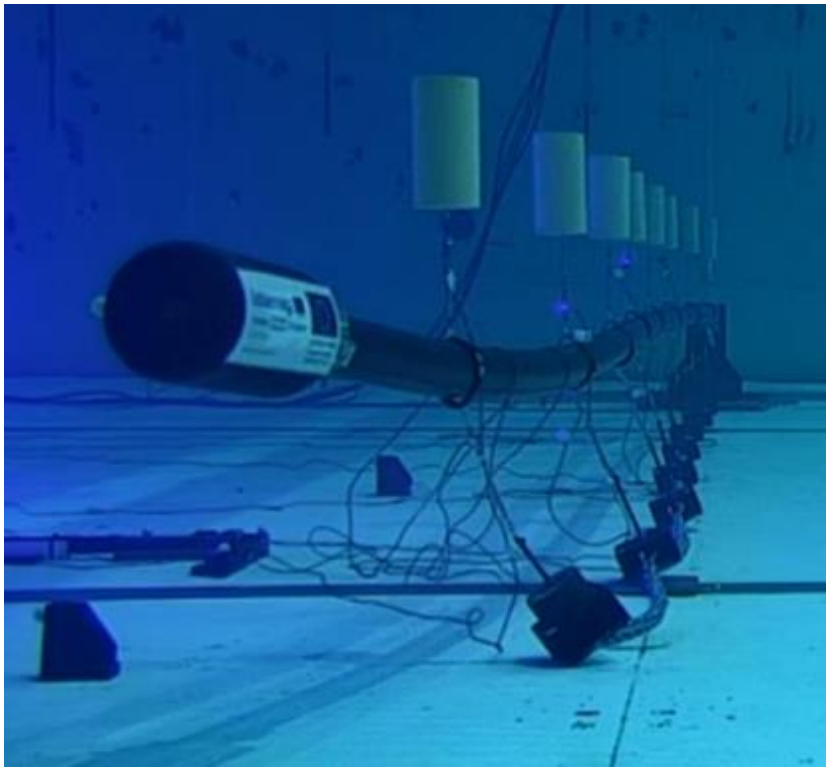

Picture 3-10: Slanted CW under the action of the current inducing a moment on the CW holder.

3.4.1.2. General Behavior of the Pipe Flexible System

3.4.1.2.1. Clump Weights X Displacements

Experimental Setup

Focusing on the regular waves 90° heading tests for a Pi of 10bar (**tests 75 - 77**), the displacements in the x-direction of three CWs, mainly located close to the pipe free end, are reported in this section.

The location of the recorded CWs is detailed in Sketch 3-1. CW5 is equipped with the Qualysis target Q12, CW7 with Q11, and CW8 with Q10.

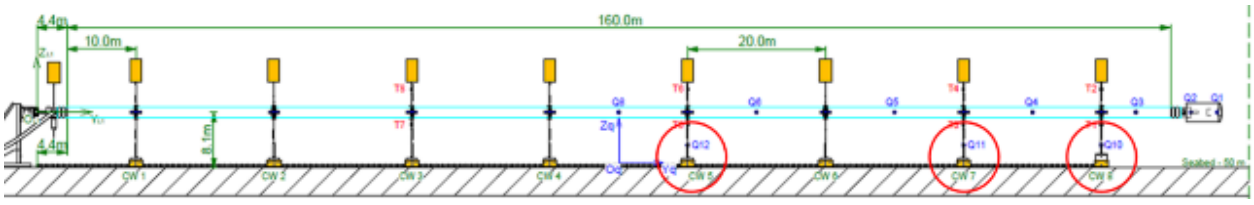

Sketch 3-1: Location of the Qualysis targets on the tracked clump weights for Configuration 1.

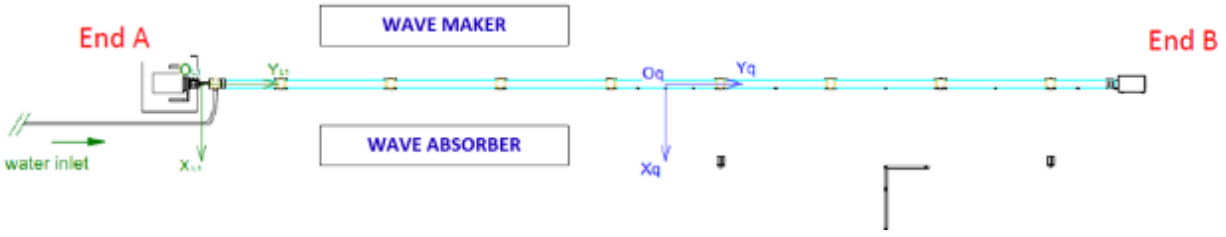

Sketch 3-2: Top view of the reference frame.

Experimental and Numerical Time Signal Comparison for the 90° incident regular waves

(a)

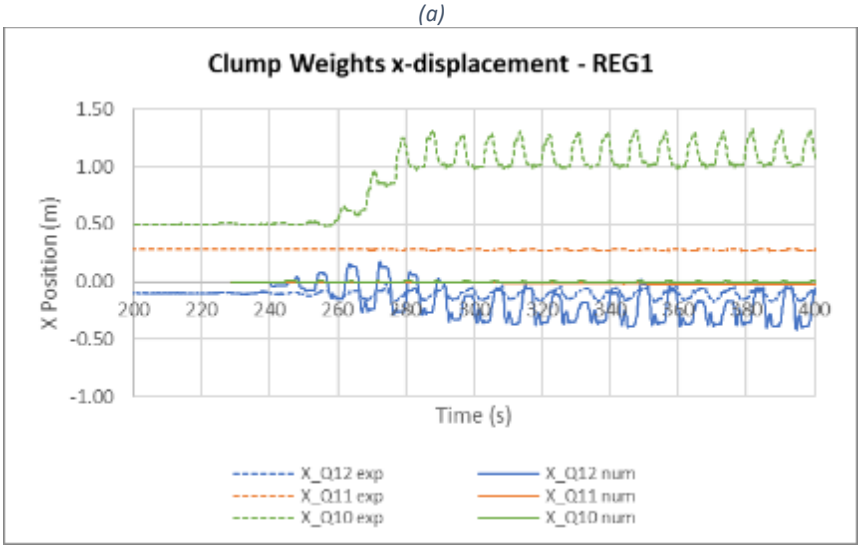

(b)

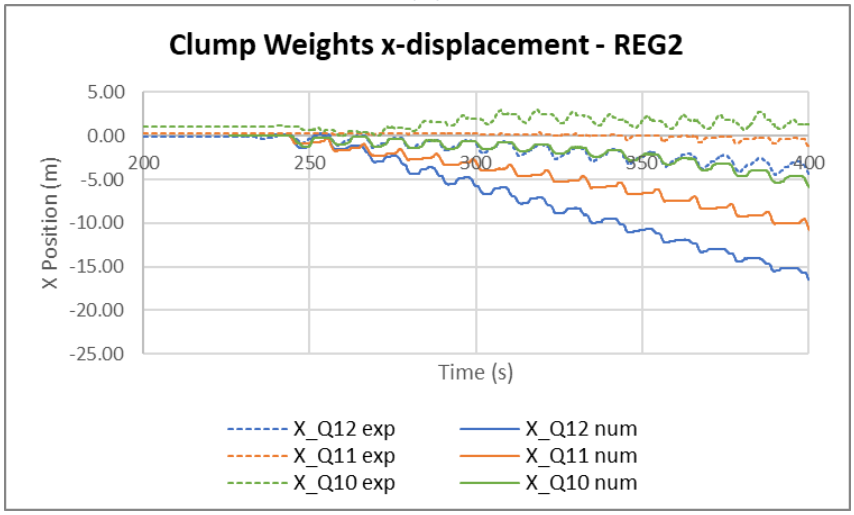

(c)

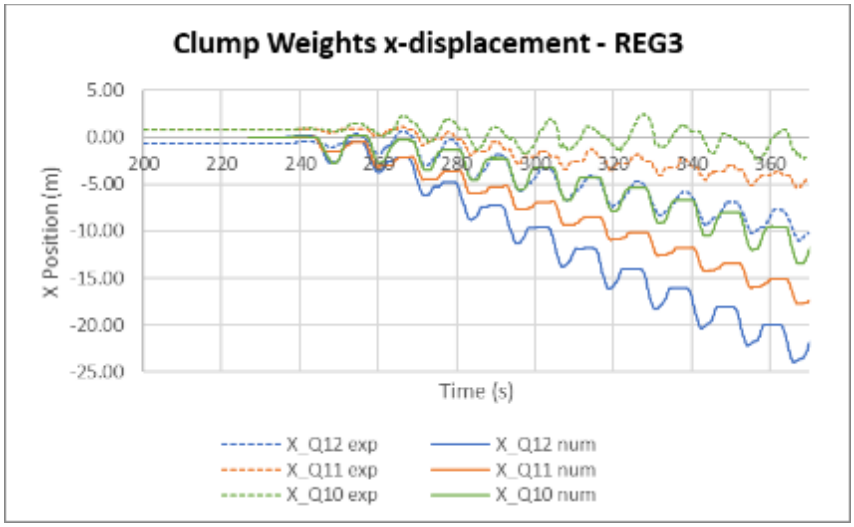

Figure 3-18: Comparative study of the experimental and numerical clump weights transverse offsets for (a) REG1, (b) REG2, (c) and REG3.

- For REG2 and REG3 especially, the closer to the pipe center, the greater the x-offset towards the wave maker (negative value). This means that the CW, and the flexible pipe in turn, adopt a general bent shape.

- **REG 1**:
  - X_Q10 exp. is moving towards the wave absorber, while X_Q11 exp. is stagnating and X_Q12 exp. is evolving in the opposite direction, towards the wave maker.
  - X_Q10 num. is maintaining a null value (unlike its analog), X_Q11 num. is increasing very faintly (opposite trend as the exp. analog), and X_Q12 num. is slightly moving towards the wave maker.

  - After investigation, it was found that the CW are moving during the ascending phase of the orbital water particle motion, allowing a lifting of the CW close to the free pipe end, and thus a suppression of friction forces. However the square wood plate thickness prevented the CW7 (Q11) to be lifted high enough. This caused CW7 to be stuck at its initial position, and restricted CW5 motion towards the wave absorber due to the chain (Q12).
  - The difference between the X_Q10 values is most likely explained by the fact that since only partial CW lifting arose under the small REG1 (slanted CW only), the model could not reproduce the reduction of friction due to the modelling of the CW with 3D buoy.
- **REG 2 :**
  - The flexible pipe is adopting a bend shape under the action of the regular wave (Picture 3-11). The two CW placed at the pipe extremity remains on the rectilinear axis of the starting position, while the other CW evolve towards the wave maker to allow the curved position of the flexible pipe.
  - This bend position of the flexible pipe is possible due to the higher wave height of REG2, which generates a CW lift high enough to displace CW7 (initially stuck because of the square wood place).

Picture 3-11: Transversal view of the flexible pipe system Configuration3 with the visible b*end shape of the flexible pipe system under the action of a 90° heading REG2 (test 76).*

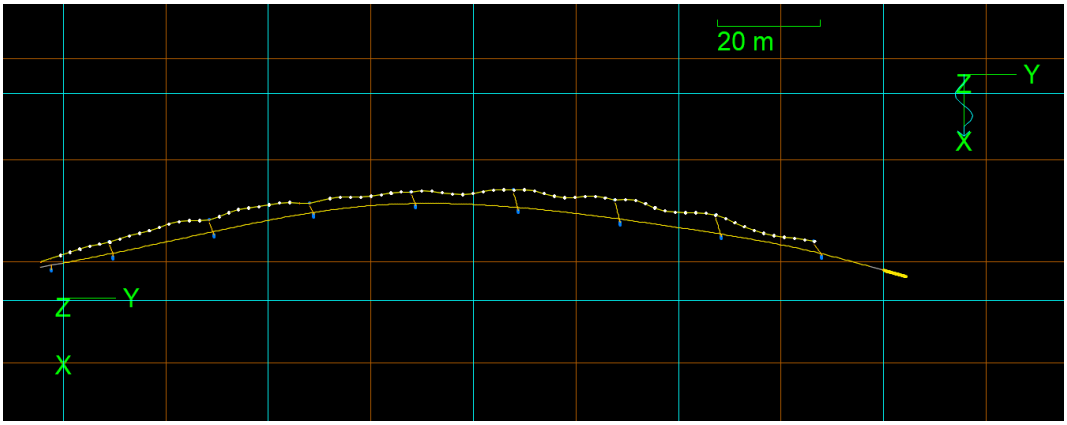

Figure 3-19: Plan view of the numerical reproduction of Configuration 3 under a 90° incident REG2 t = 350s (test 76).

- The numerical model yields however greater CW displacements, as after adopting a curved position, the CWs are further pushed by maintaining their bent shape. This can partially be explained by the hindrance caused by the square wood plate, which delays the x-offset in the basin tests.

- **REG 3 :**
  - Both the experimental setup and the numerical model adopt a curved shape which is maintained why being pushed towards the wave maker.
  - The CW displacement tendencies are now respected for all the CW, despite the numerical model yielding larger x-displacements. In order to investigate about this divergency a succinct sensibility study about the flexible pipe hydrodynamic coefficients is conducted hereafter.

The rather counter-intuitive x-displacement of the CW towards the wave maker (negative), rather than towards the wave absorber, was linked to the wave phase which happens to cause the pipe to be at the bottom position of the orbital motion caused by the wave, when it is positioned towards the wave absorber. Thus the CW are in contact with the seafloor and the friction prevents transverse motion in that direction.

Inversely, when the pipe is leaning in its circular motion towards the wavemaker, it so happens that it is positioned upwards in the circular motion and thus the CW are lifted upwards, and they are not in contact with the seafloor anymore (no friction) which allows the transverse motion of the flexible pipe towards the wave maker.

Hydrodynamic Coefficients Sensitivity Study

Given that the flexible pipe system of the second campaign is allowed to move laterally, it is sensible to refine the applied hydrodynamic coefficients of the flexible pipe specifically for each studied sea condition. The previous section presents the CW displacement under REG3, which main wave parameters are reported in Table 6 in Ref. 3 at model scale (given that the Froude similitude was used).

According to the Sarpkaya graphics (Ref. 3, Figure 14 and 15), the hydrodynamic coefficients for this specific test under REG3 are as follows:

$$C_D \approx 1.7 \text{ and } C_m \approx 0$$

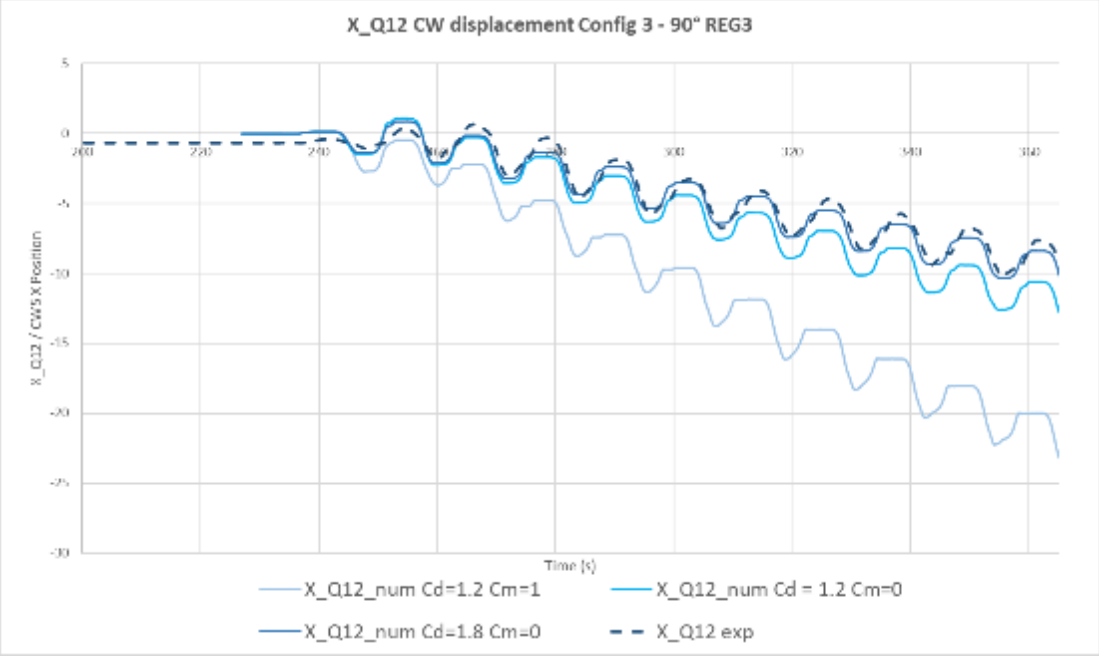

Figure 3-20: Comparative study of the experimental and numerical CW5 transverse offset, measured by Q12 for a 90° incident REG3. The numerical time signals are repeated for the same CW5 but with varying hydrodynamic coefficient values.

Figure 3-20 clearly illustrates that:

- The refined values of the flexible pipe hydrodynamic coefficients for REG3 lead to a CW transverse motion of the same order of magnitude as the experimental one.
- The added mass coefficient seems to have a greater impact than the drag coefficient.

As the flexible pipe is now allowed to move in the transverse plan, the hydrodynamic coefficients should be adjusted for each sea condition.

Comparative Observations about the Experimental and Numerical Response under 0° incident regular waves

Regarding the 0° wave heading tests the following observations are made:

- No CW transverse motion was predicted by the numerical model, while the tests recorded minor oscillations around the initial position.
- Vertical lifting of the CW is present in both the experimental and numerical data.
- It can be observed that the amplitude of the vertical motion of the CW, is often slightly overestimated by the numerical model, and rarely the other way around.

3.4.1.2.2. Flexible Pipe X-Displacements

To assess the flexible pipe motion in the x-direction and to compare the recorded behavior with the numerical model, the position of the flexible pipe at 100s from mid pipe length to the strainer is plotted in Figure 3-21, for each regular waves for a nominal Pi of 10 bar. An additional test with REG2, but with a Pi of 40 bar is also included.

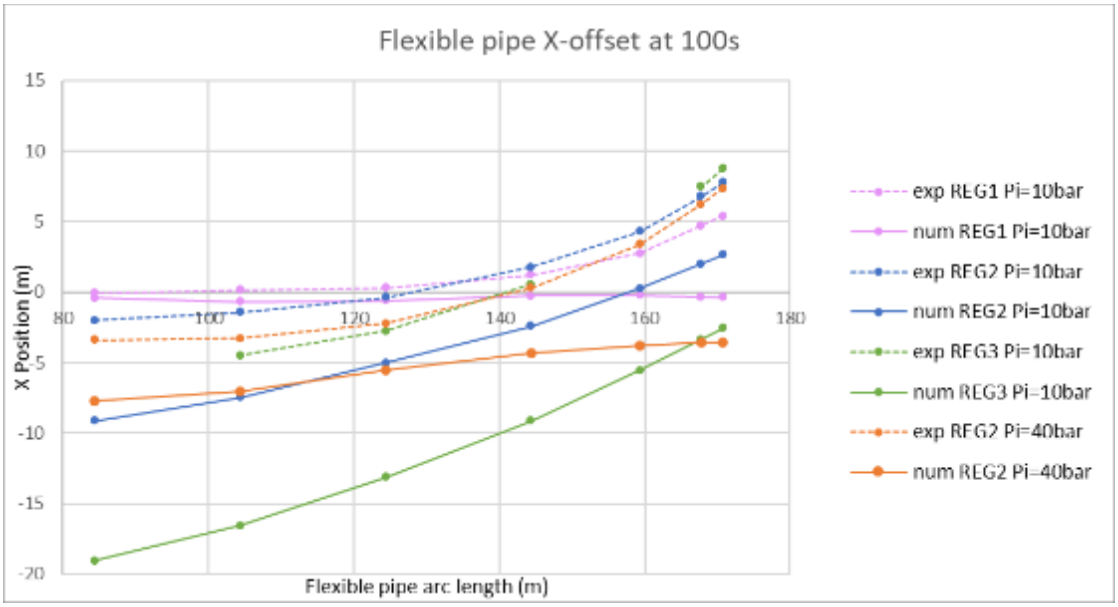

Figure 3-21: X-offsets along the second half of the flexible pipe length in function of the incoming regular wave and the internal pressure at t=100s.

- The shape distortion of the flexible pipe at the pipe free extremity towards the wave absorber (positive X value) is clearly visible on the experimental graphs (dashed lines).
- The higher the wave height, the higher the x-offset. This trend holds for both the experimental and numerical results.
- Under regular waves, the previously mentioned bent shape is formed before being pushed all together (for a wave powerful enough), which increases the x-offset.

- While the shape between the basin tests with a Pi of 10bar and the one with 40bar yield the same flexible pipe distortion under the action of REG2, however the numerical model graph shows a difference in shape. The numerical model with a Pi of 40 bar produces a less bent flexible pipe distortion.

- In agreement with the observations made in Section 3.4.1.2.1, the numerical model overestimates the pipe transverse motion. Specifying the flexible pipe hydrodynamic coefficients for a given sea condition fixes this overestimation, as illustrated in Figure 3-22 for REG3.

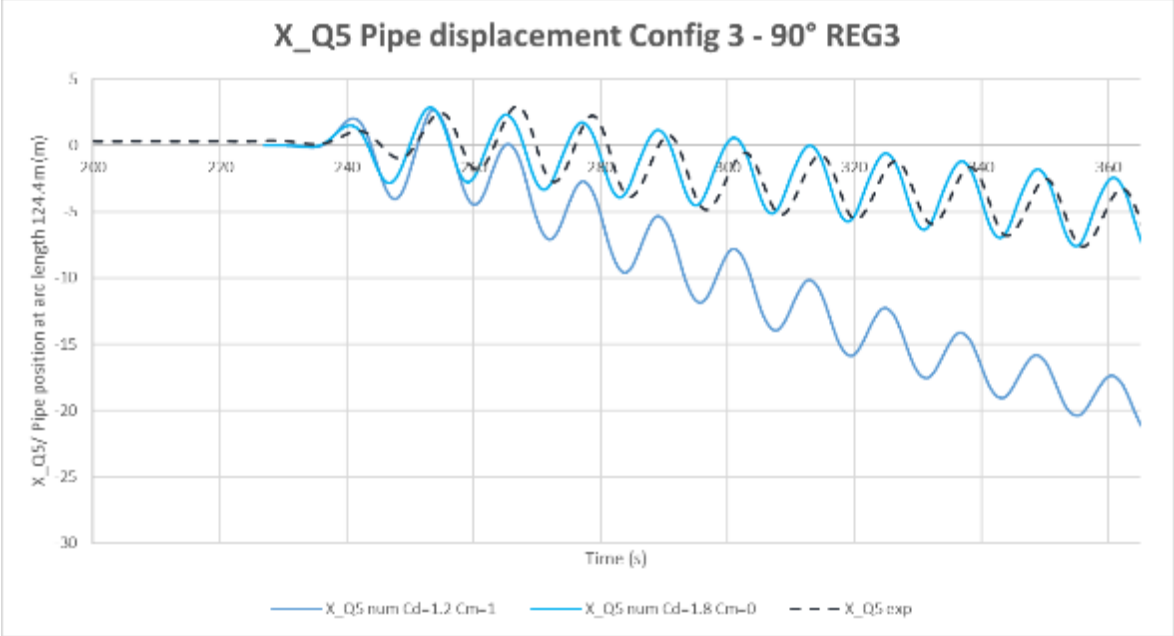

Figure 3-22: Comparative study of the experimental and numerical transverse offset of the flexible pipe at arc length 124.392m, measured by Q5 for a 90° incident REG3. The numerical time signals are repeated for the same pipe location but with varying hydrodynamic coefficient values.

Figure 3-23 depicts the vertical motion of the flexible pipe at the section on which the strainer is mounted. As the most 'favorable' wave for the 'whiplash effect' observation, REG3 with a heading of 0°, was chosen to assess the potential amplification motion at the pipe free end.

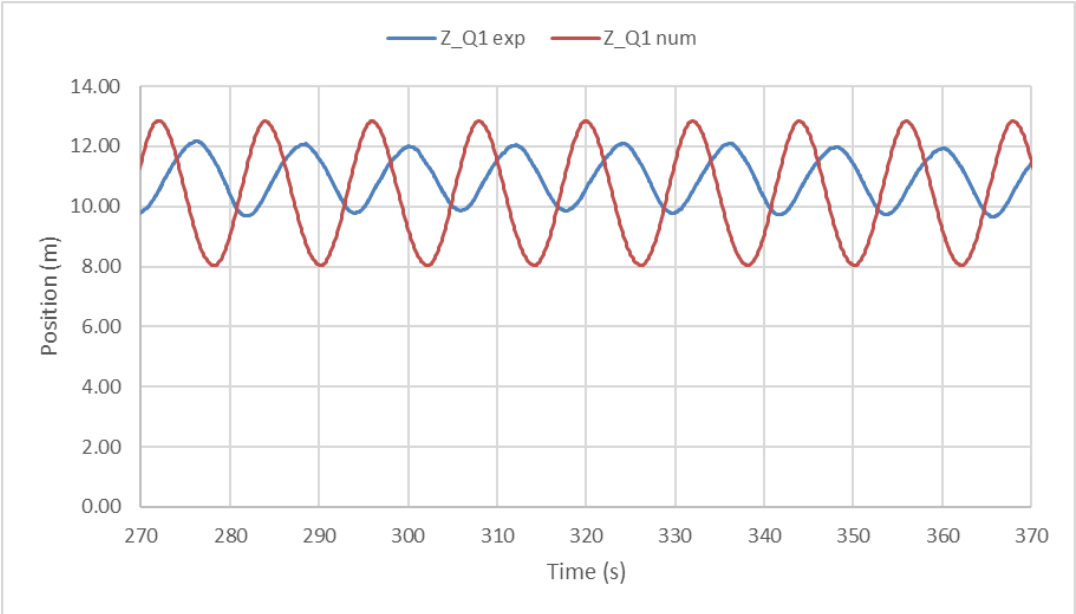

Figure 3-23: *Temporal evolution of the experimental strainer vertical motion recorded by Q1 and its numerical analog (wave heading of 0° REG3).*

- The amplitude of the strainer vertical motion oscillation is approximately of 1m for the experimental prototype and of 2.5m for the numerical model. Once again, the numerical model slightly overestimates.
- No resonance of the strainer motion or so-called "whiplash effect" was observed.

3.4.1.2.3. Anchor Sling Tensions

The initial AS tension are analyzed hereafter to get an order of magnitude of the static tension values in the recorded AS.

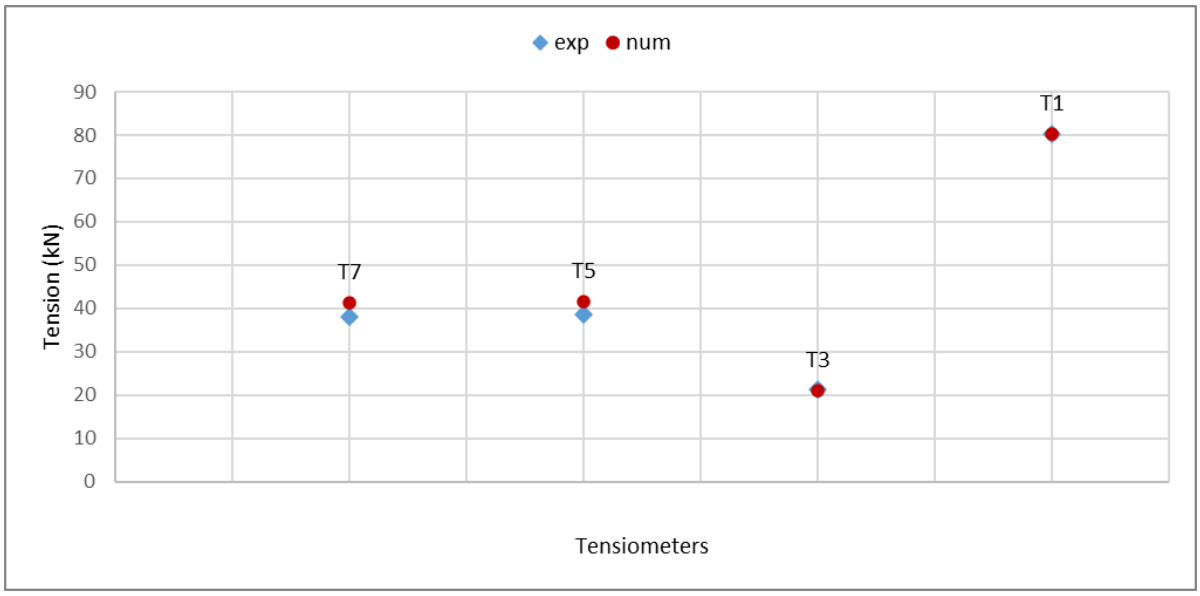

Figure 3-24: Static tension in the anchor slings.

- Globally, the static tension in the AS is 40kN along the flexible pipe, for both the experimental data and the numerical results.
- T3 and T7 (located close to the pipe free end) are respectively displaying a tension around 20kN and 80kN, again for both the experimental data and the numerical results. This tendency is caused by the higher buoyancy of the strainer which slightly bends the flexible pipe to allow the strainer to position itself above the flexible pipe height.
- AS7 tension, recorded by T3, is associated with slack events due to its relatively low value.

A specific comparison study is presented hereafter in Figure 3-25, under the form of a temporal signal cross-checking to verify the identification and predictive ability of the numerical model of the slack events in the AS. This analogy specifically focused on T3.

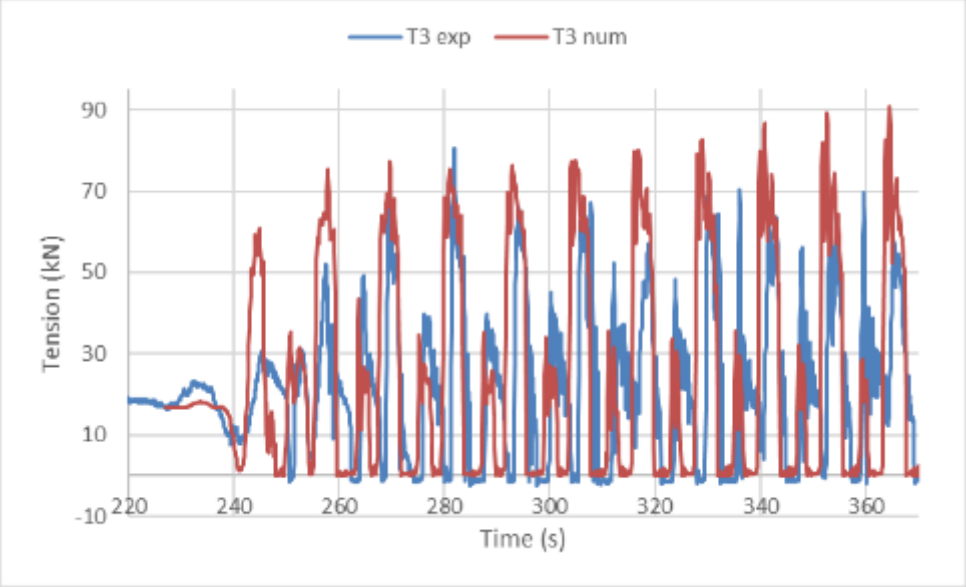

Figure 3-25: Temporal evolution of the experimental anchor sling 7 tension recorded by T3 and its numerical analog.

- Both experimental and numerical signal are identifying slack events in the anchor sling 7 of a very similar signal pattern.
- The numerical model seems to be slightly overestimating the high tension peak of the slack event.
- Note that even if not shown, the numerical model sometimes predicts slack events in other AS even when the experimental tests did not record any, but never the other way around.

3.4.1.2.4. Buoyancy Sling Tensions

Similarly to the AS tension comparison, Figure 3-26 compares the BS static tensions and Figure 3-27 presents a time series analogy to assess the signal pattern predictive ability of the numerical model about the BS tension signal.

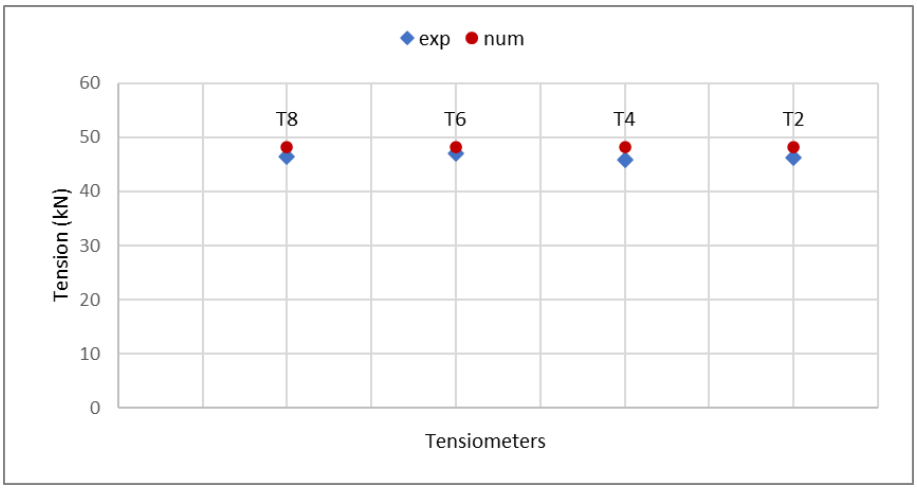

Figure 3-26: Static tension in the buoyancy slings.

- The static BS tension is close to the same for each BS.
- The numerical BS tension is slightly overestimated: 48kN. While the numerical BS tension are comprised between 46kN and 47kN.

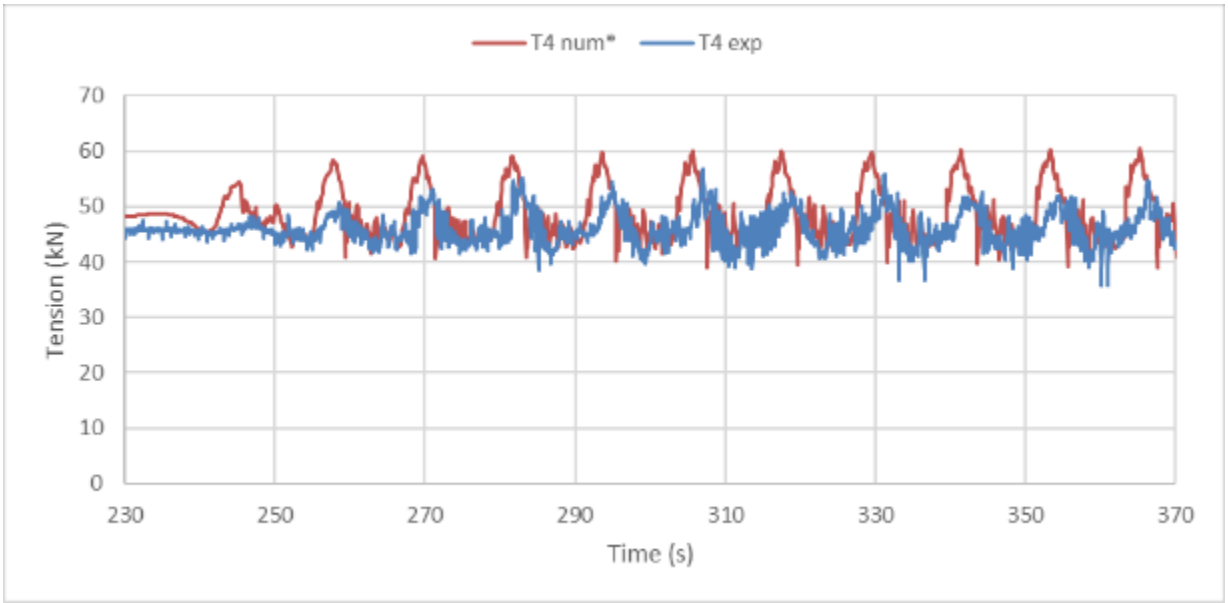

Figure 3-27: Temporal evolution of the experimental buoyancy sling 7 tension recorded by T4 and its numerical analog.

- Again, the pattern of the tension signal is well reproduced by the numerical model, to the exception of a slight over estimation of the tension amplitude.
- Similarly, the model has a tendency to overestimate the amplitude of the signal, but not the other way around.

3.4.2. Flexible Pipe Systems Stability Tests

To further test the built numerical model, three different irregular waves IRR1Y, IRR10Y, and IRR100Y, with or without current were tested to meet more realistic sea conditions. All three anchoring configuration were tested, for both a wave heading of 90° and 0°. This section focusses on the sea heading of 90°. Note that the irregular waves were used in the numerical model were designed after the JONSWAP spectrum with the specified Hs and Tp provided values. One test was reproduced identically, by using the experimental time history signal, filtered down to 2Hz.

- Pipe Stability 90° (current Irr1Y Irr10Y Irr100Y Irr100Y+current)
  - Config 1 : **tests 22-26**
  - Config 2 : **tests 27-31**
  - Config 3 : **tests 32-36**
- Pipe Stability 0° (current Irr1Y Irr10Y Irr100Y Irr100Y+current)
  - Config 1 : **tests 57-61**
  - Config 2 : **tests 47-51**
  - Config 3 : **tests 42-46**

3.4.2.1. CW/Chain X-Displacements

The transverse offset of the CW for each 3 anchoring configurations is reported in the following table after 500s of exposure to the considered 90° incidence sea condition. Note that the CW starting x-offset of the experimental data was removed in the following table for the sake of comparison.

		Q12 exp	Q12 num	Q11 exp	Q11 num	Q10 exp	Q10 num
Current 90°	Config. 1	0.7	0.0	0.8	0.0	2.7	1.1
	Config. 2	2.1	0.7	2.1	0.6	2.8	3.0
	Config. 3	1.0	0.3	1.3	0.0	2.6	0.5
IRR10Y 90°	Config. 1	0.1	0.0	0.0	0.0	-0.1	-0.4
	Config. 2	0.0	-0.3	0.2	0.1	-0.1	0.1
	Config. 3	-0.7	-0.3	0.0	-0.7	1.2	-1.6

Table 3-10: CW transverse position at CW5 (Q12), CW7 (Q11), and CW8 (Q10) after a 500s exposure to the considered sea environment (90°) for the 3 anchoring configurations.

- Focusing on the experimental data:
  - The current creates a significant transverse motion of the CW. The closer to the pipe free end, the greater the CW x-offset.
  - The irregular wave produces no significant transverse motion. When looking at the temporal evolution of the CW10 x-displacement signal (provided below), it is visible that under the action of an irregular wave only, the flexible pipe oscillates more or less around its initial position.
  - The more significant transverse offset values for Configuration 3 (IRR10Y) are misleading as CW7 was stuck because of the square wood plate elevation preventing a lifting of CW7, resulting a perturbation of the CW transverse motion. In fact, the tests conducted for configuration 1 did not use the square wooden plate, and Configuration 2 CW holders being free of weights, they are slightly lifted, thus not affected by the square wooden plate.

- Configuration 2 seems to be the less stable (highest transverse displacement), when subjected to the current. However this suggestion is to be taken with caution as the test conditions were not identical for each configuration (i.e. presence of square wooden plate).

- When comparing with the numerical results:
  - Overall, the numerically reproduced test conducted under current predict smaller CW displacements. This attributed to the fact that VIV was not included in the numerical model.
  - The current case yields a null motion for Configuration 1, except for a very small displacement at CW8 (closest to the pipe free end). This is mainly due to the modelling of the CW with 3D buoys preventing a slanted position (as observed in the basin) and thus a reduction of friction.
  - Again, the misleading of Configuration 3 under IRR10Y may be caused by the square wooden plate restricting the motion of CW7.
  - Configuration 2 outmost CW8 has an almost identical transverse offset with the experimental data.

For the sake of accuracy a succinct comparative study with the exact same sea elevation time signal, depicted in Figure 3-28, was conducted.

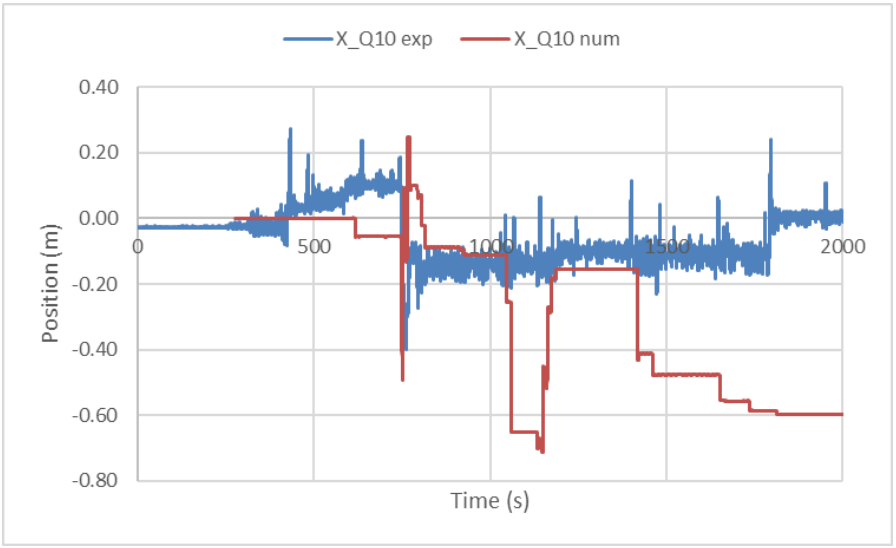

Figure 3-28: Temporal evolution of CW8 (X_Q10) transverse motion exposed to IRR10Y (Configuration 1) with the initial x-offset removed from the experimental data.

- The experimental CW8 transverse motion under IRR10Y is mainly static with minor fluctuations.
- The numerical graph globally follows the experimental trend, when taking into account the initial distorted position of the flexible pipe system in the basin yielding an x-offset. Starting 1000s, the numerical motion diverges from the experimental data. This could be caused by the basin floor irregularity retaining the numerical CW.
- In conclusion, the difference between the experimental and the numerical x-offset value reported in Table 3-10 is not due to the use of a JONSWAP signal rather than the exact same irregular wave.

3.4.2.2. Flexible pipe X-displacements

Again, note that the flexible pipe starting x-offset of the experimental data was removed in the following table for the sake of comparison.

		Q8 exp	Q8 num	Q5 exp	Q5 num	Q1 exp	Q1 num
Current 90°	Config. 1	2.0	1.5	2.6	1.7	4.8	3.1
	Config. 2	3.6	2.0	3.7	2.5	4.6	5.8
	Config. 3	2.3	1.8	3.0	1.8	4.5	2.5
IRR10Y 90°	Config. 1	1.9	0.2	1.3	0.3	1.7	-0.4
	Config. 2	0.1	-0.1	0.3	0.4	1.2	-0.5
	Config. 3	-1.8	0.5	-0.7	0.1	-0.2	0.3

Table 3-11: Flexible pipe transverse position at an arclength of 84.4m (Q8), 124.4m (Q5), 170.8m (Q1, located on the strainer) after a 500s exposure to the considered sea environment (90°) for the 3 anchoring configurations.

- Focusing on the experimental data:
  - The flexible pipe transverse motion follows the same trends described in Section 3.4.2.1., the numerical model yields larger transverse motions. The flexible pipe offset value are however higher given the associated sling inclination.
  - As mentioned in the previous section, the transverse motions under irregular waves are actually close to nonexistent given that, the pipe globally oscillates around its starting position.
- When comparing with the numerical results:
  - Again, the experimental data are globally higher than the numerical results for the test exposed to current.
  - The difference in tendencies for the pipe transverse motion under irregular waves is explained by the difference in irregular wave signal. See the graph comparison below for a direct comparison using the exact sea elevation signal in the numerical simulation.

Figure 3-29 provides a comparison between the pipe motion signal in the x-direction at both the pipe mid-length and at the pipe free extremity, at the strainer level, for the exact same irregular wave signal.

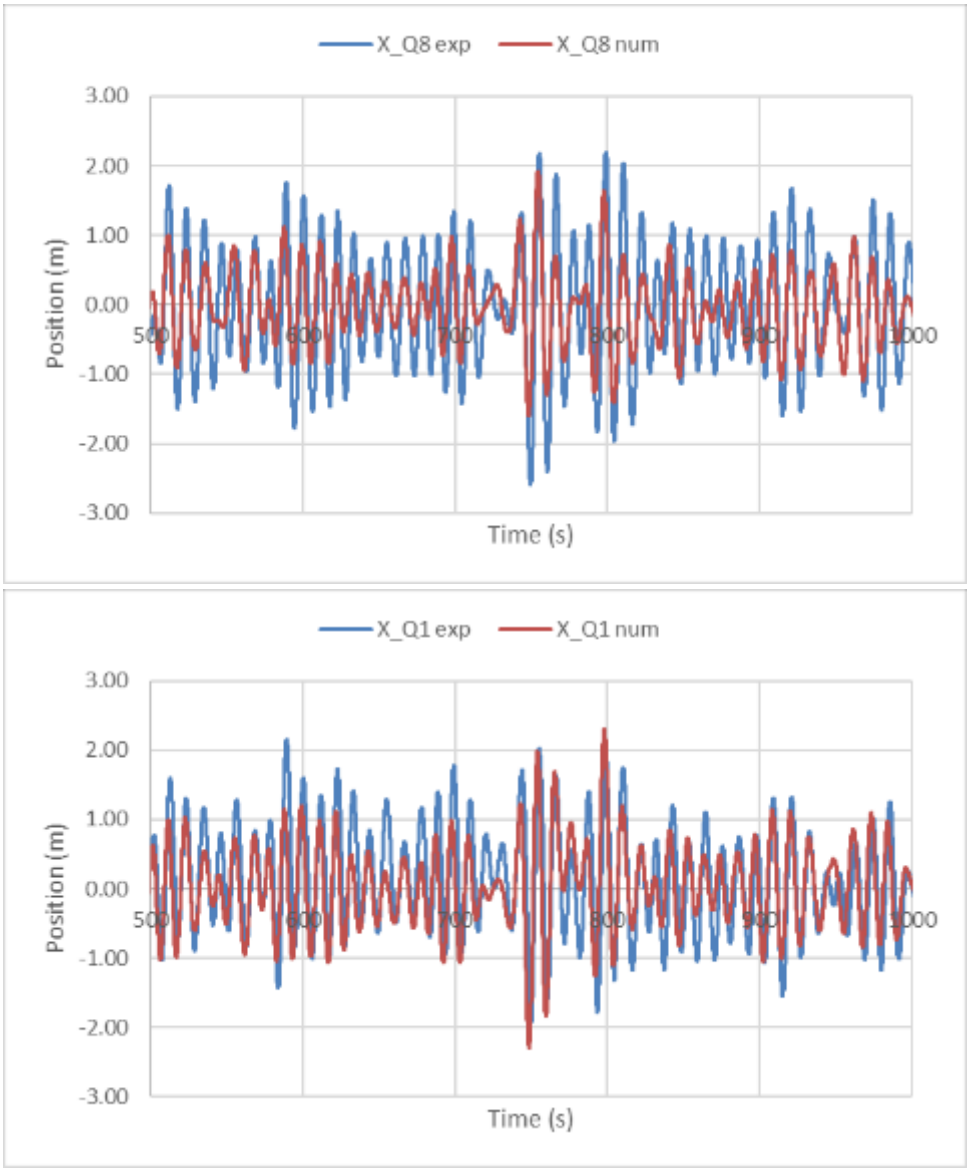

Figure 3-29: Temporal evolution of the flexible pipe at mid-length (X_Q8) and the strainer (XQ1) transverse motion exposed to IRR10Y (Configuration 1) with the initial x-offset removed from the experimental data.

- Looking at the comparative study of the time signals of the experimental tests and the numerical results, it is straightforward that under the same irregular wave signal, the numerical model predictability concerning the pipe motion is on point.
- However, it seems that the experimental data oscillations are slightly larger.

3.4.3. Buckling Tests

Initially 2 types of buckling were scheduled to be tested: namely the so-called '*initial buckling*' referring to the local deformation adopted by the flexible when bringing two neighboring clump weights together and the '*zig-zag*' flexible shape referring to the shape of the flexible pipe when the clumps weights are imposed with transverse offsets (Test matrix attached to Ref. 4).

However, due to the flexible pipe stiffness:

- For an internal pressure higher than 5 bar, it was not possible to make the pipe buckle when only moving two neighboring clump weights, may it be for the *'initial buckling'* or the *'zig-zag'* shape methodology.
- The only way to bend the pipe was to allow a collapse of the pipe, approximately at the middle, by moving almost all the clump weights transversally, so to create a 'v-shape' with the flexible pipe (Picture 3-12).
- The central transverse offset has to be significant enough for the buckle collapse to be hold at a nominal Pi of 10 bar (at least 10m).

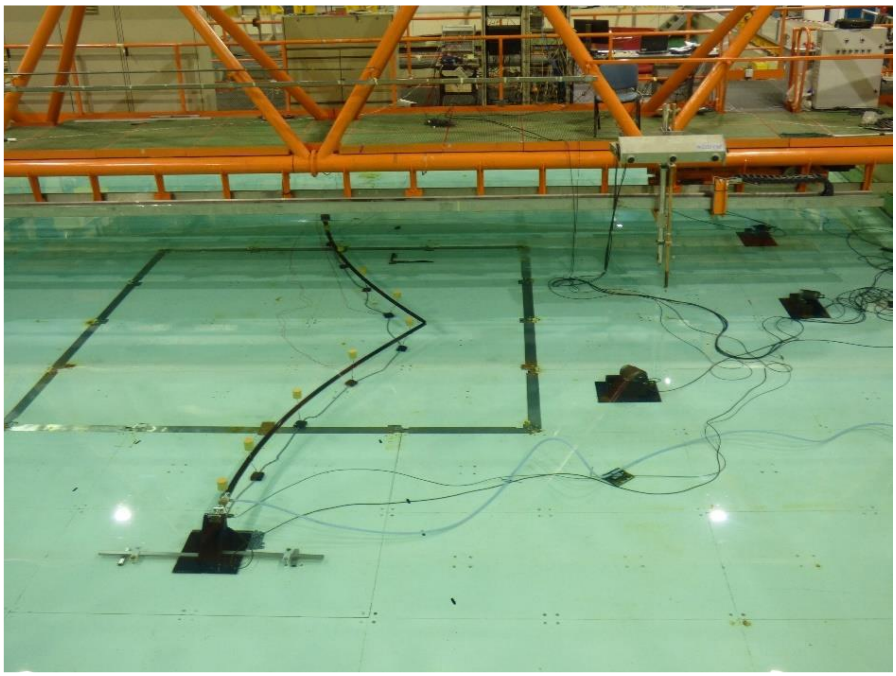

Picture 3-12: Collapsed buckling of the flexible pipe system at the pipe mid-length.

- However, the **shape deformation of a solid not covered by the Orcaflex software.** Hence, all the buckling tests were not reproduced numerically, and no comparative studies were conducted. Additionally, a collapse is to be avoided to guarantee a flow condition.
- For internal pressures greater than 10 bar, the flexible pipe is simply too stiff to even allow a buckle-typed deformation.
- During the experimental buckling tests conducted at 5 or 10 bar (with a collapse), it was observed that for a small enough central transverse offset (minimum of 10m still) REG3 is powerful enough to initiate a motion of the CW towards their initial rectilinear position.

3.5. 2nd Campaign Conclusions

To conclude this 2nd campaign, the fundamental observations and findings are listed in Section 3.5.1. The transition towards the 3rd campaign is justified in Section 3.5.2.

3.5.1. 2nd Campaign Key Points

- The axial stiffness of the flexible pipe was characterized for tension below 1000kN, and the strain vs. effective tension characterization curves were defined as bi-linear for internal pressures higher than 5bar.
- The bending stiffness was re-defined with the mean of underwater tests and was found to be lower than the one defined during the 1st campaign. Two methods were used for the EI calibration. A straightforward calibration of the z-elevation profile of the flexible pipe as a function of the Pi and a calibration of the X-natural period of the flexible pipe. Both methods lead to very close results when the frequency response of the decay test in the x-direction is single-peaked.
- Both axial and lateral seabed friction coefficient for the different anchoring components were defined. The calibration of the numerical friction tool, revealed the difficulty of calibration the axial seabed friction coefficient of the chain, given that the initial chain buckle position is unknown by Orcaflex. In fact moving the basin test seafloor up and down to change configurations, slightly modifies the chain position which has a high impact on the overall friction of the chain.

- The flexible pipe tested in the basin presented an initial distorted shape at the pipe free end, generating a significant transverse offset (shape memory).

- Under small 90° incident regular waves, the flexible pipe system adopts the u-bent position induced by the water particle circular motion, by maintaining its first and last CW on its starting position axis. For REG3, the flexible pipe system moves transversally in additions to the previous remark.
- Under the action of the current, the CW are getting into a slanted position and the flexible pipe system is being pushed transversally by the current. Note that the CW were modelled with 3D buoys Orcaflex object in the numerical model which prevented the slanting position of the CW. Additionally, the VIV observed at the buoys level could not be reproduced by the numerical model as VIV was not included.
- During the 90° incident regular wave comparison study, the numerical model transverse motions were found to be overestimated. Calibrating the hydrodynamic coefficient values of the flexible pipe for a given sea condition allowed to fall back on the same transverse experimental displacement at both the flexible pipe and CW level.

- No resonance effect at the pipe free end (at the strainer) were observed for 0° incident regular waves.

- The irregular wave tests testing for the different flexible pipe system configuration stability were well predicted by the numerical model. The AS and BS static tension and temporal evolution were

globally reproduced by the numerical model. The slack event high tension peaks were however sometimes over-estimated by the numerical model. The flexible pipe transverse motions were very well reproduced by the numerical model. The CW transverse motions however were not properly predicted by the numerical model, mainly because of the VIV omission and the use of 3D buoy Orcaflex object. Additionally, note that the CW7 was initially placed on a basin seafloor irregularity which was then covered by a wood plate which also obstructed the CW7 transverse motion due to the added thickness reducing the CW lifts and thus friction reduction.

3.5.2. Towards the 3rd Campaign

- List of suggestions to improve the numerical model and the calibration methodology:
    - Use 6D buoys for the CW modeling
    - Consistent re-alignment of the prototype in the basin
    - Deepen the calibration of the anchoring components friction coefficients, by multiplying the experimental calibration tests, the current tests, and making sure no basin floor irregularities are present, especially under the anchoring components

- Most of the tests of the 2nd campaign test matrix were included based on phenomena observed during the SubmaFlex/Via Marina projects which was using a different flexible pipe: one elongating under pressure. Hence the 3rd campaign will be using a flexible pipe similar to that of the Via Marina, in order to test for the pipe behavior in presence of a non-collapsed buckling.

- Additionally, the use of a 2nd flexible pipe will allow to test for the adaptability of the developed numerical tool calibration methodology.

- The objectives of the 3rd campaign are as follows:
    - Characterize the new flexible pipe with the developed methodology
    - Test the axial tension characterization (with both pipe ends fixed) under external sea conditions, for both flexible pipe
    - Assess the pipe behavior when encountering a small seabed slope
    - Assess the pipe behavior when one sling is broken (both BS and AS)

4. Third Campaign

4.1. Model Scale Experimental Campaign

4.1.1. Flexible Pipe System Design

The flexible pipe system used in the third campaign is the same as the one of the 2nd campaign, as described in Section 3.1.

The few novelties of the third campaign are listed as hereafter:

- Only 2 anchoring configurations were used: Configuration 1 (CW only) & Configuration 2 (Chain only)
- A second flexible pipe (Picture 4-1) elongating under pressure, was tested using the exact same system, mainly for the buckling tests.

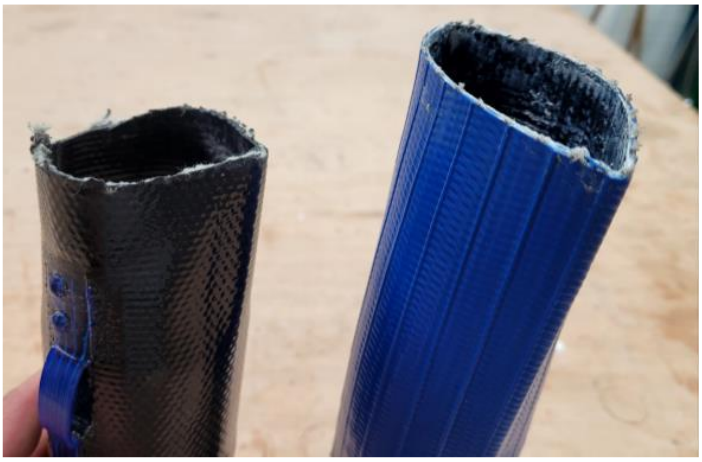

Picture 4-1: Pipe A retracting under pressure (left-hand side) and pipe B elongating under pressure (right-hand side).

4.1.2. Experimental Campaign

This section acts as an executive summary of the basin test report (Ref. 7). A succinct description of the test matrix is first provided, as well as a list of the main observations made during the experimental campaign, which are of interest for the Orcaflex model calibration.

4.1.2.1. Experimental Procedure

As detailed in the Section 3.3.1, the two test batches used for the calibration of the axial stiffness of the flexible pipe were conducted on pipe B. The flexible pipe axial stiffness was first assessed with the underwater pulley system for various internal pressure in **tests 2-5.** As a complementary step, the axial tension of the naked flexible pipe was then measured by fixing both pipe ends and gradually increasing the internal pressure in **test 1.**

Similarly, bending stiffness tests and decay tests were conducted for pipe B for both the anchoring configurations 1 and 2, respectively **tests 12 and 33, and tests 13-16 and 34-37**.

Regarding the characterization tests, the weight in water was experimentally verified for both pipes (Table 4-1), to provide a more accurate result. This is important for the calibration tests relying on the z-elevation profiles for low pulling tensions especially, which are sensitive to the mass in water, as mentioned in Section 3.3.1.

During the axial stiffness preliminary characterization of Pipe B in the air medium (Ref. 7, Section 11.1.2.), the pipe B was noticed to exhibit hysteresis : for identical cycle of internal pressure finishing with a decompression to 0bar, the flexible pipe lengthening is variable.

For the actual configuration response tests, the batches were conducted as such:

- Pipe B – Pipe Behavior with initial buckling (both ends fixed): **tests 6-11**
- Pipe B – Pipe Stability with initial buckling (fixed/free end): **tests 27-32**
- Pipe B – Pipe Stability with straight initial configuration: **tests 17-26 & 38-47**

- Pipe A – Pipe Stability with straight initial configuration in damaged condition (1 broken sling): **tests 48-85**
- Pipe A – Pipe Stability with straight initial configuration with a bump at seabed level: **tests 88-107**

4.1.2.2. Observations of Interest

The present section lists the unexpected observations made during the 3rd experimental campaign, which could be useful to understand the behavior of the physical model in the basin during the calibration of the Orcaflex numerical model. These remarks are for most of them, mentioned in Ref. 7, Section 12.

As thoroughly described in Ref. 7, Section 5.8., two rectangular wood plates [13.6 m x 2 m x 0.1 m] were added under CW2 and CW8 (Picture 4-2**Erreur ! Source du renvoi introuvable.**), adding an additional thickness at these two locations which can have an impact in the transverse motion of the flexible pipe system, as seen during the calibration of the 2nd campaign.

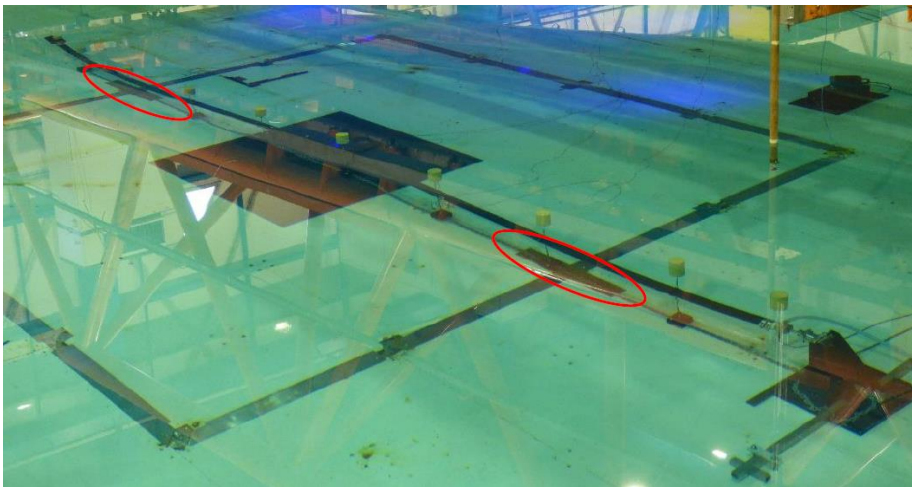

Picture 4-2: Location of the two rectangular wood plate underneath CW2 and CW7.

It should also be mentioned that the Qualysis targets supposedly positioned on the pipe center line depicted in red in Picture 4-3, can happen to be slightly shifted. Most likely, the pipe undergoes torsion potentially caused by the CW misalignment which can brings the QT downwards, as shown in Picture 4-3. As a result, divergencies in the pipe Z-position between the numerical and the experimental results, should be considered by taking this trend into account (especially when calibrating the numerical model on the pipe z-elevation profile, as in Sections 4.3.1 and 0).

Similarly, during the axial stiffness tests on Pipe B which used a pulley system, it was noted that the depending on the pulling forces hauling in the boot, the vertical aluminium beam was bending towards the flexible pipe (Picture 4-4). The higher the pulling force, the higher the vertical beam displacement. More importantly, this displacement is thus leading to a variable reference point location, regarding the end of the vertical beam. Again, this trend should be remembered when considering the uncertainty on the axial bending calibration (Sections 4.3.1).

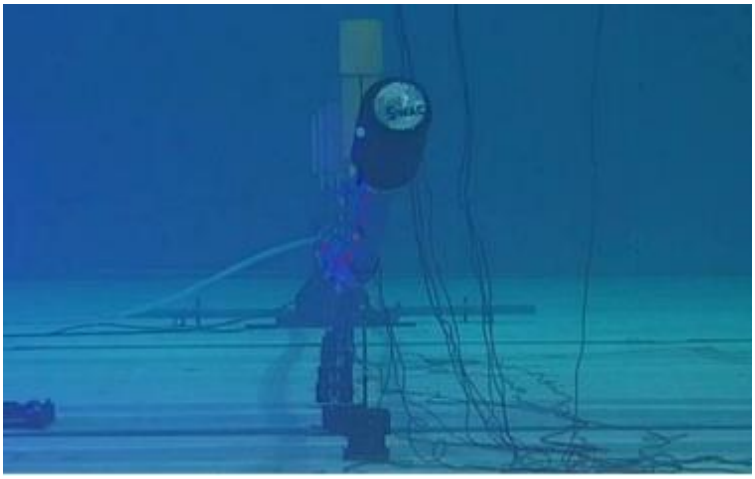

Picture 4-3: Focus on the Qualysis target's location along the flexible pipe B (test 33). The pipe mid-line is depicted in red.

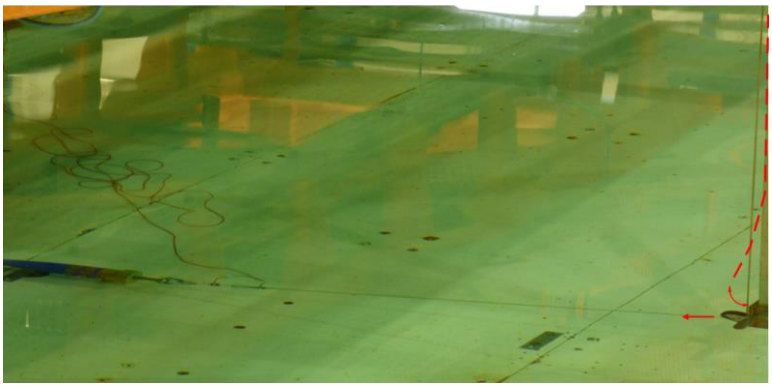

Picture 4-4: Pulley system used in tests 2-5 to characterize the pipe B axial stiffness.

Incidentally, it happens that the buoy used to make the weighting end connection B neutrally buoyant, when the flexible pipe system is fixed at both ends was unintentionally kept during the entirety of the third campaign (Picture 4-5). As a result, this additional buoy was included in the numerical model for the sake of consistency. Moreover, this additional buoy also caused the flexible pipe to buckle towards the water surface when at very low internal pressure (Picture 4-6).

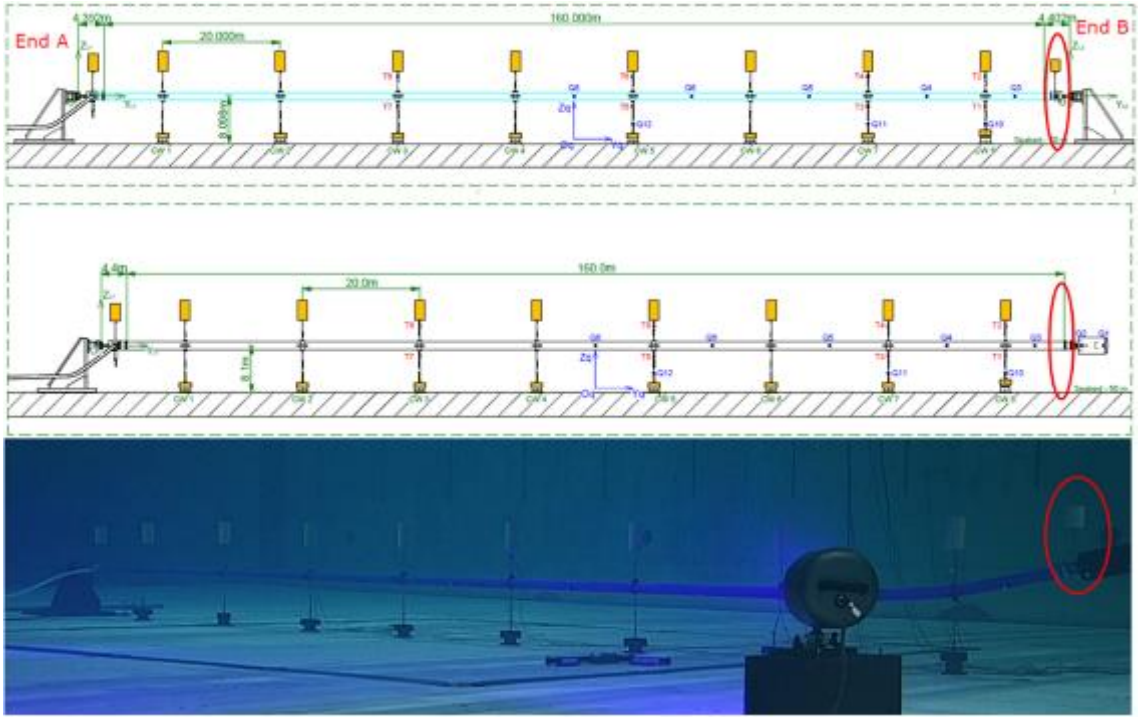

Picture 4-5: Drawings of the flexible pipe system with both ends fixed (top), one free end and the strainer (middle) and implementation of the prototype in the basin with one free end and the strainer with the end B buoy (bottom).

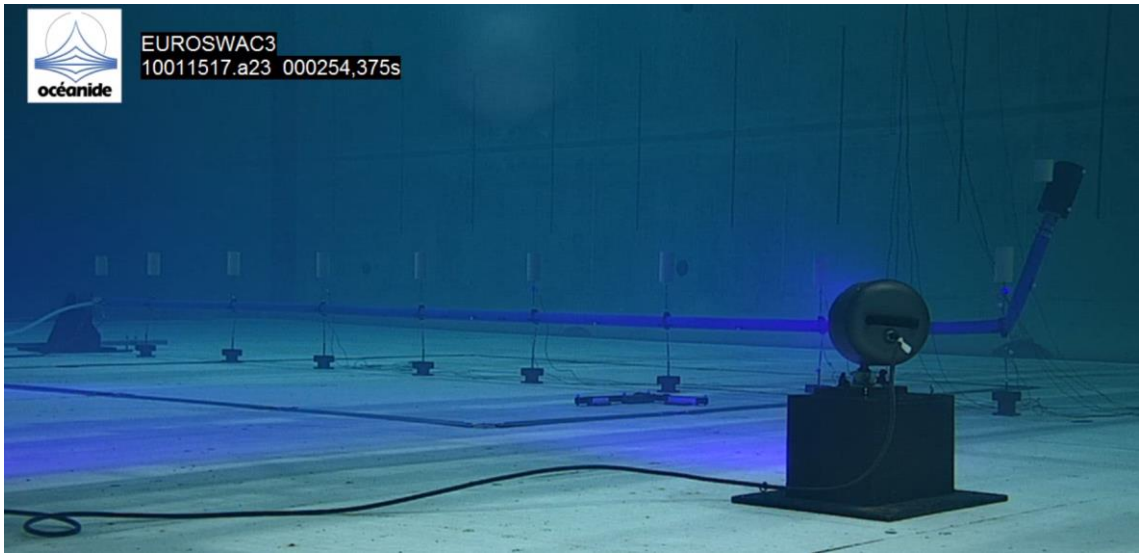

Picture 4-6: Buckle collapse of the flexible pipe towards the water surface of approximately 75° when at approximately 500kPa of internal pressure (test 12).

Regarding the tests testing for non-collapsed buckles:

- The pipe B elongating under pressure, allowed the formation of non collapsed buckles.
- The additional length trapped in the fixed inter-distance between the two connection points, thus buckles, mainly transversally and in an unpredictable trend, given the uncharacterized woven elastic material of the flexible pipe (Picture 4-7).
- For the axial tension characterisation test, the nominal distance between the fixation points corresponding to the flexible pipe and its end connection length, was increased to both avoid the flexible pipe to touch the ground at the highest Pi and to avoid any buckles.

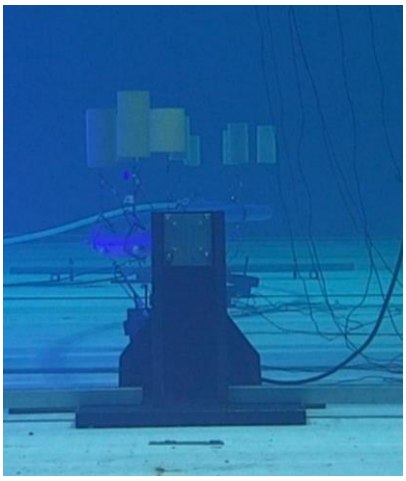

Picture 4-7: Pipe with initial buckling and both ends fixed at Pi = 40bar (test 27).

Regarding the tests investigating the flexible pipe system behaviour when lacking one sling (damaged condition):

- Intense flexible pipe system responses for damaged condition under REG2 were noted, thus all the tests scheduled for the damaged conditions under REG3 and REG3 + current, were not conducted.
- The combined effects of the additional buoy at pipe end B and the removal of the AS 8 brought the flexible pipe too close to the water surface (Picture 4-8), thus it was chosen to test for the breakage of AS 6 instead.

Picture 4-8: Flexible pipe system static sate with AS 8 removed (test excluded of the test matrix).

4.2. Numerical Model Implementation

4.2.1. Flexible Pipe, End Connection & Strainer

Erreur ! Source du renvoi introuvable. provides the main dimensions of the flexible pipe B "H2O Pompes 1340mm" and its connections used as input data in Orcaflex model.

	Length	OD	ID	Mass per unit (air)	Mass (water)	EI	EA
-	[m]	[m]	[m]	[t/m]	[kg]	[kN.m2]	[KN]
H2O Pompes 13400mm	160	1.34	1.253	195.4	2847	Note 1	Note 1
End A	4.392	1.037	0	1.837	4363	8.58E+07	9.07E+07
End B	2.4	1.199	0	1.861	-3041 (3)	8.58E+07	9.07E+07
Strainer	5.008	2.9	0	5.2		8.58E+07	9.07E+07

Table 4-1: Orcaflex input data concerning the flexible pipe "H2O Pompes", both end connections, and the strainer.

- Note 1: These results depend on the internal pressure. The evolution of the axial and bending stiffnesses in function of the pressure are respectively further specified in Section 4.3.1 and 4.3.2.

- Note 2: For the sake of simplicity, it was chosen to only implement the correct masses (in air and water) in the numerical model, when the object to model had a complex shape. As a result, the Line section diameters displayed in **Erreur ! Source du renvoi introuvable.**, have been slightly modified.

  Note 3: Since End B and the strainer were embedded together, and that the experimental mass in water was verified by combining both elements by Océanide, the mass in water is provided for both elements combined.

As observed in the calibration of the 2nd campaign, the hydrodynamic coefficients of the flexible pipe play a key role in the transverse motion amplitude since the flexible pipe is not fixed at the anchor slings anymore. **Erreur ! Source du renvoi introuvable.** provides an estimation of the hydrodynamic coefficients in Ref. 11, to be specified in the Orcaflex software.
Additionally, according to the DNV C205 Ref. 10 (Section 6.7.2.4.), it was found that when subjected to both an oscillatory motion, and a steady current which velocity is four times greater than the wave maximum orbital velocity, then the Cd of the object exposed to this sea condition can be considered to be equal to its steady value.

Sea condition	C_M	C_D
REG1	1	1
REG2	0.8	1.5
REG3	0	1.7
Current	1	1.2
Current + REG3	1	1.2

Table 4-2: Flexible pipe hydrodynamic coefficients (added mass coefficient and drag coefficient) in function of the sea condition.

4.2.2. Remaining Flexible Pipe System Components

The buoys used in the third campaign are specified in Table 4-3 hereafter.

		Buoy type 2 (1)	End A Buoy (2)	End B Buoy (2)
Shape	-	Cylinder	Cylinder	Cylinder
Volume	m3	7.56	6.71	4.57
Diameter	m	1.69	1.69	1.69
Height	m	3.38	3.00	2.04
Mass in air	kg	2645	2350	1598
Mass in water	kg	-4912	-4364	-2967

Table 4-3: Third campaign buoys main parameters.

Note 1: Buoys used in the 2nd campaign.

Note 2: Buoys used to make both pipe end connections neutrally buoyant.

Regarding the numerical modelling, the same methodology as described in Section 3.2.3 was adopted. A minor adjustment was performed on the numerical sling parameters (

		Real AS	Numerical AS	Real BS	Numerical BS
Length	m	3.46	4.43	3	3.97
Diameter	m	0.123	0.123	0.0896	0.0896
Mass in air	kg	93.3	93.3	49.3	49.3
Mass in water	kg	81.4	81.4	43	43
EA	kN	1190	1523	2046	2708

Table 4-4), to consider the difference in pipe diameters between pipe A and pipe B. The pipe B diameter is smaller, and thus the additional numerical length added to the numerical sling is smaller (0.97m instead of 1.007m).

		Real AS	Numerical AS	Real BS	Numerical BS
Length	m	3.46	4.43	3	3.97
Diameter	m	0.123	0.123	0.0896	0.0896
Mass in air	kg	93.3	93.3	49.3	49.3
Mass in water	kg	81.4	81.4	43	43
EA	kN	1190	1523	2046	2708

Table 4-4: Third campaign sling main parameters (associated to pipe B).

The anchoring components of anchoring configuration 1 and 2 used in this third campaign were kept identical as described in Section 3.2.4, in the numerical model used for this third campaign.

4.3. Numerical Model Calibration Axes

In the same manner as for the flexible pipe A, the flexible pipe B was experimentally characterized; both in terms of axial stiffness and of bending stiffness. In this section, the already introduced methodology to incorporate these data as user specified Orcaflex inputs, is presented. No further topics which could require a numerical model validation process were identified during this third campaign.

4.3.1. Axial Stiffness Calibration

The pressure dependent axial stiffness of flexible pipe B was first characterized in air with air-induced pressure, as described in Ref. 7, Section 11.1.2.

It was noticed that:

- For a given load, the flexible pipe undergoing a cycle pressure starting and finishing at 0bar, does not yield the same initial and final lengthening value.
- Similarly, for a given pressure, the flexible pipe undergoing a loading cycle starting and finishing at 0kN, does not yield the same initial and final lengthening value.
- The flexible pipe is thus demonstrating a hysteresis behavior.
- One direct consequence is the variability of the flexible pipe stiffness, and in turn the approximate estimation of its axial stiffness.

Nonetheless, the axial stiffness was assessed as defined previously (Section 3.3.1), with the combined use of **tests 2-5** and **test 1,** respectively investigating the flexible pipe axial stiffness in function of both the internal pressure (5bar-40bar) and the pulling tension (300-100kN); and by defining the exact initial pipe length in function of the internal pressure (by matching the effective tension behaviour when both pipe ends are fixed).

(a)

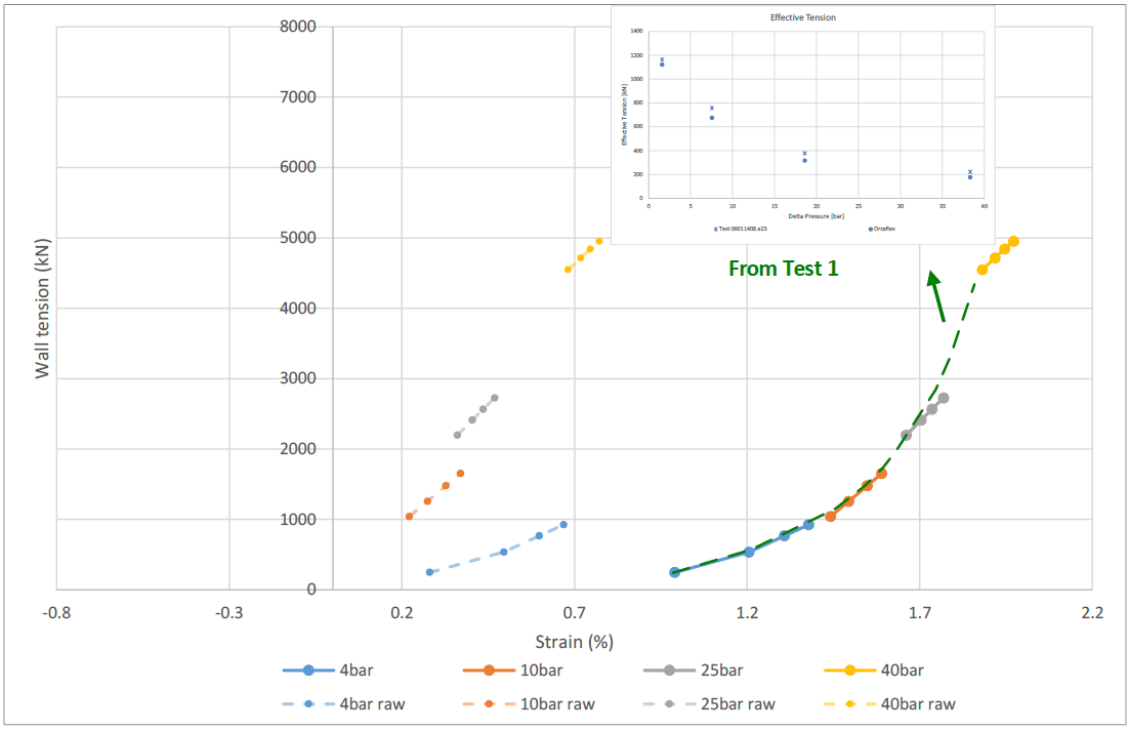

(b)

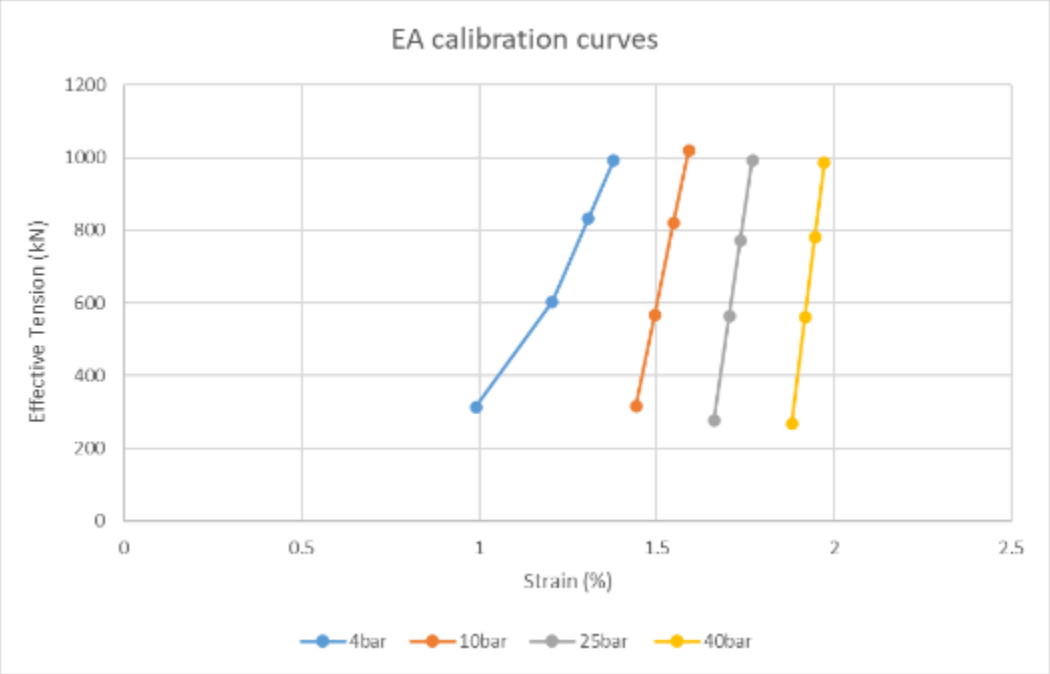

Figure 4-1: Calibrated EA curves for pipe B obtained from the 3rd campaign calibration expressed through (a) wall tension in function of the strain (%) *, and (b)* effective tension in function of the strain (%).

In the same manner as for the first campaign, the elevation profiles of the flexible pipe numerical model, for each pressure, were calibrated by iteratively modifying the EA value for a given pulling tension, until matching with the experimental ones (**tests 2-5**). The initial EA guess value is obtained from the in-air characterization tests. In doing so one strain[%]/Tw[kN] curve is obtained for each internal pressure (4bar, 10bar, 25bar, 40bar). Thanks to **test 1,** these EA characterisation curves were then adjusted so to respect the pipe effective tension (i.e., determine the initial pipe length) behavior in function of the Pi (Figure 4-1a).

It is straightforward that pipe B is elongating under pressure: this elongation ranges from 1% to 2% for internal pressures comprised between 4 and 40bar.

Additionally, it can be noticed when considering Figure 4-1b, that compared to the EA curves of pipe A, those characterizing pipe B are all linear to the exception of the 4bar one.

Similarly, these EA curves were imported in a MathCad sheet as database for linear interpolation, to obtain such an EA curve for any Pi ranging between 4bar and 40bar.

4.3.2. Bending Stiffness Calibration

As stated in Section 4.1.2.2 , the flexible pipe featured a buckle collapse at low Pi (approx. 4-5bar). Thus, the estimation of the flexible pipe EI at this PI could not be performed, given the deformation of the flexible pipe not supported by the Orcaflex software.

In agreement with Section 3.3.2, the calibration of the pipe B EI was conducted on anchoring Configuration 1, given the absence of a chain in the anchoring components. In fact, the chain exact initial position is not known by the OrcaFlex software, given the seabed immersion, the sequential aspect of the experimental tests modifying the chain position, and the approximative and not systematic chain repositioning between each test.

The experimental elevation profiles of **test 12** were used as a reference to calibrate the EI values of pipe B. For the three tested internal pressures: 10bar, 25 bar, and 40 bar, the profiles were matched so to make the "free" part of the flexible pipe system (i.e., close to the strainer) overlap with the z-profiles recorded in the basin.

In Section 4.1.2.2, the position of the QT was discussed and is reminded here, to justify the choice of reference points in the elevation profile calibration. As can be seen in Picture 4-9, most of the Qualysis targets have slightly shifted from their initial mid axis position, which led to a selection of the QT to keep as reference point for the elevation calibration. Q8 as well as Q2 and Q1 have been qualified as the closest to their theoretical position on the flexible pipe, and thus used in the EI calibration process.

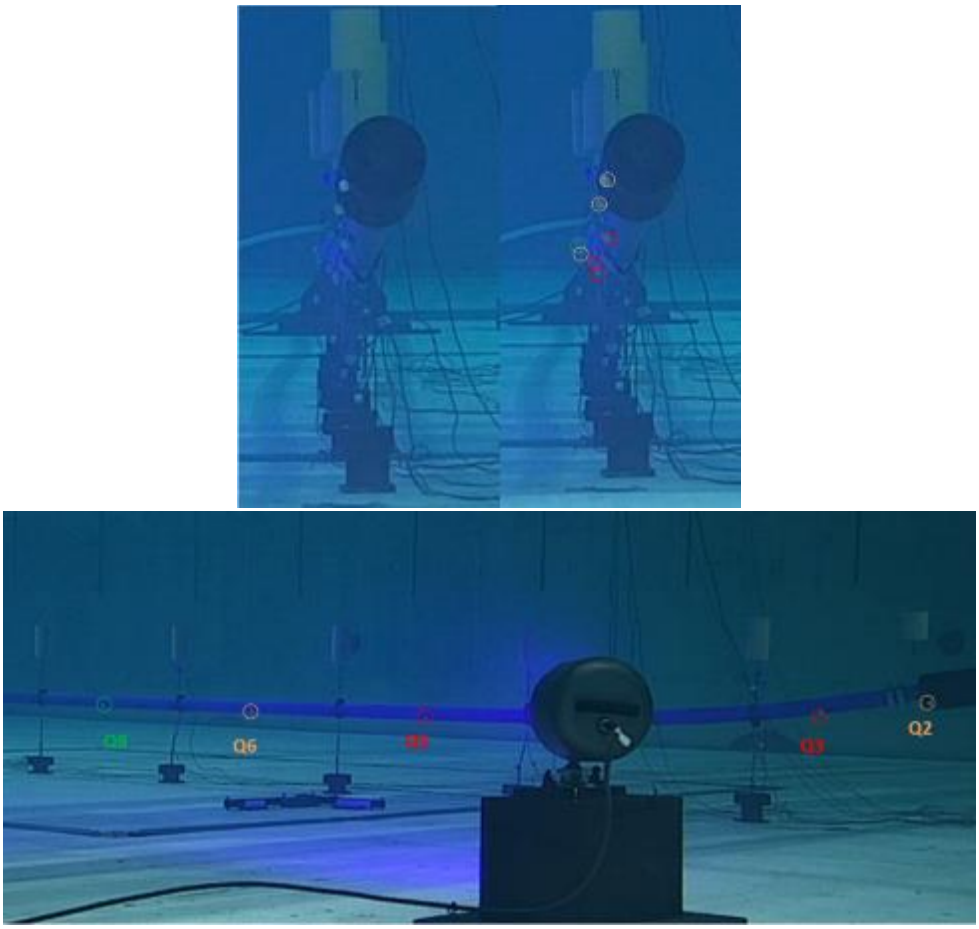

*Picture 4-9: Qualysis targets location on the flexible pipe during the bending stiffness test of configuration 1 (**test 12**), transverse view (top), and longitudinal view (b).*

It should however be mentioned that the following EI values might be slightly overestimated giventhe downwards position of Q2 and Q1 (i.e., QT on the strainer) which are still slightly misplaced with regards to their supposedly mid-axis position.

Figure 4-2 depicts the elevation profiles recorded during the experimental campaign, as well as the elevation profiles obtained from the calibrated numerical model. As introduced before, the reference points are Q8 (arc length of 84.4m), Q2 (arc length of 167.8m), and Q1 (arc length of 170.8m).

The obtained EI values are listed in Table 4-5.

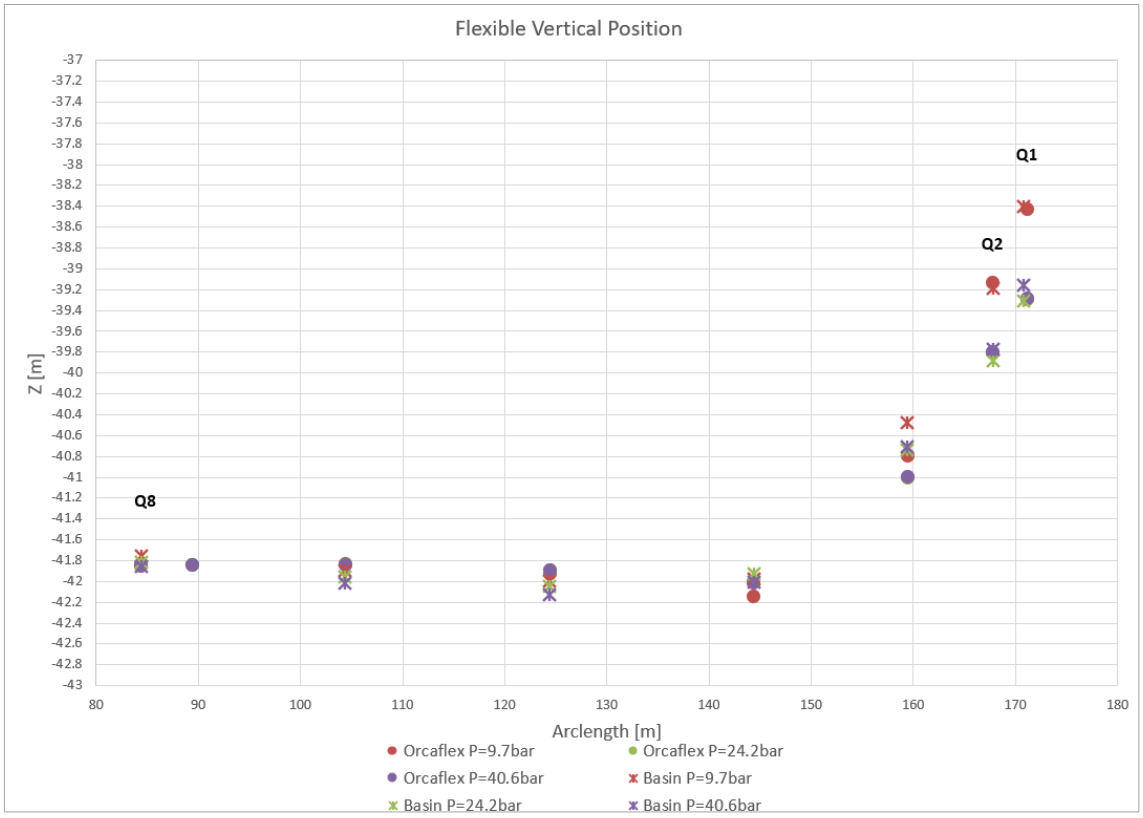

*Figure 4-2: Pipe B elevation profiles as a function of the internal pressure for anchoring Configuration 1 (**test 12**).*

Pi [kPa]	EI [kN.m2]
973	57000
2417	82000
4058	82000

Table 4-5: Pipe B EI values obtained through the elevation profile method.

4.4. Comparative Study between the Experimental and Numerical Data

4.4.1. Introduction

This comparative study concerns the five different physical models tested during the third campaign:

1. Pipe B, new pipe material that tends to elongate under pressure, anchored in configuration 1 (with clump weights only), deployed on a flat seabed and tested in irregular wave conditions,
2. Pipe B anchored in configuration 2 (with chain only) deployed on a flat seabed and tested in irregular wave conditions,
3. Pipe A, already used during the two previous campaigns, anchored in configuration 1 (with clump weights only), deployed on a bumped seabed and tested in irregular wave conditions,
4. Pipe A anchored in configuration 2 (with chain only), deployed on a bumped seabed and tested in irregular wave conditions,
5. Pipe A anchored in configuration 2 (with chain only), deployed on a flat seabed and tested in regular wave conditions considering a damage case simulating the loss of 1 of the following slings:
   - Anchor sling 6,
   - Anchor sling 7,
   - Buoyancy sling 7,
   - Buoyancy sling 8.

An OrcaFlex model of each of the 5 physical models listed above is set and calibrated using the results of two previous campaigns and the characterisation tests performed on pipe B, presented in sections 4.3.1 and 4.3.2. The objective is to apply the calibration methodology developed within the framework of this project to these 5 specific cases. Then, each environmental condition generated during the campaign is run numerically and a systematic comparison between numerical results and physical measurements is performed to validate the calibration procedure and the numerical models.

The following lists the differences existing between the numerical model and the physical model:

- The buoys and clump weights are modelled in the OrcaFlex model as 3D elements. Consequently, for these elements, only translations are considered. However, during the tests some important rotations of the clump weights have been observed.
- For irregular wave conditions, the wave elevation time series have been recomputed in OrcaFlex using the spectral characteristics of the wave. Consequently, wave elevation time series is not strictly the same between the numerical model and the physical model.
- The numerical model can be considered as a perfect world. In this model, the pipe and chain are perfectly straight at the beginning of the simulations and all elements have a perfect symmetry plane. Physical testing is real world. During the campaign, the tests are performed one after another leading to different initial conditions for the flexible pipe and the anchoring system.
- The characterisation of the friction coefficient between the chain and the tank floor was not conclusive. Consequently, a generic friction parameter has been selected.

Based on the above observations, the comparison presented in this section is more qualitative than quantitative. Finally, the objective is to show that for both numerical and physical models, the parameters of interest have the same orders of magnitude and exhibit the same tendencies.

4.4.2. Comparison Presentation

Comparison focuses on the main parameters of interest in a design point of view:

- The hydrodynamics behaviour of the pipe and thus the pipe motions at the 8 measurement locations spread along the flexible pipe,
- The axial tensions measured in the 4 anchor slings instrumented during the tests with a 1D load cell.

During the tests, it was observed that the variations of tension in the buoyancy slings are very low. This observation was confirmed by the numerical study. Consequently, this parameter is not considered as of interest for the present comparative study. In addition, for a wave heading of 90 deg, i.e., transverse to the main flexible pipe axis, the 3D motions are compared while for a wave heading of 0 deg, i.e., in-line to the main flexible axis, only vertical motions are compared as in-line and cross-flow horizontal motions are of very low amplitudes for this case.

The statistics considered in the comparisons are:

- The maximum values for the tensions in the slings that can be considered as the design values,
- And the standard deviation for the flexible pipe motions as the observed motions are low and that the extreme values are more impacted by the initial conditions of the tests that might differ between the numerical model and the physical model.

Finally, comparison is performed using 2D plots comparing the values measured during the campaign that are plotted versus results extracted from the numerical model as illustrated by the two figures below. One plot is provided for each pipe tested configuration: pipe A or B, flat or bumped seabed, without or with 1 sling loss. Each figure includes all the tests performed for each pipe condition. Finally, each point in the plot is a comparison point and the closest the point is from the line y=x the better is the comparison between the physical model and the numerical model.

The first example below shows that the numerical and physical models compare very well as all the points are close to the 'y=x' curve. This demonstrates that the numerical model well predicts the maximum tensions in the anchor slings.

The second example shows that both models exhibit a very similar tendency as the points forms a linear curve. This shows that the numerical model provides the same tendencies as the physical model but tends to underestimate the pipe vertical motions.

On all following comparisons, tensions are given in kN, and pipe motions are in meters.

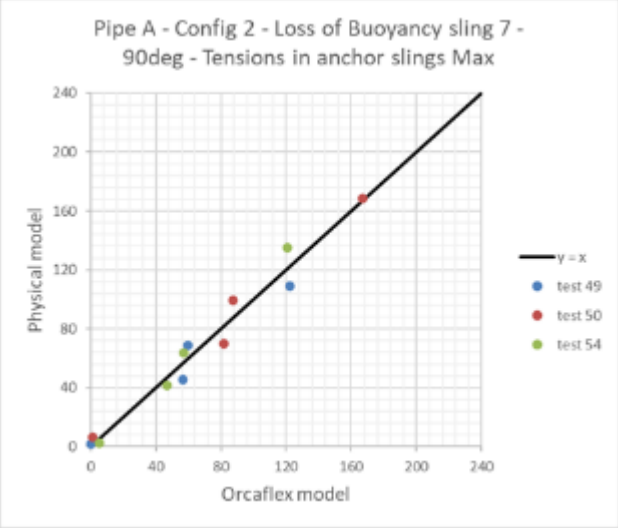

Figure 4-3: Example 1 of comparative plot between physical model and numerical model.

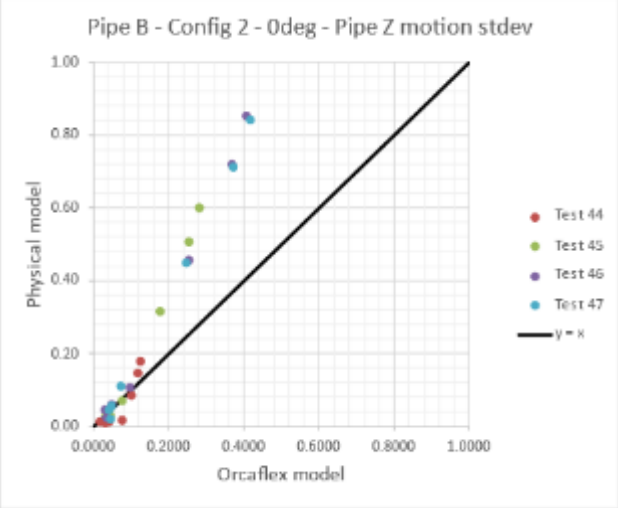

Figure 4-4: Example 2 of comparative plot between physical model and numerical model.

4.4.3. Pipe B: Comparison of Numerical and Physical Results

From the set of comparison plots provided here-after, it comes:

- For all cases, both numerical model and physical model exhibit the same tendencies and the same orders of magnitude for all parameters,
- The numerical model predicts very well the maximum tensions in the anchor slings for all cases and pipe behaviour for anchoring configuration 1, i.e., with clump weights only,
- For the chain only anchoring configuration, numerical model tends to underestimate the pipe motions. Two causes might explain these discrepancies. First, the initial position of the chain is not similar between the numerical model and the physical model. In the numerical model, the chain is rectilinear at the beginning of the simulation while in the physical model the chain initial position is impacted by the motion history of the previous test. Secondly, a typical friction coefficient was used to simulate the impact of the basin floor on the chain. Consequently, it is expected that a better characterisation of the chain friction would yield to more reliable numerical predictions.

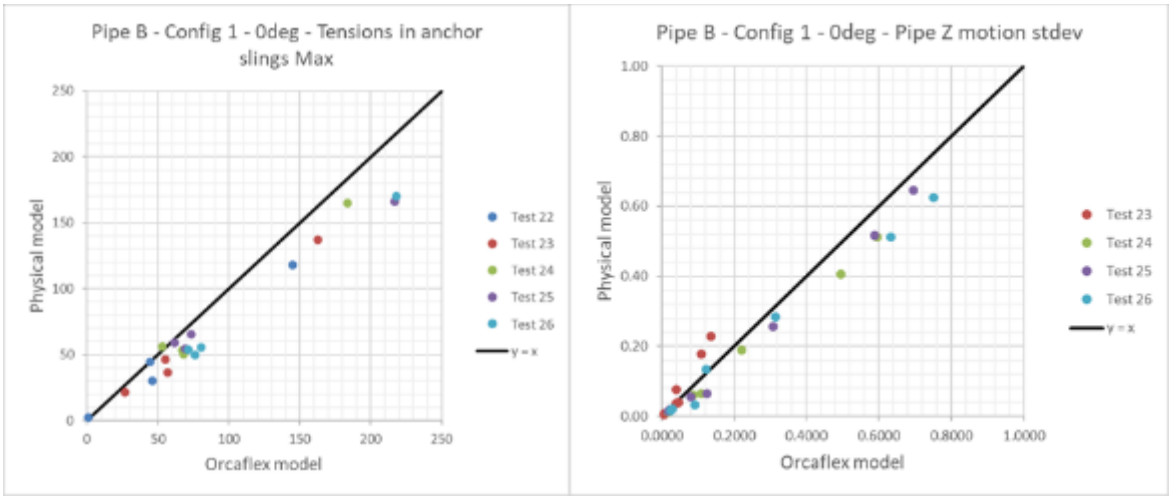

Figure 4-5: Pipe B – Configuration 1 – Wave at 0 deg.

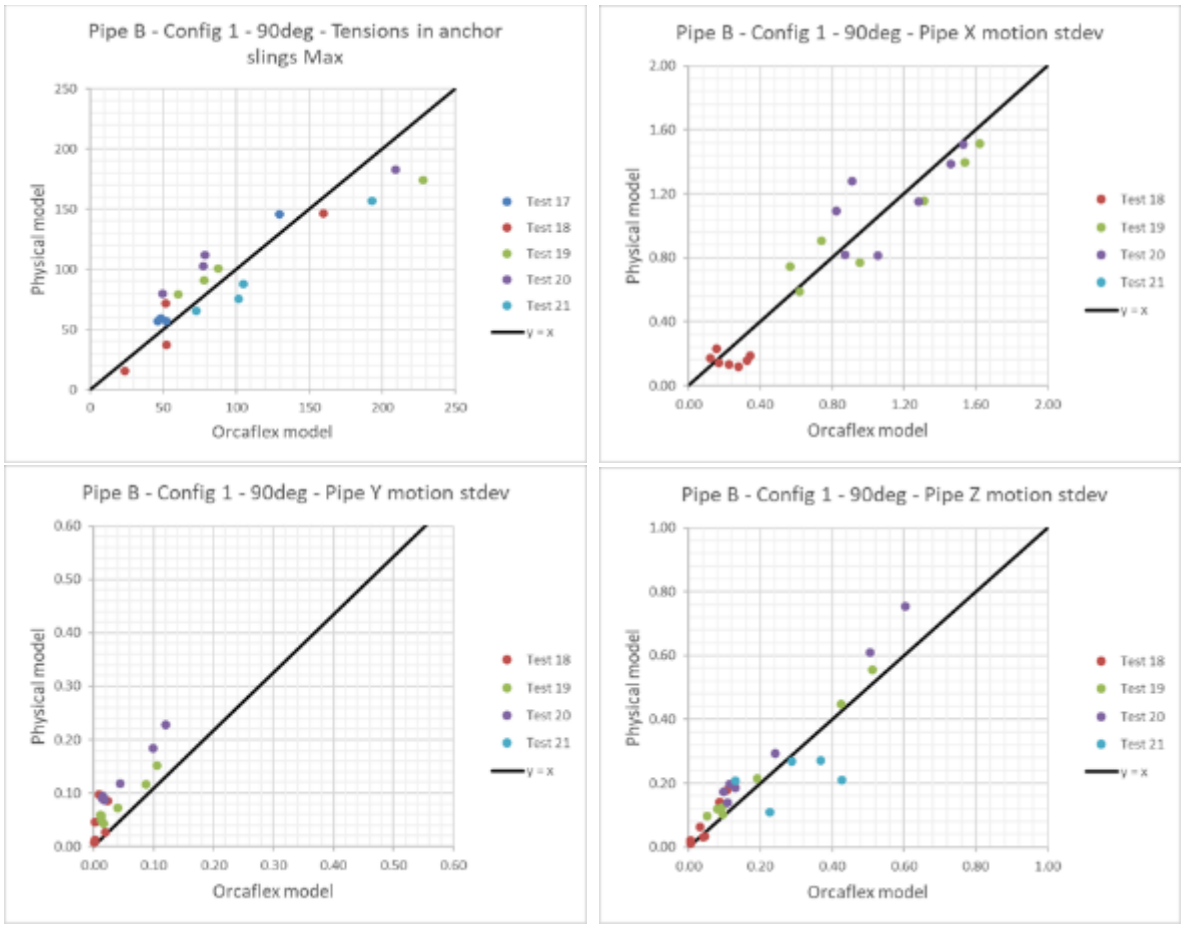

Figure 4-6: Pipe B – Configuration 1 – Wave at 90 deg.

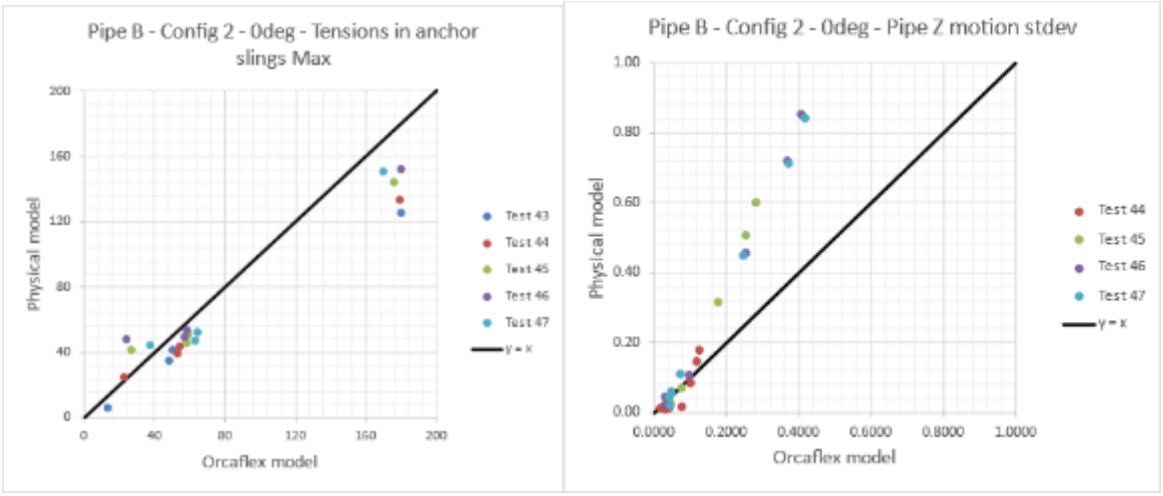

Figure 4-7: Pipe B – Configuration 2 – Wave at 0 deg.

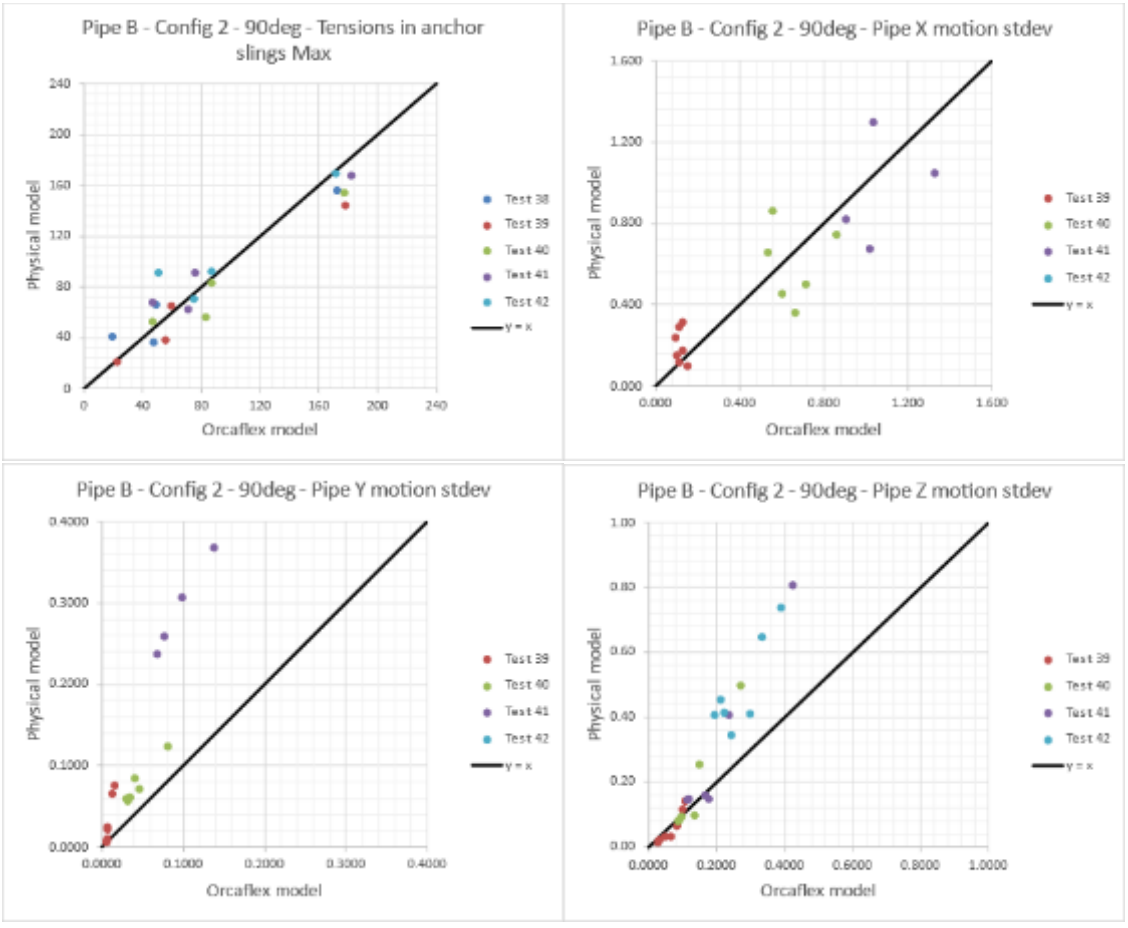

Figure 4-8: Pipe B – Configuration 2 – Wave at 90 deg.

4.4.4. Pipe A Laid on a Bump: Comparison of Numerical and Physical Results

For this configuration, comparison between the numerical model and physical model leads to the following observations:

- Again, the numerical model predicts very well the maximum tensions in the anchor slings,
- Regarding the pipe motions, even if both numerical model and physical model exhibit the same tendencies, the numerical model results exhibit more discrepancies than for the flat seabed condition. However, no clear trend can be extracted, sometimes the numerical model tends to underestimate and sometimes to overestimate the results.

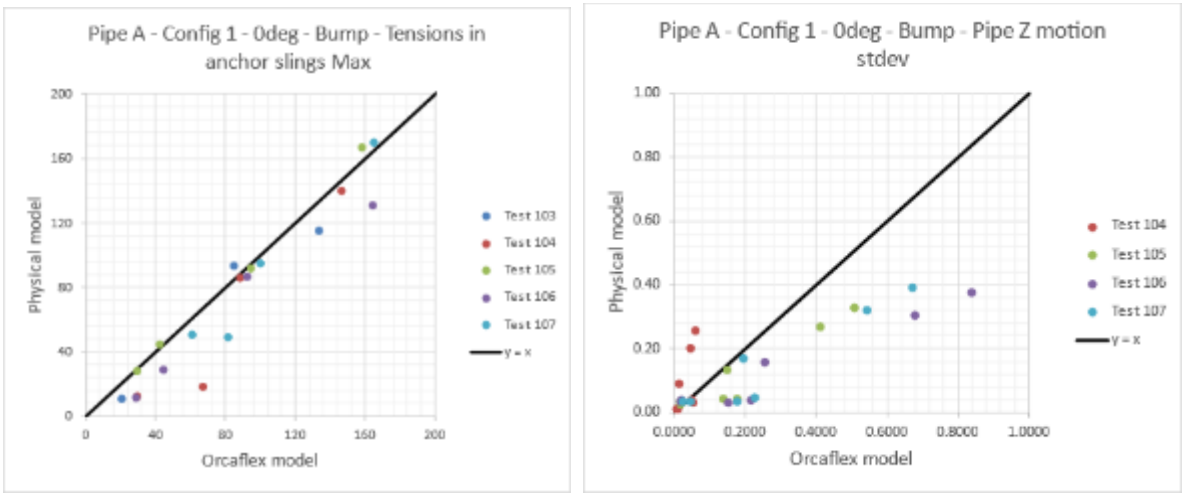

Figure 4-9: Pipe A laid on a bump – Configuration 1 – Wave at 0 deg.

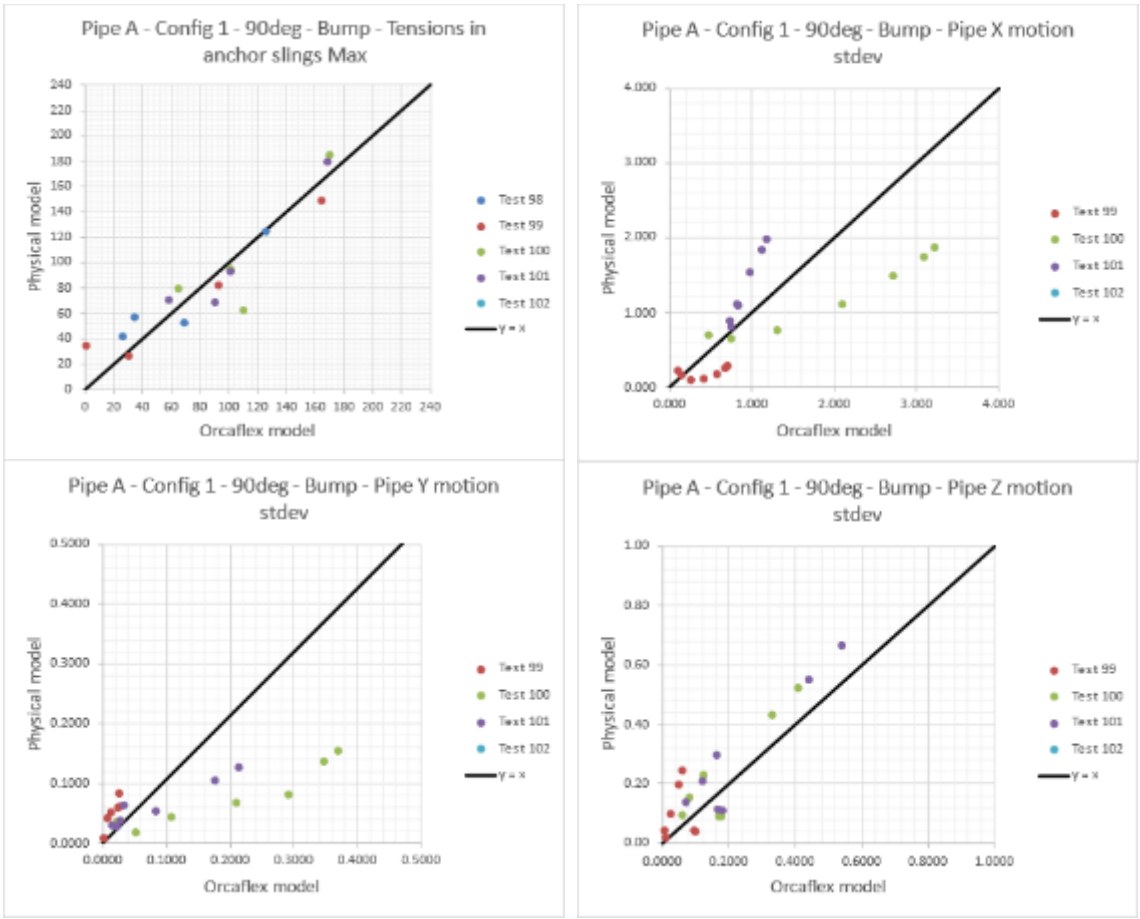

Figure 4-10: Pipe A laid on a bump – Configuration 1 – Wave at 90 deg.

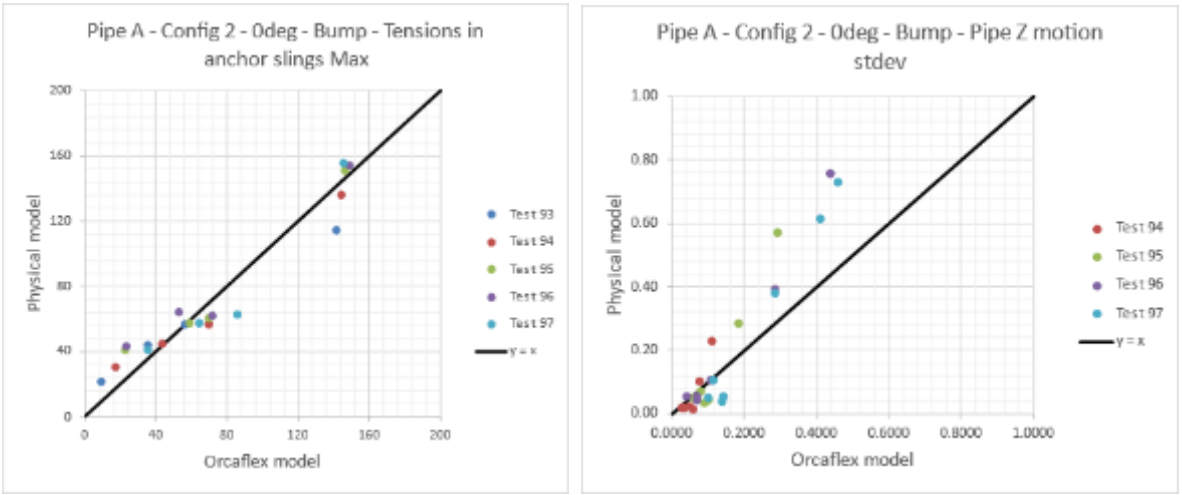

Figure 4-11:Pipe A laid on a bump – Configuration 2 – Wave at 0 deg.

4.4.5. Pipe A in Damage Conditions: Comparison of Numerical and Physical Results

Damage conditions have been tested in regular wave conditions only.

For these cases, the comparison between results from the numerical model and measurements from the physical model illustrated by the figures below shows that:

- The numerical model predicts very well the maximum tensions in the anchor slings for all cases,
- Regarding the pipe motions, the tendencies and orders of magnitude are the same between the two model. However, points are more spread than for the previous comparisons. This might be explained by the fact that during regular wave tests the system tends to drift during the tests modifying the initial conditions of the next test and impacting thus the behaviour of the pipe.

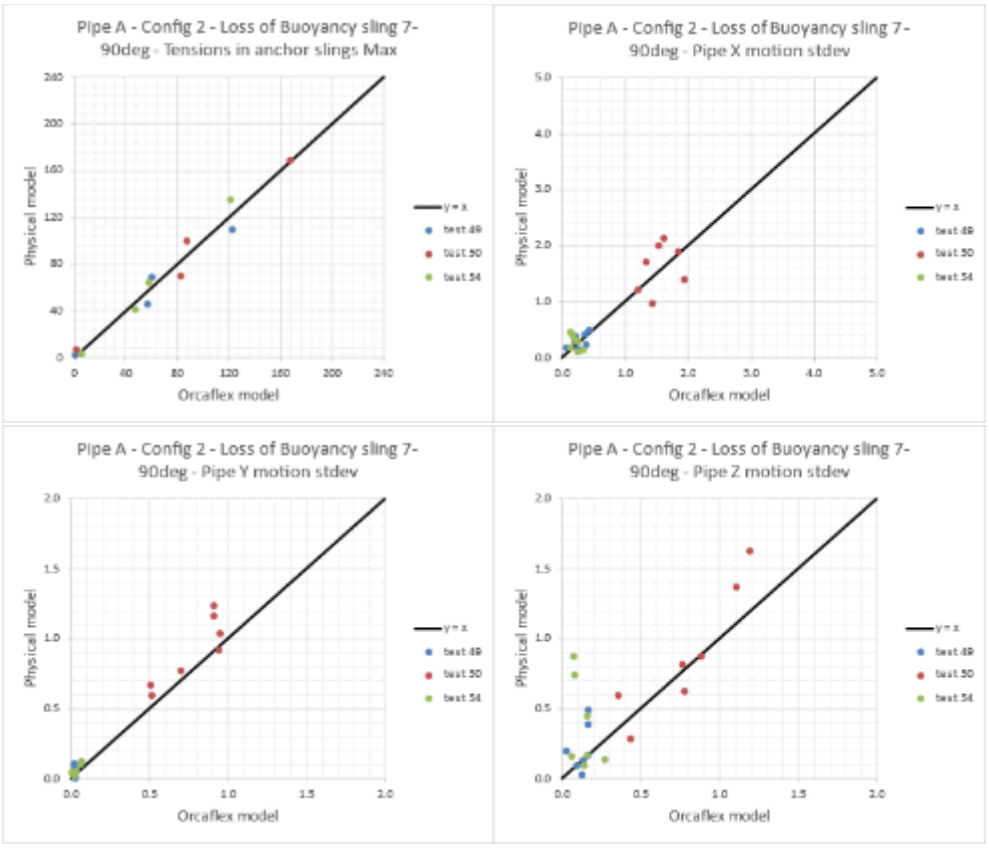

Figure 4-12: Pipe A – loss of buoyancy sling 7 – Configuration 2 – Wave at 90 deg.

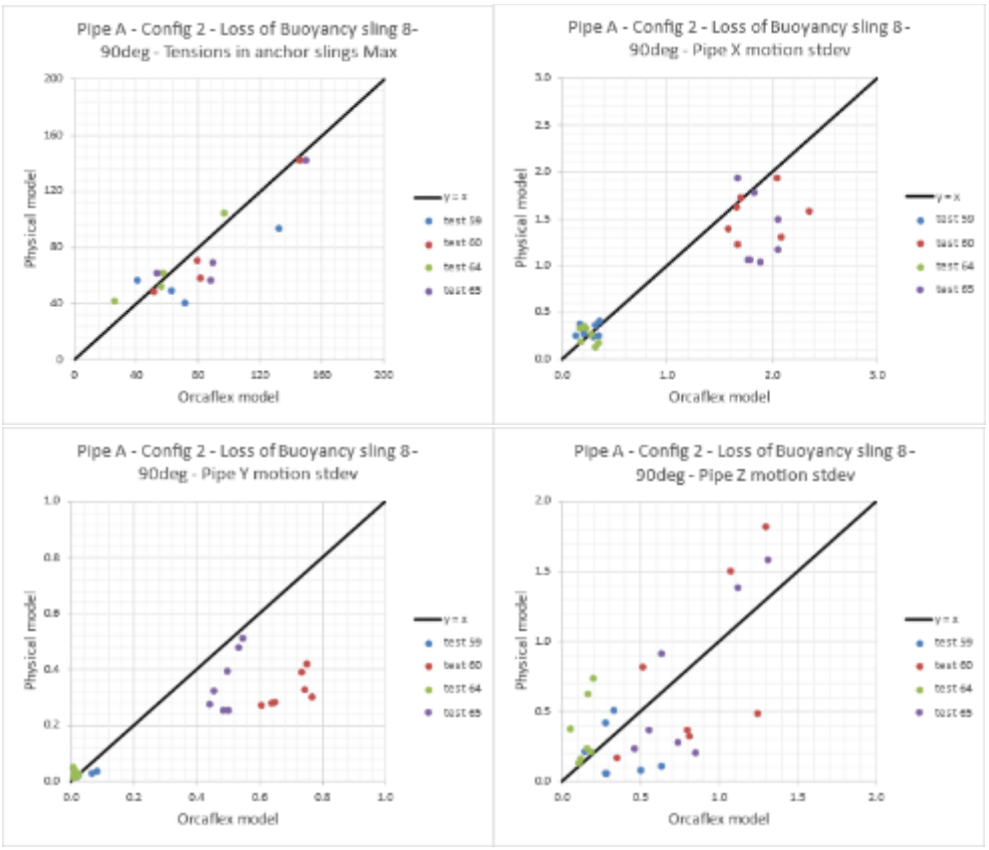

Figure 4-13: Pipe A – loss of buoyancy sling 8 – Configuration 2 – Wave at 90 deg.

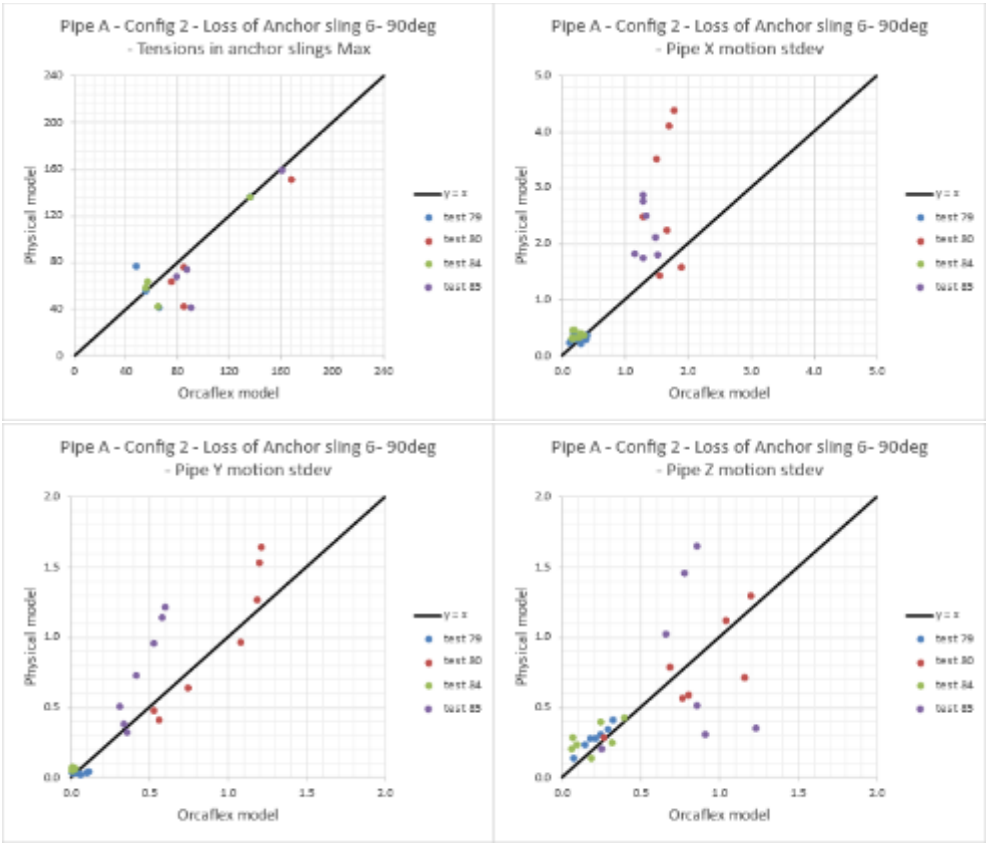

Figure 4-14: Pipe A – loss of anchor sling 6 – Configuration 2 – Wave at 90 deg.

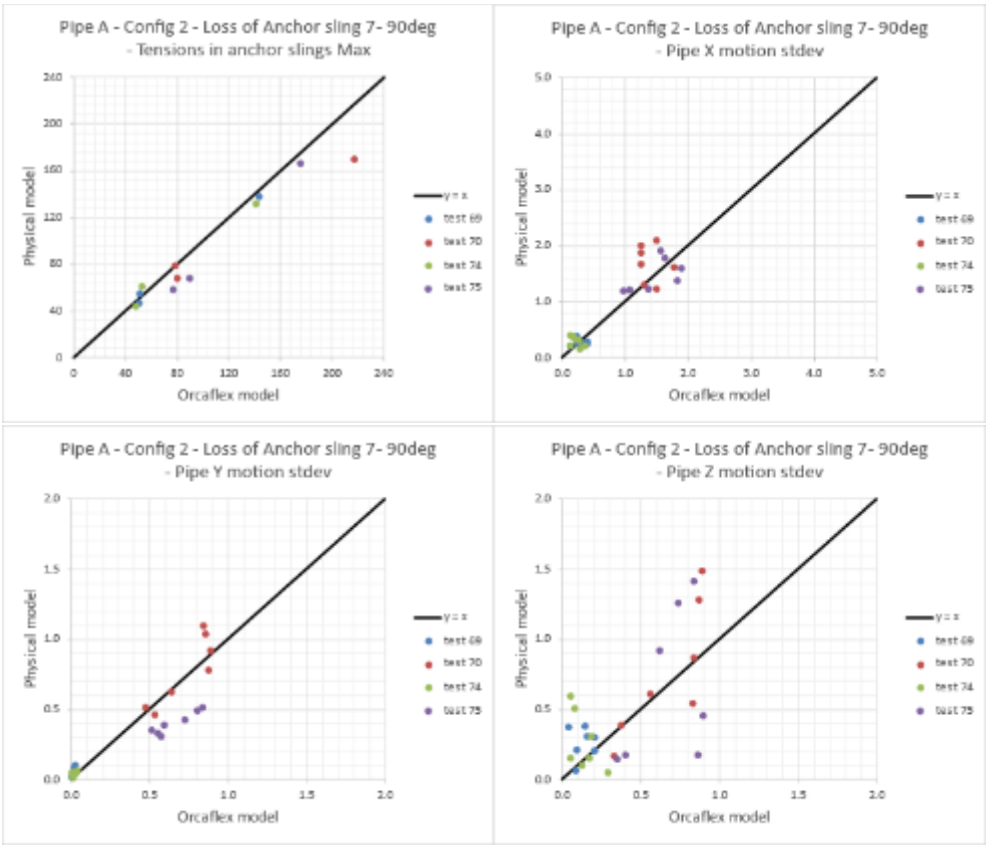

Figure 4-15: Pipe A – loss of anchor sling 7 – Configuration 2 – Wave at 90 deg.

For regular wave conditions, time domain comparison can be performed. Therefore, to complement the previous observations, a time domain comparison is performed on test n°80. The test was performed with pipe A laid on a flat seabed in configuration 2, with chain only, and considering the loss of anchor sling n°6, third sling from the pipe free end.

This comparison is performed on the 3D motions of the strainer, the 3D connection loads at pipe fixed end and the axial tensions in the anchor slings.

The numerical model and physical model compares very well. Some differences can be observed; however, values and shape of the curves are very close which shows that, on the one hand, the numerical model predicts well the values of the parameters of interest and that, on the other hand, the numerical model simulates well their dynamics responses to wave loadings.

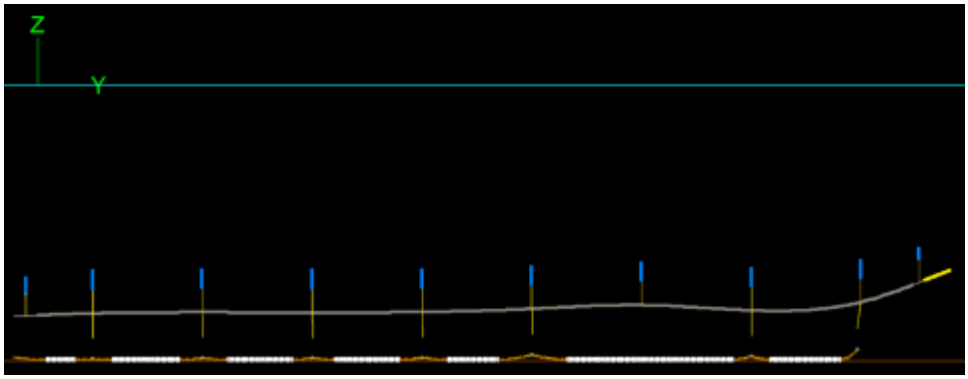

Picture 4-10: Pipe A – loss of anchor sling 6 – Test n°80 – Static state.

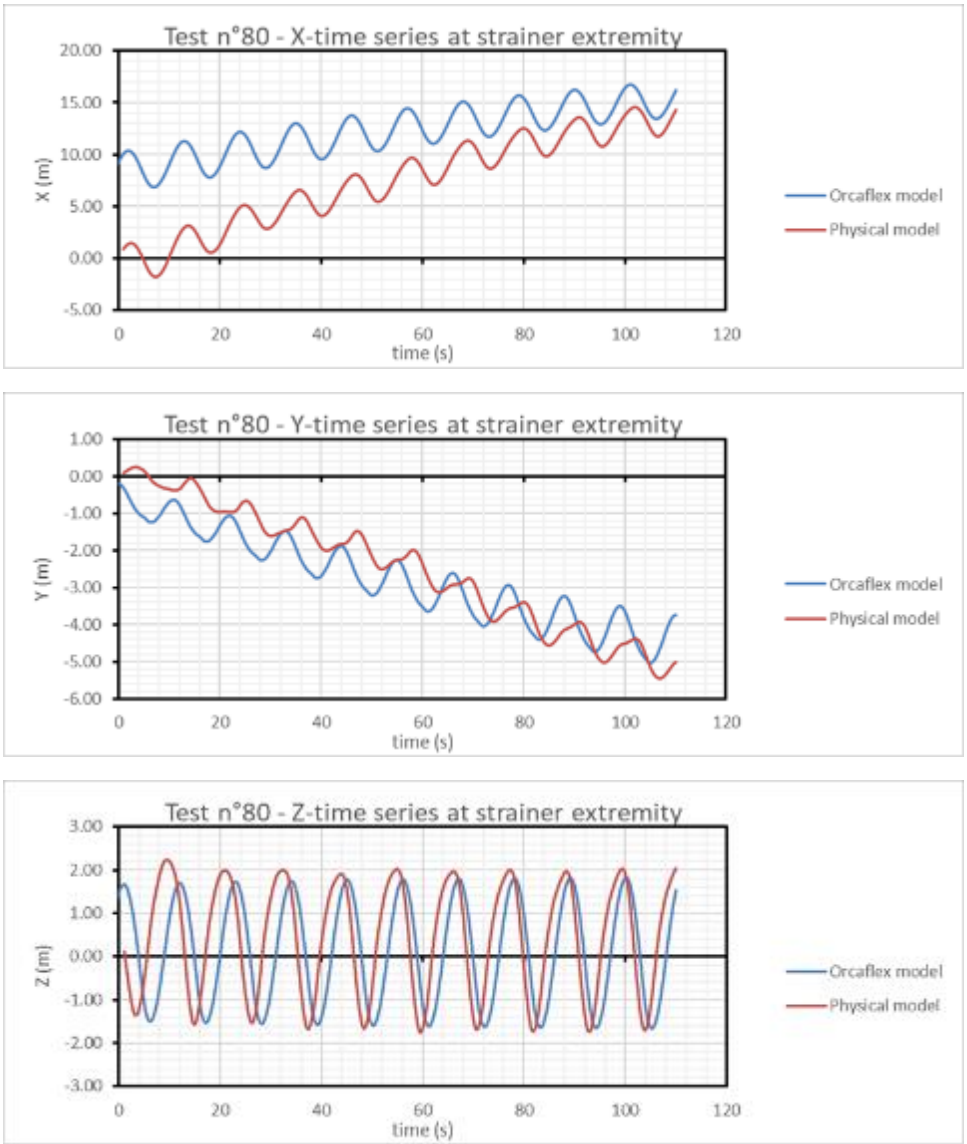

Figure 4-16: Pipe A – loss of anchor sling 6 – Test n°80 – 3D motions at strainer.

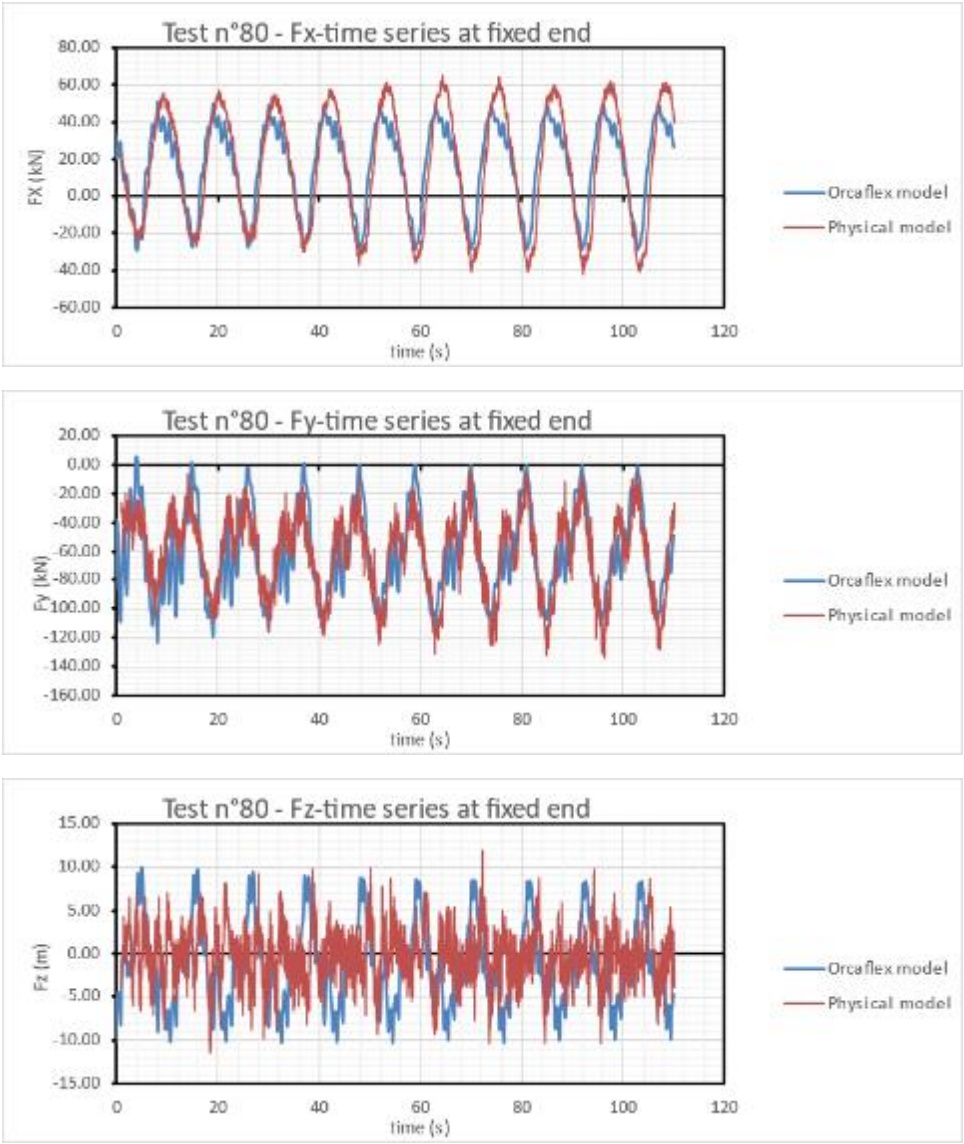

Figure 4-17: Pipe A – loss of anchor sling 6 – Test n°80 – 3D loads at pipe fixed end.

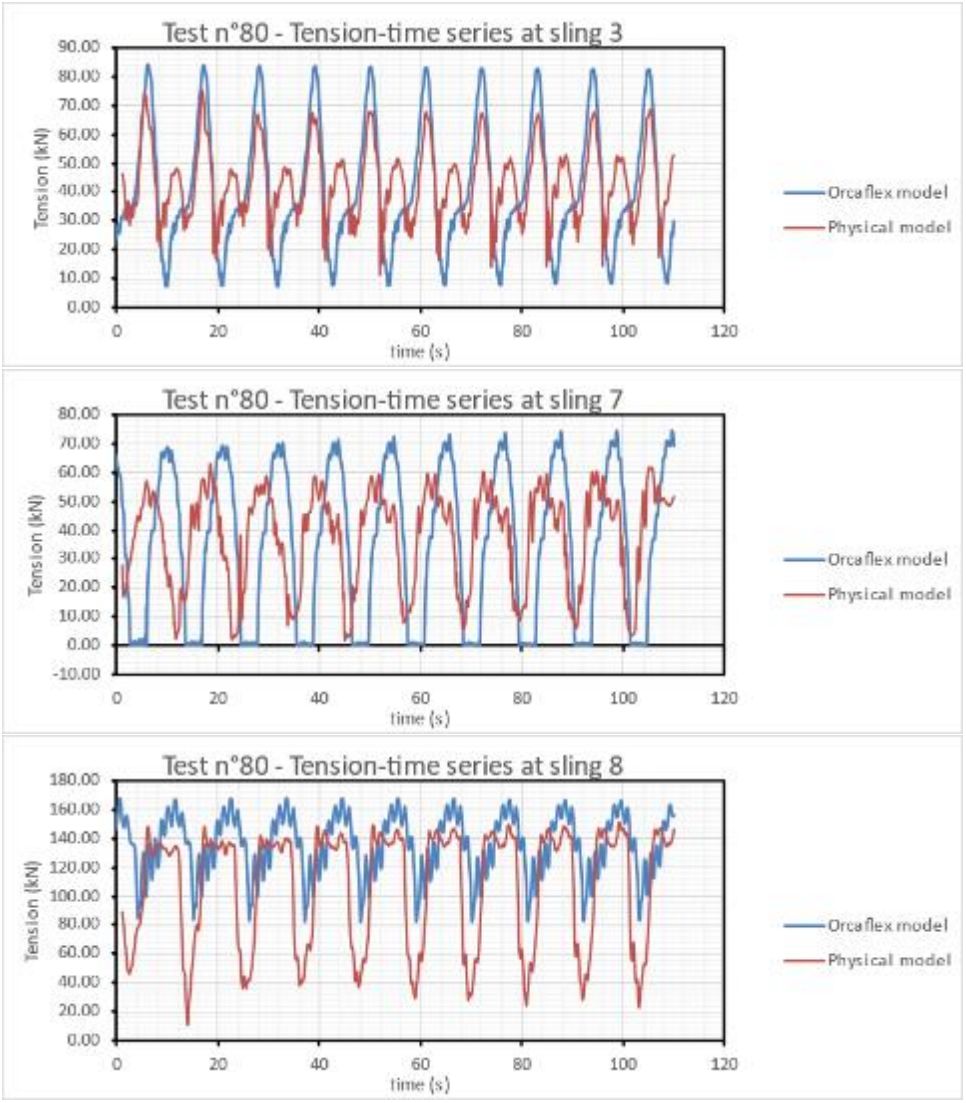

Figure 4-18: Pipe A – loss of anchor sling 6 – Test n°80 – tensions in anchor slings.

4.5. 3rd Campaign Conclusions

The following Section 4.5.1 summarizes the progress, as well as the main observations and results obtained during this third campaign.

Section **Erreur ! Source du renvoi introuvable.** discusses the identified way forwards which should be considered for possible further studies.

4.5.1. 3rd Campaign Key Points

The goals of the third campaign were:

- to validate the calibration methodology implemented to build a robust numerical model reproducing the hydrodynamical and mechanical responses of the experimental setup by using a new flexible pipe with a different mechanical response (elongating under pressure),
- to test non-collapsed buckling configurations with this new flexible pipe,
- to investigate the flexible pipe system response in specific conditions such as with one broken sling (damaged condition) and in the presence of a bump in the seabed.

As a result, the third experimental campaign featured the following novelties:

- New pipe elongating under pressure: pipe B
- Only 2 anchoring configurations were tested: Configuration 1 (CW only) and Configuration 2 (chain only)
- Damaged condition configuration: successive removal of AS 6, AS7, B7 and B8 (pipe A)
- Flexible pipe system response when placed on a bump (pipe A)
- General dynamic behavior with a straight initial configuration (pipe B)
- General dynamic behavior with an initial buckling configuration (pipe B)

In addition, the following preliminary characterization tests were also conducted in air to complement the experimental data base used for the numerical model calibration:

- The mass in water if the flexible pipe B was experimentally obtained to provide a more reliable value which precision is key for the EA and EI calibration (i.e., catenary position in the z-elevation profiles).
- The elongation of pipe B was tested at specific pressures, for an increasing loading looping back to 0kN: it was found that the elongation at 0kN before the loading process is not the same as the elongation at the offloading stage.
- The pipe B elongation was also tested through pressure cycles for given loads, and again a hysteresis behavior was noted: the initial pipe elongation value after decompression to 0bar is not identical to the elongation before undergoing the pressure cycle.
- The hysteresis behavior of pipe B (and most probably also in pipe A, through it was not investigated) is identified to reduce the accuracy of the EA calibration process, since it is currently not accounted for.

During this third experimental campaign, some unforeseen experimental phenomena arose which are listed hereafter, with the double purpose of traceability and discussing potential influence on the numerical model calibration accuracy:

- Two square wooden plates were used to palliate the irregularity of the BGO basin floor, adding a supplementary elevation under CW2 and CW7, which can influence the transverse motion of the flexible pipe system.
- The buoy used to make the weighting end B neutrally buoyant when in fixed/fixed configuration was involuntarily kept for fixed/free configurations when the floatability of the strainer already accounts for this. Thus, it was also included in the numerical model.
- This additional buoyancy made the flexible pipe collapse vertically close to the strainer for a low Pi (approx. 4bar) during the bending stiffness check test, preventing the EI calibration at this Pi.
- During the axial stiffness check tests using the pulley setup, the vertical beam was subjected to a variable flexion towards the flexible pipe system due to the increasing pulling tension. As a result, the accuracy of the EA calibration is reduced.
- Similarly, the actual z-position of the QT which is meant to be on the pipe midline axis, is slightly variable from one QT to another (tendency to point downwards) which impact the EI calibration, since it relies on the elevation profile (yields higher numerical EI than in reality).

Concerning the axial and bending stiffnesses of pipe B and the associated numerical model calibration, the following conclusions are made:

- The pipe B EA curves are depicting a pipe elongating under pressure: this elongation ranges from 1% to 2% for internal pressures comprised between 4 and 40bar.
- The EA curves for the internal pressures of approximatively 10bar, 20bar, and 40bar are all linear, while the one characteristic of a Pi of 4bar is bilinear.
- The EI obtained from the numerical calibration on the experimental elevation profiles are likely to be higher than the real value given the torsion of the flexible pipe (not allowed in numerical model) which brings the QT downwards when comparing the initial z-position on the pipe midline axis. This could explain smaller pipe motion amplitude, especially at the pipe free end.

The systematic comparison between the numerical model and physical model has shown that:

- The numerical model provides the same tendencies and the same orders of magnitude for most of the cases.
- The numerical model well predicts the maximum tensions in the anchor slings for all cases.
- The numerical model exhibits more discrepancies regarding the flexible pipe motions. However, both numerical model and physical model show small motions of the pipe at the wave frequencies, demonstrating the consistent hydrodynamics behaviour of the modelled flexible pipe. In addition, it is highlighted here that the motions predicted for the anchoring configuration 1, with clump weights only, compare better to the numerical model than for the anchoring configuration 2, with chain only. It is reminded that the initial position of the chain is not similar between the numerical model and the physical model. In the numerical model, the chain is rectilinear at the beginning of the simulation while in the physical model the chain initial position is impacted by the motion

history of the previous test. In addition, a typical friction coefficient was used to simulate the impact of the basin floor on the chain. Consequently, it is expected that a better characterisation of the chain friction would yield to more reliable numerical predictions.

Finally, the calibration methodology developed using the results of the two first campaigns was applied to the cases investigated during the third campaign. **The comparative analysis between the numerical model and physical model tends to demonstrate that OrcaFlex software can be used to investigate the hydrodynamic behavior of a flexible pipe system and to design the main elements of such a concept.** In addition, the calibration methodology developed using results from tests with pipe A has been applied with success to another pipe material exhibiting a different response to internal pressure variation. **As a conclusion, the developed numerical tool and associated calibration methodology can be used to design an actual flexible intake pipe for future SWAC systems.**

4.5.2. Way Forward: Recommendation for Further Investigations

In general, it was observed that the calibration of the numerical model should preferably rely on a large experimental basis. Concretely, it is thus preferable to conduct several repetitions of the tests identified as “calibration tests” (i.e., used to derive OrcaFlex input data such as the EI, EA, seabed friction coefficient, …) rather than testing for an extensive number of configurations.

Moreover, several aspects of the numerical model could be improved in terms of level of accuracy in the input data/allowed hypotheses. The following list is made based on observed experimental phenomena in the basin:

- As stated in Section 3.5.2, the use of 6D Buoy Orcaflex objects for the modeling of the CW would yield more accurate results, based on the observed slanted positions occurring when subjected to current.
- Similarly, it is reminded that the anchoring chain initial position before each test is unknown by the software and assumed to be rectilinear. In reality, this initial position is modified by the experimental uncertainties and the previous tests motion history. A meticulous repositioning of the chain between each test or a motion tracking system, combined with an extensive characterisation the chain friction would yield a more reliable transverse displacement for flexible pipe system using a chain in their anchoring configuration.
- In the same way, allowing torsion at the pipe level would avoid data divergences due to this phenomenon, as noted during the EI calibration.
- A thorough characterization of the tested flexible pipe hysteresis would allow a more accurate estimation, and thus calibration of the EA.

5.Conclusions

The objective of this study was to investigate the feasibility of using the OrcaFlex software to model and design a flexible SWAC pipe. More precisely, the subsequent steps were followed:

- Production of an experimental data base through the realization of 3 experimental campaign at the Océanide's BGO FIRST basin.
- Design and optimization of the flexible pipe system based on its experimental hydrodynamic response.
- Calibration of a numerical model with OrcaFlex and demonstrate the suitability of this software for such a project.

Each experimental campaign was guided by specific objectives which are reminded hereafter:

- 1st campaign: Investigate flexible pipe system behavior to calibrate a numerical model with a simplified prototype fixed at the basin floor to refine the conceptual design.
- 2nd campaign: Test for a more realistic design including a strainer at the system free end, and proper anchoring configurations.
- 3rd campaign: Study specific cases such as, the use of a new flexible pipe featuring a different mechanical response, behavior on a non flat seabed and behavior in case of a broken sling.

The following list summarizes the main concepts to consider during the design conception and refinement:

- Keep the flexible pipe at a certain distance from seabed with floating modules to avoid damages caused by friction.
- Optimize the buoy distribution to both avoid taught-slack events in the slings and minimize number of buoys for economical reasons.
- Ensure the knowing of the flexible pipe mechanical response under pressure (if not specified by the provided) by experimental preliminary testing.
- Prefer several repetitions of characterization tests to reduce the uncertainty of the input data in the software used for the numerical model (i.e., EI; EA, seabed friction coefficient) rather than testing for an extensive number of configurations.
- Determine the design tension and maximum pipe position offset, respectively with fixed anchoring points, and with modular anchoring components (i.e., stackable CW system) for instance.
- Test for or investigate the response of your flexible pipe system for specific situations such as:
    - Broken sling
    - Evolution of a local deformation (i.e., a pipe buckling) through a cycle of pressure or subjected to various sea conditions
    - Bumpy seabed
    - Effect of strainer presence at pipe free end
    - Potential amplification of pipe motion amplitude at pipe free end

The calibration methodology of the flexible pipe system numerical model with OrcaFlex includes the calibration of the following physical quantities:

- the axial stiffness calibration of the flexible pipe as a function of the internal pressure (in terms of strain [%]/wall tension [kN])
- the bending stiffness calibration of the flexible pipe as a function of the internal pressure
- the seabed friction coefficients of the anchoring components
- the flexible pipe hydrodynamic coefficients in case of allowed transverse motion

The current calibration process is based on the following characterisation tests, which should be repeated for better data input accuracy:

- EA: underwater axial stiffness test & underwater axial tension characterization
- EI: underwater tracking of flexible pipe elevation profiles as a function of the internal pressure or decay test (consider X-natural frequencies)
- μ_s: underwater axial and transverse pulling test related to displacement for each anchoring component
- C_A and C_D: transverse motion recording under various sea conditions

The main conclusions of each experimental campaign are summarized as follows:

- 1st campaign:
  - Global response of the simplified flexible pipe system prototype, when subjected to regular waves
  - Determination of the design tension
  - Validation of the buoys size and spreading
  - First definition of the numerical model calibration methodology
  - Observation of a hyperstatic state of the flexible pipe system due to the fixation state at both ends and at the basin floor
- 2nd campaign:
  - Global response of the flexible pipe system comprising a strainer at the free end and an anchoring configuration, when subjected to both regular and irregular waves
  - Attempt to investigate specific response of the flexible pipe system when featuring a buckling --> failure to form a buckling without collapse with the first flexible pipe (i.e., shortening under pressure)
- 3rd campaign:
  - Global response of the flexible pipe system with the new flexible pipe (i.e., elongating under pressure under irregular waves)
  - Specific response of the flexible pipe system with the pipe shortening under pressure when placed on a bump
  - Specific response of the flexible pipe system with the pipe shortening under pressure when featuring one broken sling

To conclude, the EuroSWAC project has enabled to gain insight on the following points listed hereafter:

- SWAC flexible pipe section design conception and refining procedure
- Order of magnitude of system design outputs

- Determination of typical test matrix content to be used for the study of a flexible pipe system hydrodynamic behavior and its numerical model calibration (i.e., produce a useful experimental data base)
- List of trends to consider in the design optimization of the experimental flexible pipe system design (i.e., typical flexible pipe system behavior to be cautious of, or seabed features to consider when designing a flexible pipe system)
- Calibration methodology for flexible pipe system numerical model building
- Validation of Orcaflex software suitability for this type of project, the limitation lies in the level of accuracy of the input data and the considered modeling hypotheses (the higher the precision in input data the closer the to reality the numerical outputs are)